INFORMATION TO USERS

This manuscript has been reproduced from the microfilm master. UMI films the text directly from the original or copy submitted. Thus, some thesis and dissertation copies are in typewriter face, while others may be from any type of computer printer.

The quality of this reproduction is dependent upon the quality of the copy submitted. Broken or indistinct print, colored or poor quality illustrations and photographs, print bleedthrough, substandard margins, and improper alignment can adversely affect reproduction.

In the unlikely event that the author did not send UMI a complete manuscript and there are missing pages, these will be noted. Also, if unauthorized copyright material had to be removed, a note will indicate the deletion.

Oversize materials (e.g., maps, drawings, charts) are reproduced by sectioning the original, beginning at the upper left-hand corner and continuing from left to right in equal sections with small overlaps. Each original is also photographed in one exposure and is included in reduced form at the back of the book.

Photographs included in the original manuscript have been reproduced xerographically in this copy. Higher quality 6" x 9" black and white photographic prints are available for any photographs or illustrations appearing in this copy for an additional charge. Contact UMI directly to order.

.

UMI

Analysis of mass flow and enhanced mass flow methods of flashing Refrigerant-22 from a small vessel

Nutter, Darin Wayne, Ph.D.

Texas A&M University, 1994

ANALYSIS OF MASS FLOW AND ENHANCED MASS FLOW

METHODS OF FLASHING REFRIGERANT-22 FROM A SMALL VESSEL

A Dissertation

by

DARIN WAYNE NUTTER

Submitted to the Office of Graduate Studies of
Texas A&M University
in partial fulfillment of the requirement for the degree of

DOCTOR OF PHILOSOPHY

December 1994

Major Subject: Mechanical Engineering

ANALYSIS OF MASS FLOW AND ENHANCED MASS FLOW

METHODS OF FLASHING REFRIGERANT-22 FROM A SMALL VESSEL
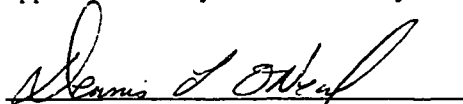
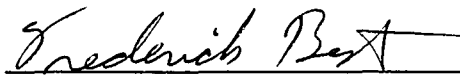A Dissertation

by

DARIN WAYNE NUTTER

Submitted to Texas A&M University
in partial fulfillment of the requirements
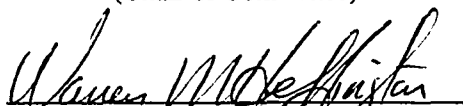for the degree of

DOCTOR OF PHILOSOPHY

Approved as to style and content by:

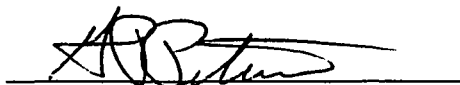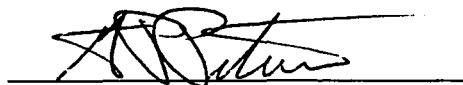|	
Dennis O'Neal	Frederick Best
(Chair of Committee)	(Member)
Warren Heffington	George Peterson
(Member)	(Head of Department)
George Peterson	
(Member)	

December 1994

Major Subject: Mechanical Engineering

ABSTRACT

Analysis of Mass Flow and Enhanced Mass Flow Methods of Flashing

Refrigerant-22 from a Small Vessel. (December 1994)

Darin Wayne Nutter, B.S., Oklahoma State University;

M.S., Oklahoma State University;

Chair of Advisory Committee: Dr. Dennis O'Neal

The mass flow characteristics of flashing Refrigerant-22 from a small vessel were investigated. A flash boiling apparatus was designed and built. It was modeled after the flashing process encountered by the accumulator of air-source heat pump systems. Three small pyrex glass vessels were used to hold the refrigerant and allow for visualization studies of the flashing process. Baseline experiments were run varying initial pressure, initial refrigerant amount, orifice diameter, and vessel geometry. Three sets of experiments were run using two passive enhancement methods (the addition of steel balls and the addtion of small amounts of oil) and one active enhancement method (the addition of an immersion heater). Furthermore, a lumped-parameter analytical model was developed from basic thermodyamic principles that predicted the rate of depressurization for the flashing refrigerant.

The study showed that the initial refigerant amount and the orifice size had the greatest influence on the mass flow and pressure characteristics during each sixty second test. The initial pressure and vessel volume had less of an impact under the condtions

tested. Two of the enhancement methods consistantly increased the amount of refrigerant flashed during the tests as compared to the baseline data for the same intial conditions. The addition a 1 cm layer of 3.6 mm steel balls to the base of the vessel increased the amount flashed from 21% to 81% and the addition of the 215-watt flat-spiral immersion heater the increased the amount flashed from 47% to 111%. Foaming at the vapor-liquid interface was observed with the refrigerant-oil mixture experiments as two of the eight test conditions averaged an increase while six averaged a decrease, ranging from a 21% increase to a 27% decrease. The analytical depressurization model predicted general pressure and mass flux trends, and revisions to the model improved pressure predictions to within ±11%.

ACKNOWLEDGMENTS

I would like to express my gratitude to Dr. Dennis O'Neal for his continued support and guidance throughout my pursuit of this degree. His encouragement over the last five years and long hours spent reviewing this manuscript are well appreciated. Furthermore, his proven abilities and accomplishments will be difficult to emulate and a sizable goal to aim for during my career.

I would like to thank my advisory committee members, Dr. Warren Heffington, Dr. George Peterson, and Dr. Frederick Best for their assistance. I would also like to thank Dr. Yassin Hassan for substituting for Dr. Best during my final examination and Dr. David Bessler for being my graduate council representative.

It should be noted that Dr. Warren Heffington contributed a great deal to the development of my professional abilities and attitudes. He should be acknowledged for not only his financial support though the LoanSTAR program and the Industrial Assessment Center, but also for his considerable contribution of time and energy spent on my behalf.

I would like to acknowledge and thank the Texas Energy Research Appropriation Program (ERAP) and American Society of Heating, Refrigerating, and Air-Conditioning Engineers (ASHRAE) for their financial support. I would like to recognize the Trane Company and the Carrier Corporation for their equipment donations and technical support and advice given to this project.

Special thanks should be given to my wife, Jeanne, who continually supported me though the latest stage of my career. She has unselfishly spent her valuable time and efforts raising our three children (Austin, Abbie, and Anna). Many memories were formed over the last five years as Jeanne and I had two children born in College Station and developed many lifelong friendships. I am thankful to my parents (and family) for their continued encouragement and assistance. Also, I am greatful to my father-in-law and mother-in-law who gave so much and asked for so little. Finally, I would like to acknowledge that my faith in Jesus Christ as my Lord and Savior gave me the perserverance to perform this task and allowed me to keep my work in perspective.

DEDICATION

To my loving wife Jeanne,

and our children:
Austin Wayne who loves to fish,
Abbie Jean who loves to sing, and
Anna Catherine who loves to hug.

TABLE OF CONTENTS

TABLE OF CONTENTS (Continued)

LIST OF TABLES

LIST OF TABLES (Continued)

LIST OF FIGURES

LIST OF FIGURES (Continued)

LIST OF FIGURES (Continued)

LIST OF FIGURES (Continued)

LIST OF FIGURES (Continued)

LIST OF FIGURES (Continued)

LIST OF FIGURES (Continued)

NOMENCLATURE

$A =$ area (m^2)

$B =$ frequency factor of iterations between molecules (1/sec)

$C =$ flow coefficient

$C^* =$ defined by eqn. (3.16)

$erf =$ Gaussian error function

$g =$ acceleration due to gravity (m/sec^2)

$G =$ mass flux (kg/m^2-sec)

$h =$ enthalpy (kJ/kg)

$I =$ mechanical equivilant of heat (unitless)

$J =$ rate of nucleation events (events/m^2-sec)

$k =$ slip ratio

$K =$ Boltzmann's constant (J/K)

$\dot{m} =$ mass flow rate (kg/sec)

$M =$ mass (kg)

$N =$ number

$P =$ pressure (kPa)

$\dot{Q} =$ rate of heat transfer (KW)

$t =$ time (sec)

$T =$ temperature (°C)

$u =$ internal energy (kJ/kg)

$v =$ specific volume (m^3/kg)

$V =$ velocity (m/sec)

$\dot{W} =$ rate of work transfer (KW)

$x =$ quality

$z =$ elevation (m)

NOMENCLATURE (Continued)

Greek Symbols

$\alpha =$ thermal diffusivity (m^2/sec)

$\beta =$ heterogeneity factor

$\phi =$ defined by eqn. (3.22)

$\pi =$ pi

$\rho =$ density (kg/m^3)

$\sigma =$ surface tension (mN/m)

Subscripts

$1\phi =$ single phase

$A =$ Avagadro's number

$b =$ blowdown

$cr =$ critical flow

$d =$ discharge

$f =$ liquid (fluid) phase

$g =$ vapor (gas) phase

$i =$ interior fluid

$o =$ entering orifice

$q =$ quasi-equilibrium (static)

$s =$ solid

$sat =$ saturated condition

$v =$ vapor phase

$\infty =$ inner temperature

CHAPTER I

INTRODUCTION AND PROBLEM STATEMENT

INTRODUCTION

Flash boiling occurs when the pressure of a liquid suddenly drops below its

saturation pressure, causing the liquid to vaporize. Flash boiling is a phenomenon

common to many engineering applications. The nuclear power industry initiated flash

boiling research because of the safety concern regarding loss-of-coolant-accidents

(LOCA) in the 1960s. Flashing also occurs in liquefied gas storage vessels, desalination

equipment, safety relief valves, steam generating systems, heat exchangers, vegetable puff

dryers, and refrigeration and air-conditioning equipment. Most experimental efforts have

used water as their experimental fluid. Japanese researchers (Hanaoka et al., 1990 and

Maeno et al., 1987) have recently used Refrigerant-113. No R-22 experimental data on

flash boiling has been found in the literature.

Flash boiling occurs in many air-source heat pumps during start-up and the defrost

cycle. The systems are typically charged with R-22. Many heat pumps utilize an

accumulator, a small tank in the refrigerant system, to store excess refrigerant. During

start-up or initiation of the defrost cycle much of the refrigerant is in the accumulator. At

the onset of the defrost cycle, the pressures within the heat pump equalize, and up to 50%

This dissertation follows the format of the *Transactions, American Society of Heating, Refrigerating, and Air-Conditioning Engineers.*

of the system's refrigerant floods into the accumulator and outdoor heat exchanger

(Miller,1987). The compressor reduces the suction pressure below the refrigerant's

saturation pressure, causing the liquid refrigerant to boil. Several minutes pass before an

appreciable amount of refrigerant leaves the accumulator and begins to circulate through

the system and defrost the outdoor heat exchanger. An increase in the rate that the

refrigerant leaves the accumulator would shorten the defrost cycle and improve the overall

efficiency of the heat pump.

Additional knowledge of the flash boiling phenomenon could have immediate

applications in the air-conditioning industry; however, more research is needed to better

understand the flash boiling process. Mayinger (1988) states, "Further experiments have

to be performed to study flashing behavior, phase separation, critical mass flux , and two-

phase pressure loss of chemical substances."

BACKGROUND

The first pressurized-water reactor power plant, a 60-MW(e) reactor located in

Shippingport, Pennsylvania, began generating electricity in 1956. It was designed to

maintain the coolant fluid at pressures around 2250 psia, which is higher than the

saturation pressure corresponding to the maximum temperature in the reactor. Therefore,

the coolant is held as a liquid (El-Wakil, 1984). The need for fundamental understanding

of flash boiling was necessary in nuclear reactor applications because of the safety

concerns about possible loss-of-coolant-accidents.

A generalized qualitative description of flashing and two-phase flow during depressurization from a vessel follows. Rapid depressurization begins at some initial pressure that is equal to or higher than the liquid's saturation pressure. Once the pressure drops below the saturated conditions, bubbles form at the first available nucleation sites, causing the liquid to flash boil. Guhler et al. (1979) observed three kinds of boiling phenomena as the pressure in the vessel drops below the liquid saturation pressure: interfacial boiling, bulk boiling, and heterogeneous boiling on the vessel surfaces. Next, the liquid-vapor mixture within the vessel swells and the pressure increases. Initially, the vapor production within the vessel is greater than the volumetric flow rate of the vapor exiting the vessel. Once the vapor production and flow rate equalize, the pressure starts to fall and the swell begins to recede. Flash boiling can be a rapid and violent process that frequently lasts only a few seconds in small vessels.

PROBLEM STATEMENT

The objective of this research was to characterize the effects of pressure, temperature, orifice size, vessel size, initial refrigerant level, and boiling enhancement techniques on the mass flow produced by flashing Refrigerant-22 from a small vessel. The author concentrated on measurable variables related to the heat pump application previously mentioned (i.e., pressures, temperatures, and mass flow rate). The eight steps necessary to reach the objective were:

1.   to review of the literature from previous flash boiling research,
2.   to design and build an experimental apparatus for flash boiling experiments,

3.   to develope an analytical model

4.   to perform flash boiling experiments using Refrigerant-22 as the fluid,

5.   to discuss the variables that influence the flashing process,

6.   to compare baseline experimental data with data from enhanced boiling experiments,

7.   to compare experimental data with the model, and

8.   to revise the model as necessary.

The available literature on flash boiling provided insight into the phenomenon of flash boiling and an understanding of the mechanisms that control it. The measurable properties important to the proposed research were pressure, temperature, exit throat area, initial refrigerant amount, vessel geometry, and mass flow rate.

The experimental apparatus was designed to allow fundamental flashing experiments, visualization studies, and "enhanced" flashing experiments. The apparatus used a transparent vessel, allowing for visualization studies. The vessel was instrumented with thermocouples mounted inside to measure the temperature gradient during the flashing process. The top of the vessel was removable so the enhanced surfaces or immersion heaters could be placed inside for some of the experiments. A pressure transducer was mounted on the top of the vessel. Three different sized orifices were constructed for easy installation. The flashed vapor was piped to a large "semi-infinite" tank initially set at 120 kPa. A fast-acting solenoid valve located between the flash vessel and the tank was opened to initiate each flashing experiment. A data acquisition system collected the real-time data. Each experiment began by filling the flash vessel to the desired liquid level, temperature, and pressure. After checking the apparatus, the

experiment began by electronically triggering the solenoid valve and data acquisition system. At that point, some of the refrigerant in the flashing vessel boiled into the large tank.

Multiple experiments were performed varying the pressure (and corresponding initial temperature), orifice size, vessel geometry, and refrigerant amount. The refrigerant pressures used were similar to those an accumulator experiences during defrost initiation of a residential sized air-source heat pump. Different orifice sizes, vessel geometry, initial pressure, and initial refrigerant liquid levels were investigated to determine their influence as potential variables in the flashing phenomenon with respect to the mass flow. In addition to the traditional flash boiling tests, experiments were run using enhanced boiling surface material, a flat spiral electric immersion heater, and small amounts of oil.

This dissertation provides an analysis of the mass flow of flashing R-22 from a small vessel. Chapter II presents a critical review of available and relevant literature. Chapter III provides the development of an analytical model for the flashing process. Chapter IV describes the experimental apparatus and lists step-by-step procedures used for running the flashing experiments. Chapter V presents results from the baseline experiments including analysis of important parameters. Qualitative descriptions of the flashing process are also provided. The results from the enhanced flashing experiments are discussed and compared with baseline results in Chapter VI. Chapter VII includes the comparison of the analytical model with the baseline experimental data as well as a

discussion of two revisions to the model. Finally, Chapter VIII summarizes the work, presents conclusions from the research, and lists recommendations for further work.

CHAPTER II

LITERATURE REVIEW

The literature review found that no flashing research has been performed using R-22 as the experimental fluid. The available literature on flashing provided insight into the phenomenon and an understanding of the mechanisms that control flash boiling. This literature review critiques the relevant existing literature regarding the flashing phenomenon. Early research efforts are discussed as well as the literature that discussed measurable factors influencing the flashing mass flow. The factors applicable for this research were primarily pressure, exit orifice area, vessel geometry, and initial refrigerant amount (or mass). Additionally, existing analytical models, critical mass flow models and literature related to enhanced flash boiling are also discussed. Finally, conclusions from the literature review are stated.

BACKGROUND

The need for fundamental understanding of flash boiling first became apparent in nuclear reactor applications because of safety concerns about possible loss-of-coolant-accidents (LOCAs). The bulk of literature available presents both applied and analytical information for sizing pressure relief valves for pressure vessels (First and Huff, 1989; Fauske, 1988; and Huff, 1982). Several events can lead to a pressure rise within a vessel. Some examples are excessive heating, loss of agitation, incorrect sequence of addition of

reactant, leak of heat transfer media into vessel, and e3xternal fire around reactor (Swift et al., 1983). Leung and Fauske (1987) tested 55 fluids for proper emergency vent sizing. R-22 was not among the tested fluids. Experiments concentrated on fluids commonly used as nuclear reactor coolants or on volatile and caustic fluids that could have rapid increases in pressure.

An early and commonly referenced article is Hooper and Kerba's (1969) "The law of flashing." They first defined the "static" pressure as the average pressure within the liquid for the twelve milliseconds following the initial minimum pressure (or pressure undershoot). As illustrated in Figure 2.1, this "quasi-equilibrium" pressure (or static pressure) is lower than the saturation pressure and higher than the blowdown (minimum) pressure. Flashing experiments using thirteen fluids were run. The fluids were ethyl alcohol, methyl alcohol, n-propyl alcohol, acetone, ethyl acetate, n-propyl acetate, hexane, cyclohexane, heptane, toluene, Freon 113, carbon tetrachloride, and water. Hooper and Kerba (1969) concluded that the static pressure was independent of the initial and blowdown pressures; furthermore, that it was a function only of the initial liquid temperature and physical properties of the fluid. The equation below was determined to best approximate the experimental data:

$$\left(\frac{P_q}{\rho_f h_{fg} l} \right) = 0.318 \left(\frac{\rho_g}{\rho_f} \right)_{T_{s,i}}^{\frac{4}{3}} \tag{2.1}$$

TIME (sec.)
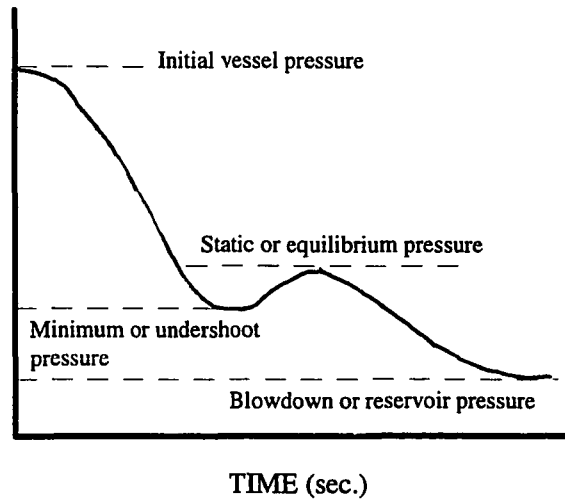
Figure 2.1. Illustration of depressurization process.

Hooper and Luk (1974) used high speed cameras to observe the flashing phenomenon in a

U-tube flashing apparatus and deduced three major influences that kept the internal static

pressure constant: conduction of heat to the surface of the liquid, instabilities in the

surface of the liquid layer created by convection of warmer liquid, and nucleation and

bubble growth in the bulk liquid. The determination of the static pressures were

interesting, but no direct application of these finding were found. Researchers have

referenced this article, but there has not been a reason identified to investigate the static

pressure phenomenon further.

MASS FLOW

The main emphasis of this dissertation is on the mass flow characteristics for the flashing process. This section reviews the literature covering mass flow characteristics for "traditional" flashing from a small vessel as well as the available literature related to enhanced flash boiling using passive and active boiling techniques. It was found in the literature that the mass flow is primarily dependent on initial vessel pressure, initial refrigerant level (or amount), and exit orifice area.

The initial pressure affects the amount of flashed vapor that will be generated and the rate of pressure drop during the flashing process. Nakamura et al., (1985) provided a useful qualitative description of flashing and a good discussion of the influence of initial pressure, nozzle throat diameter, and initial water level on flashing. They built an experimental apparatus that flashed water from a 0.071 m^3 (305 mm ID by 1000 mm) vessel using three initial pressures (294, 392, and 490 kPa) and three orifice diameters (5, 7, and 9 mm), and three initial water levels (322, 481, and 570 mm). The authors plotted their experimental data (pressure, water level, and temperature vs. time) and presented qualitative conclusions. They concluded that a higher initial pressure resulted in more vapor production and a larger depressurization rate. Furthermore, they concluded that a larger exit orifice diameter caused a more rapid rate of depressurization. The larger orifice diameter allowed more vapor to be generated during the first part of flashing. Nakamura et al., (1985) stated that experiments with higher initial water levels had larger exiting mass flow rate.

Nakamura et al., (1985) also developed a complex equation for pressure change within the vessel. Two of the five assumptions made for their lumped parameter analysis were uniform mixing in the layer of vapor and liquid with no variations in temperature or density existing, and that the void fraction in the mixed layer was the average vessel void fraction observed during the experiments. These assumptions are contrary to findings of Guhler et al. (1979) who measured a large temperature gradient in the vapor above the agitated liquid, and learned that the gradient continued to exist until the vessel was emptied. Approximate temperature differences as large as 30 °C were observed. Also, pictures of the flashing Refrigerant-12 at several time intervals (0.4, 1.1, 11.3, 42.7, 145.5, and 250.3 seconds) were published. It was evident from these pictures that, during the first three time intervals (0.4, 1.1, and 11.3 seconds), the void fraction at the mixed layer during this time was not equal to the average value since portions of the vessel did not have any bubbles forming ($\alpha=0$) while other sections had void fractions of approximately 0.4. Although these two assumptions were oversimplifications, Nakamura's calculated pressures agreed quite well with the measured experimental pressures. The vessel pressures for all three orifice sizes (5, 7, and 9, mm) gradually decreased and did not have a pressure undershoot. None of the orifices were large enough to cause anything other than choked flow during the first few seconds of the flashing process.

Grolmes and Fauske (1984) presented a one-dimensional lumped derivation of the rate of depressurization. Their derivation used the general mass and energy equations for a fluid leaving an adiabatic vessel, assuming negligible kinetic and potential energy. The

Clapeyron equation was also used in the derivation. Averaged properties for the vessel as a whole and local properties entering the discharge opening were required as well as ancillary relations for both mass flux and the vapor mass fraction entering the discharge opening were needed. Fauske, et al. (1984) used this equation combined with the mass flux and vapor mass fraction to determine the predicted rate of depressurization for R-12. The experimental data agreed with the predicted for the first ten seconds of the flashing period. Pressures were slightly underpredicted for the next 20 seconds. Other authors (Hardy and Richter, 1986) used empirical correlations in their analysis of pressure and two-phase swelling.

Guhler et al. (1979), Hanaoka (1990), and Grolmes and Fauske (1984) also discussed the influence of the exit orifice area. In every case, these researchers found that for a larger area orifice, the internal pressure of the vessel fell more quickly. Also, the liquid swell increased for larger orifice areas. The time for a vessel to reach the minimum pressure was dependent on the orifice size. Hanaoka et al. (1990) used a 0.7×10^{-3} m^3 vessel, an initial vessel pressure of approximately 390 kPa, and five orifice diameters ranging from 3-20 mm. They found that this time decreased in inverse proportion to the orifice area. Furthermore, the quality of the fluid exiting the vessel had a significant influence on the mass flow. Grolmes and Fauske (1984) ran flashing experiments using R-12 and two orifice sizes (1.59 mm and 4.76 mm). Their vessel was 1.23×10^{-3} m^3 in volume and the initial vessel pressure was set at 655 kPa. They found that a smaller orifice had very little, if any, two-phase discharge, but the larger orifice produced seven

seconds of two-phase discharge with more rapid pressure decrease and mass loss. The initial mass flow rate was two to three times greater for the experiments that used the larger orifice.

Guhler et al. (1979) explained that another influencing factor was the state of the fluid as it exited the orifice. Any entrained liquid carried out of the vessel by the vapor drastically increased the exiting mass flow. They ran flashing experiments to study the adequacy of the design of railroad tank car safety valves. Their scaled-down experimental apparatus included a 1.2 liter vessel through 1.59 mm and 4.76 mm orifices and used R-12 as their working fluid. All experiments were run using an initial vessel pressure of 580 kPa. Results from their experiments led to the conclusion that the exit quality was dependent on the liquid level and its proximity to the exit port. Critical choked flow was found to occur in some of the experiments that had small exit areas and large internal pressures. Based on measured pressures, theoretical choked flow lasted 18 seconds for the larger orifice (4.76 mm) and considerably longer for the smaller orifice (the actual length was not published).

Guhler et al. (1979) also compared measured mass flow rate to theoretical mass flow rate of compressible vapor through an orifice. They showed a plot of the total mass out and mass flow rates (predicted and actual) for a 4.76 mm diameter orifice (Figure 2.2). Predicted values were initially somewhat higher than actual mass flow rates, but gradually approached measured values. Their theoretical values gave a good order-of-magnitude estimate of the mass flow rate during the latter stages of flashing. However, the authors
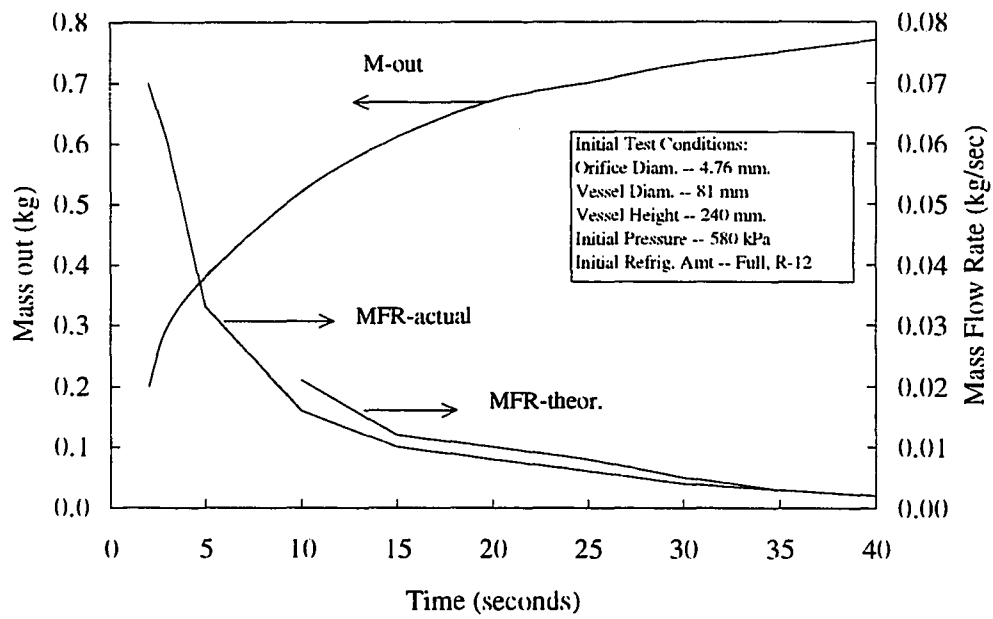
Figure 2.2. Mass out and mass flow rate (actual and theoretical) by Guhler, et al., 1979.

neglected the more transient initial 3blowdown period. No theoretical analysis was provided for the influence of vapor entrainment or two-phase flow exiting the vessel.

Finally, Peterson et al. (1984) found mass transfer rates for flashing of initially subcooled R-11 to be 10-12 times greater than evaporation alone because of agitation of the liquid and entrained droplets in the exiting vapor. The tests were performed over a small pressure range between 40 to 54 kPa. The authors defined an empirical flashing factor as the ratio of mass transfer of flashing liquid to the mass transfer of evaporating liquid. Their paper showed that the mass flux for flash boiling had a much greater magnitude than that of evaporation alone, but the empirical data were of little value since it was only for small pressure drops (40 to 54 kPa) and the experiments were run using only one fluid (R-11).

EXISTING CRITICAL FLOW MODELS

This section discusses several of the existing classical critical flow models applicable to flashing a fluid from a small finite vessel through an orifice. Critical flow occurs when the flow is maximized while traveling through a small flow path such as an orifice or broken pipe. Under these conditions, the mass flow rate dependent only on the upstream pressure and is independent of the downstream lower pressure (Kim, 1993). The flow can either be single phase vapor reaching sonic velocity at the smallest cross section or it can be two-phase flow traveling at velocities well below sonic. Two-phase

critical flow is more complicated to describe mathematically (Wallis, 1980) than single-phase flow.

Attempts to model the mass flow of flashing fluids (i.e., critical flow models) have progressed over the last few decades. Most of these two-phase models have been developed in an effort to improve the design of pressure relief valves. The major difficulty with most of the existing models is that they require information that is not easily measured. For example, several of the models need the void fraction or some local pressure, like the pressure at the orifice throat, that was not available in this research. In some cases these desired local values can be estimated by theory. Several references provide a good discussion of the "classical" two-phase critical flow models related to this research (Moody, 1965; Levy, 1965; Henry and Fauske, 1971; Wallis, 1980; and Grolmes and Leung, 1984).

The author evaluated existing 2-phase critical mass flow models to use with his analytical modeling (Mayinger, 1988; Huff, 1985; Wallis, 1980; Grolmes and Leung, 1984; Henry and Fauske, 1971; Fauske, 1985; Fauske et al., 1984; Fauske et al., 1983). The homogeneous equilibrium model (HEM) and homogeneous frozen model were examined and are discussed below. Visualization studies showed that the flashing process was two-phase very little of the time. Therefore, the critical flow model for single-phase choked flow was also used in the modeling.

Homogeneous single-phase flow through an ideal orifice is characterized by assuming a constant velocity across the exit plane (Moody, 1965). For isentropic flow

where enthalpy and specific volume are functions of pressure only, the critical mass flux is given by:

$$G_{crlo}^2 = -\frac{\partial P}{\partial v}$$ (2.2)

The homogeneous equilibrium model (HEM) is an extension of the single-phase compressible choked flow above. It assumes that the two phases are in thermodynamic equilibrium with equal velocity and temperature during expansion through an ideal nozzle (Moody, 1965 and Wallis, 1969). The vapor and liquid velocities are considered the same. In other words, the slip ratio, which is defined as the ratio of vapor to liquid phase velocities (k), is unity. In addition, the quality of the mixture is introduced by two thermodynamic relations (enthalpy, h, and specific volume, v). This leads to an expression for the HEM given as:

$$G_{cr,HEM}^2 = \frac{-1}{\frac{dv_f}{dP} - \left(\frac{v_{fg}}{h_{fg}}\right)\frac{dh_f}{dP} + x\left[\frac{dv_{fg}}{dP} - \left(\frac{v_{fg}}{h_{fg}}\right)\frac{dh_{fg}}{dP}\right]}$$ (2.3)

The homogeneous equilibrium model was developed for predicting the critical mass flux in long pipes where there is sufficient time for the flow to reach an equilibrium condition (Moody, 1980). This is supported by the research of Henry and Fauske (1971) who found that the HEM tends to underpredict the flow rate for flashing boiling from a small vessel.

The homogeneous frozen model (HFM) was developed for homogeneous flows in short pipes or nozzles where it is assumed the fluid travels through the nozzle without

time to change quality. This model (HFM) tends to yield a good prediction of the mass

flux, but generally underpredicts the critical pressure ratio (Henry and Fauske, 1971).

Mayinger (1988) found that the HFM predicts the higher critical mass flux when

compared to the HEM. The HFM assumes the flow is homogeneous, velocities of vapor

and liquid phases are equal (k=1), and there is no mass transfer between phases (dx/dt =

0). An expression for the homogeneous frozen model is written below (2.4).

$$G^2_{cr,HFM} = \frac{-1}{x\frac{\partial v_g}{\partial P}+(1-x)\frac{\partial v_f}{\partial P}}$$ (2.4)

ENHANCED FLASH BOILING

This section includes a discussion of the related phenomena that occurs during

enhanced flash boiling. Among others, the following topics are discussed: superheated

liquid, spinodal limits, homogeneous nucleation, heterogeneous nucleation, pressure

undershoot, passive boiling, active boiling, nucleation sites, and enhanced surfaces.

Finally, the literature that led to the design of the enhanced flashing included in this

research is discussed.

Superheated liquids can be reached by an isobaric or isothermal path (Cole, 1974).

Flash boiling occurs during an initially isothermal depressurization process. A theoretical

maximum amount of superheat exists before a superheated liquid is no longer metastable

and must become vapor. This theoretical maximum is called the thermodynamic limit of

superheat or the spinodal limit. Vapor bubble formation within a superheated, pure liquid is called homogenous nucleation and can approach superheat temperatures near the spinodal limit (Blander and Katz, 1975). Lienhard et al. (1978) achieved pressure undershoots that came within 2.7 °C of the spinodal line while flashing water from a long, 1.27 cm diameter pipe. Grolmes and Fauske (1974) found that if the liquid was pure enough and also free of nucleation sites, flash boiling began at the liquid surface and not in the bulk liquid. They observed superheat temperatures as high as 60 °C for R-11 and 55 ° C for methane. No such data were available for R-22. In contrast, vapor formation at the interface between a metastable superheated liquid and another phase (usually a solid or liquid impurity) is called heterogeneous nucleation (Carey, pg. 138). Superheat temperatures are much lower for heterogeneous nucleation.

Figure 2.1 shows the typical depressurization process. Alamgir and Lienhard (1981) defined the pressure undershoot as the pressure difference between the fluid's saturation pressure and the blowdown (or minimum) pressure during flashing. Several researchers, including Alamgir and Lienhard (1981) and Hanaoka et al. (1990), have attempted to predict the pressure undershoot by adding a heterogeneity factor, β, to the theory of homogeneous nucleation equations (see equation 2.5). A heterogeneity factor of unity would occur at the maximum limit of superheated liquid.

$$(P_{sat} - P_b) = \sqrt{\frac{16\pi\sigma^3 / 3KT}{\ln\left(\dfrac{N_A B}{v_f J}\right)}}\beta \qquad (2.5)$$

Modifications to equation (2.5) have been suggested (Alamgir and Lienhard, 1981 and

Guhler, et al., 1979), but Hanaoka, et al. (1990) stated that only minor alterations of the

final predicted values resulted from the changes. All necessary values for equation (2.5)

are known from experimental data allowing the calculation of the heterogeneity factor for

different initial conditions.

The heterogeneity factor for the experiments performed by Alamgir and Lienhard

(1981) ranged form 0.055 to 2×10^{-7} from experimental data available in the literature and

from their experiments using a 5.08 cm (2 inch) tube. In all cases, water was used as the

working fluid. Maeno et al. (1987) ran flashing experiments using R-113 and found

heterogeneity factors ranged from 10^{-4} to 10^{-2}. Their data showed that the initial liquid

temperature (initial vessel pressure) affected the heterogeneity factor. The experiments

with lower initial liquid temperatures had smaller heterogeneity factors. Hanaoka et al.

(1990) studied liquid flashing under rapid depressurization using both R-113 and R-11 as

experimental fluids. Their two Pyrex flashing vessels were both 50 mm inside diameter.

The lengths were 400 mm and 600 mm. They ran experiments with varying orifice sizes

(3-20 mm) and also some with an inserted 8 mm diameter polished test rod to determine

its influence on flash boiling (i.e., the heterogeneity factor). They found heterogeneous

factors that ranged from 10^{-4} to 5×10^{-3}. It was observed that vapor first formed at the

liquid surface and then on the test piece and walls, leading finally to the entire bulk liquid undergoing vapor formation. Furthermore, it was found that more explosive flashing occurred when the test rod was in the liquid. Hanaoka, et al.(1990) were the only researchers to qualitatively compare differences between heterogeneity factors for a flashing liquid with and without an introduced nucleation test piece. However, no data were provided on the individual heterogeneity factor. Their paper appears to contradict itself regarding the importance of the added test rod. They first state that the immersion test rod had no distinct effect on the pressure undershoot. Then later in the paper, they state that all added nucleation factors tend to decrease the heterogeneity factor. The current research investigates this question directly by running flash boiling tests with and without added nucleation sites.

Similar to the test rod mentioned above, enhanced boiling techniques are common place in the heat transfer field. Many comprehensive review articles or complete texts on enhanced heat transfer exist (Thome, 1990; Reay, 1991; Bergles, 1988; and Webb, 1981). Enhancement techniques have been classified according to two categories: 1) passive -- which require no direct application of external power and 2) active -- which need external power. A combination of more than one enhancement technique is called compound enhancements. For example, passive techniques include treated surfaces, rough surfaces, extended surfaces, displaced enhancement devices, swirl flow devices, surface tension devices, liquid additives, coiled tubes, and surface catalysis. Active techniques include mechanical aids, surface vibration, fluid vibration, electrostatic fields, other electrical

methods, injection, suction, rotation, and induced flow instabilities. This research investigates two passive techniques (added steel balls and oil additive) and one active technique (electric resistance immersion heater).

Literature closely related to this part of the current research includes Chuah and Carey (1987) who compared the difference in boiling characteristics between small glass spheres with low density and poor thermal conductivity and small copper spheres having high density and high thermal conductivity. A small layer of spheres was placed at the bottom of a boiling pool of water. Experiments were run measuring heat transfer coefficients for varying heat fluxes of 20 kW/m^2 and 100 kW/m^2. Their experiments showed that wall superheat increased for the glass spheres and it decreased for the copper spheres. Increased nucleation and fluid motion was encouraged by the added layer for either type of bead. The copper sphere experiments were found to have heat transfer coefficients twice as high as those for ordinary pool boiling at the same heat flux, while the glass beads showed less of an improvement. An important conclusion was that the boiling curve was found to be insensitive to the particle size or thickness of the layer. Similarly, Webb (1983) experimented with a nearly spherical coating of particles and concluded that particle diameter has very little effect on heat transfer enhancement, but the preferred particle thickness was three to four layers. It should be remembered that the above discussed articles were for isobaric or small pressure drop conditions (as in an evaporator) and the current research differs because the initial flashing processes are close to isothermal with large pressure drops.

The current research also investigates the importance of an active enhanced boiling technique by adding electric resistance heat to the R-22 while flashing. Kunk and Lester (1982) and Sakurai et al. (1978), among others, have looked at maximum heat flux and the transition from nucleate to film boiling around small diameter heated wires during depressurization. However, no literature was found presenting data on how heat addition influenced the mass flux during flash boiling.

CONCLUSIONS

The need to understand the mechanisms controlling flash boiling phenomenon first became apparent because of safety concerns with loss-of-coolant-accidents. The available literature primarily focuses on this and the related design of pressure relief valves. Additional knowledge of the flashing phenomenon could have immediate applications in the air-conditioning industry.

The literature provided insight into the factors (initial pressure, exiting orifice, and liquid amount) that control the mass flow as a high pressure fluid is flashed from a vessel. In general, higher initial pressures cause more vapor production and larger depressurization rates. Greater initial fluid amounts result in more mass leaving the vessel. The exiting orifice also influences the mass flow rate. A larger orifice allows more vapor to be generated during the initial stages of flashing. Exiting conditions are further restricted if there are choked flow conditions at the orifice. While analytical models have been developed and data presented for water and other fluids, their validity when R-22 is

used has not been previously studied. The literature does not provide information regarding enhanced flash boiling. It contains thorough coverage of enhanced boiling that concentrates on increasing the heat flux; however, research regarding increased mass flux during flash boiling was not found.

The following topics should be investigated to better characterize the flashing process of R-22 from a small vessel: 1) mass flow rates with varied initial pressures, orifice sizes, vessel sizes, and refrigerant amounts; 2) analytical model; and 3) mass flow rates using passive and active enhanced boiling techniques.

CHAPTER III

DEVELOPMENT OF ANALYTICAL MODEL

A model for predicting the flashing vessel's rate of depressurization (dP/dt) was derived from basic thermodynamic principles as shown below. The model required an additional expression for exiting mass flux. Classical single-phase choked flow and the two-phase homogeneous equilibrium models were chosen to describe the mass flux and are also described. A list of primary simplifying assumptions used in the derivations were:

1. adiabatic vessel -- no heat transfer to and from the thick vessel during the short test (60 seconds),
2. absence of shaft work -- no work into and out of vessel,
3. negligible kinetic energy effects -- fluid within control volume initially at rest and fluid exiting control volume having calculated maximum velocities to be about 14 m/sec or 0.1 kJ/kg of kinetic energy.
4. negligible potential energy effects -- stationary control volume.
5. constant volume -- rigid vessel,
6. saturated conditions -- fluid within the vessel was experimentally found to be saturated during the initial few seconds of the tests before becoming superheated.
7. equal phase velocities through orifice -- entrained liquid droplets travel at the same velocity of the vapor.

DERIVATION OF DEPRESSURIZATION MODEL

A model for depressurization was published by Grolmes and Fauske (1984) and tested against experimental data with good agreement for Freon-12 (or R-12) by Guhler, et al., (1979). The model developed here follows closely that developed by Grolmes and Fauske. As illustrated in Figure 3.1, the vessel was treated as an adiabatic one-dimensional lumped entity with the control volume containing the vessel and ending just prior to the orifice opening.
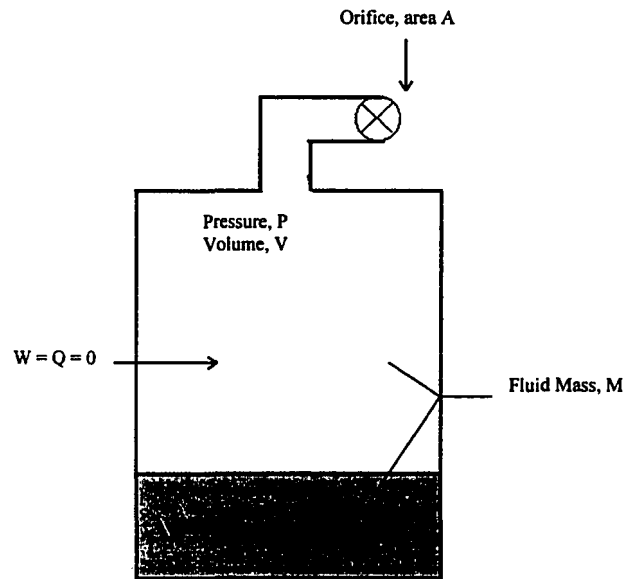
Figure 3.1. Sketch of vessel.

First, the conservation of mass principle, equation (3.1), states that the change in mass in the control volume is equal to the mass into the control volume minus the mass leaving the control volume.

$$
\begin{bmatrix} \text{change of mass} \\ \text{contained within} \\ \text{the control volume.} \end{bmatrix} = \begin{bmatrix} \text{amount of mass} \\ \text{entering the control} \\ \text{volume} \end{bmatrix} - \begin{bmatrix} \text{amount of mass} \\ \text{exiting the control} \\ \text{volume} \end{bmatrix} \qquad (3.1)
$$

or in instantaneous time rate form,

$$
\frac{dM}{dt} = \sum_{in} \dot{m} - \sum_{out} \dot{m} \qquad (3.2)
$$

Because there was no mass flow into the control volume, $\dot{m}_{in}$ was equal to zero. The mass leaving the control volume was expressed in terms of the mass flux and area or

$$\dot{m}_{out} = GA \qquad (3.3)$$

Therefore, for a top-vented vessel with a single exit port, the conservation of mass principle led to equation (3.4) where M is the mass of refrigerant remaining in the vessel, G is the mass flux, and A is the area of the exit port.

$$\frac{dM}{dt} = -GA \qquad (3.4)$$

Next, conservation of energy, equation (3.4), states that the change in energy in the control volume is equal to the energy entering the control volume minus the energy leaving the control volume.

$$\begin{bmatrix} \text{change in the amount} \\ \text{of energy within the} \\ \text{control volume} \end{bmatrix} = \begin{bmatrix} \text{amount of energy} \\ \text{entering the control} \\ \text{volume} \end{bmatrix} - \begin{bmatrix} \text{amount of energy} \\ \text{exiting the control} \\ \text{volume} \end{bmatrix} \qquad (3.5)$$

or in instantaneous time rate form,

$$\frac{dE}{dt} = \dot{Q} - \dot{W} + \sum_{in} \dot{m} \left(u + Pv + \frac{1}{2}V^2 + gz \right) - \sum_{out} \dot{m} \left(u + Pv + \frac{1}{2}V^2 + gz \right) \qquad (3.6)$$

where E is the total energy of the system, $\dot{Q}$ is the time rate of heat transfer, $\dot{W}$ time rate of change of work energy, $\dot{m}$ is the mass flow rate of the fluid, u is the specific internal

energy of the fluid, P is the pressure of the fluid, v is the specific volume of the fluid, g is the acceleration due to gravity, and z is the elevation. With the assumptions that no external work or heat energy were added to the vessel and since $\dot{m}_{in} = 0$, (3.6) was reduced to the following.

$$\frac{dE}{dt} = -\sum_{out} \dot{m}\left(u + Pv + \frac{1}{2}V^2 + gz\right) \qquad (3.7)$$

The assumption of an adiabatic process was confirmed experimentally, although not unequivocally, by insulating the exterior of Vessel I during a flashing test. Results found that the amount flashed (0.134 kg) equaled the lowest amount flashed (out of three experiments) for the tests without insulation at the same initial conditions. Because of the short length of the experiments (60 seconds) and the thickness of the vessel there was insufficient time for heat energy to be transfer from the surroundings.

The expression reduced further by assuming that the potential and kinetic energy terms were negligible. Maximum velocities at the entrance of the orifice were calculated to be about 14 m/sec or 0.1 kJ/kg of kinetic energy transferred from the vessel. Furthermore, the control volume was stationary making the potential energy term negligible. The symbols u and e_o represented the specific internal energy of the vessel and specific total energy of the fluid leaving the control volume and entering the orifice (noted by the subscript, o), respectively.

$$\frac{dE}{dt} = -\dot{m}_{out}\left(u + Pv\right)_o = -\dot{m}_{out}e_o \qquad (3.8)$$

The total energy of the control volume, E, was defined as the sum of the kinetic, potential and internal energies. As discussed above, both the kinetic and potential energies were assumed to be zero resulting in E = U where U is the total internal energy within the control volume. In terms of specific internal energy E = Mu where M is the total mass of the refrigerant within the control volume. This includes the assumption that the internal energy of the vessel wall was negligible because of the short duration of each test. This was used along with (3.3) to obtain equation (3.9).

$$\frac{d(Mu)}{dt} = -GAe_o \tag{3.9}$$

The left hand side of equation (3.9) can be expanded with the chain rule.

$$\frac{d(Mu)}{dt} = M\frac{du}{dt} + u\frac{dM}{dt} \tag{3.10}$$

Next, with the assumption that the refrigerant in the vessel was saturated at a given quality, x, the internal energy term can be expanded to (3.11) where u_f is the specific internal energy for the liquid phase and u_{fg} is the difference between the liquid and vapor phase specific internal energies.

$$u = u_f + xu_{fg} \tag{3.11}$$

Saturated conditions were found to be the case (see Figure 5.26) for five of the first six seconds for a test at the following test conditions: Vessel I, 575 kPa, 0.23 kg, and 5.56 mm diameter orifice. Temperature measurements for other tests that utilized either a

smaller orifice or a larger initial amount of refrigerant showed that the quality of the exit

fluid was saturated for up to 20 seconds of the 60 second test before becoming a

superheated vapor. Incorporating (3.11) into (3.10) yielded:

$$\frac{d(Mu)}{dt} = M\frac{d(u_f + xu_{fg})}{dt} + u\frac{dM}{dt} \qquad (3.12)$$

Using the chain rule again and rearranging, this was expanded to (3.13).

$$\frac{d(Mu)}{dt} = Mu_{fg}\frac{dx}{dt} + u\frac{dM}{dt} + M\left(\frac{du_f}{dt} + x\frac{du_{fg}}{dt}\right) \qquad (3.13)$$

Multiplying the third term on the right hand side of (3.13) by $\frac{dT}{dT}$ (where T is the fluid

temperature) and pulling out a $\frac{dT}{dt}$ term resulted in (3.14).

$$\frac{d(Mu)}{dt} = Mu_{fg}\frac{dx}{dt} + u\frac{dM}{dt} + M\frac{dT}{dt}\left(\frac{du_f}{dT} + x\frac{du_{fg}}{dT}\right) \qquad (3.14)$$

With the right hand side bracketed term defined as C^* and recalling (3.9) yielded (3.15)

below.

$$\frac{d(Mu)}{dt} = Mu_{fg}\frac{dx}{dt} + u\frac{dM}{dt} + MC^*\frac{dT}{dt} = -GAe_o \qquad (3.15)$$

Rearranging (3.15) reduced to the equation below.

$$C^{\bullet} \frac{dT}{dt} + u_{fg} \frac{dx}{dt} = -\frac{GA}{M}(e_o - u)$$

(3.16)

Now, an expression for dx/dt is required. For a constant volume vessel, (3.17) was expanded to (3.18) with the use of the chain rule.

$$\frac{d(Mv)}{dt} = 0$$

(3.17)

$$M \frac{dv}{dt} + v \frac{dM}{dt} = 0$$

(3.18)

Introducing the quality term for specific volume, v, and expanding it with the chain rule yielded (3.20).

$$v = xv_g + (1-x)v_f$$

(3.19)

$$\frac{dv}{dt} = v_g \frac{dx}{dt} + x \frac{dv_g}{dt} + \frac{dv_f}{dt} - x \frac{dv_f}{dt} - v_f \frac{dx}{dt}$$

(3.20)

Rearranging and using $v_{fg} = (v_g - v_f)$ gave (3.21).

$$\frac{dv}{dt} = v_{fg} \frac{dx}{dt} + (1-x) \frac{dv_f}{dt} + x \frac{dv_g}{dt}$$

(3.21)

By multiplying the second and third term of (3.21) by $\dfrac{dT}{dT}$ and introducing the term ϕ

which is defined below, (3.21) became

$$\frac{dv}{dt} = v_{fg}\frac{dx}{dt} + \phi\frac{dT}{dt}.$$

(3.22)

where

$$\phi = x\frac{dv_g}{dT} + (1-x)\frac{dv_f}{dT}$$

(3.23)

Next, by using (3.22) and (3.4), (3.18) was expanded and rearranged into the expression
below for $\dfrac{dx}{dt}$.

$$\frac{dx}{dt} = \frac{v}{v_{fg}}\frac{GA}{M} - \frac{\phi}{v_{fg}}\frac{dT}{dt}$$

(3.24)

Now, (3.16) and (3.24) was combined to make (3.25).

$$\frac{dT}{dt}\left(C^{*} - \frac{u_{fg}\phi}{v_{fg}}\right) = -\frac{GA}{M}\left(e_o - u + \frac{u_{fg}v}{v_{fg}}\right)$$

(3.25)

By multiplying the left hand side of (3.25) by dP/dP and introducing the Clapeyron

equation, $\dfrac{dT}{dP} = T\dfrac{v_{fg}}{h_{fg}}$,an expression including dP/dt was obtained. The Clapeyron

equation allows the change in enthalpy during vaporization at a constant temperature to

be evaluated using tabulated property data (Moran and Shapiro, 1988).

$$\frac{dP}{dt}\frac{Tv_{fg}}{h_{fg}}\left(C^{\bullet} - \frac{u_{fg}\phi}{v_{fg}}\right) = -\frac{GA}{M}\left(e_{o} - u + \frac{u_{fg}v}{v_{fg}}\right) \qquad (3.26)$$

The final expression for the rate of depressurization was derived by rearranging (3.26).

$$\frac{dP}{dt} = \frac{-\dfrac{GA}{M}\left[(u+Pv)_{o} - u + u_{fg}\dfrac{v}{v_{fg}}\right]}{T\dfrac{v_{fg}}{h_{fg}}\left[C^{\bullet} - \phi\dfrac{u_{fg}}{v_{fg}}\right]} \qquad (3.27)$$

The model allowed for the evaluation of all four initially set variables (initial pressure, initial refrigerant amount, orifice size, and vessel volume) as was done for the baseline flashing experiments. A relationship for mass flux, G, was required for calculation of equation (3.27). Three critical flow models (single-phase critical flow model, the two-phase homogeneous equilibrium model, and the two-phase homogeneous frozen model) were examined for developing expressions for the mass flux and are discussed below.

DEVELOPMENT OF CRITICAL FLOW MODELS

Three classical single-component critical flow models were examined for use in the depressurization model. Two-phase flow models called the homogeneous equilibrium model (HEM) and homogeneous frozen model (HFM) as well as the expression for single-phase critical flow expression were used to predict the mass flux value needed in the depressurization model. The theoretical development of each flow model is briefly described below.

Homogeneous single-phase critical (or choked) flow through an ideal orifice is
characterized by assuming a constant velocity across the exit plane (Moody, 1965).
Critical flow is the maximum flow possible at a given upstream pressure and is
independent from the downstream pressure (Kim, 1993). For isentropic flow where
enthalpy and specific volume are functions of pressure only, the critical mass flux is given
by:

$$G_{1\phi}^2 = -\frac{dP}{dv} \qquad (3.28)$$

The general form of the two-phase critical flow equation is given in equation
(3.29). It was derived from the momentum equation by neglecting viscous dissipation
and assuming one-dimensional steady flow (Kim, 1993; Hsu and Graham, 1976). The
slip ratio, k, is defined as ratio of the vapor to liquid phase velocities.

$$G_{cr}^2 = \frac{-1}{\dfrac{\partial}{\partial P}\left\{\dfrac{[k(1-x)v_f + xv_g][xk+(1-x)]}{k}\right\}} \qquad (3.29)$$

The HEM uses the assumption that the vapor and liquid velocities are considered
the same and in equilibrium with each other. In other words, the slip ratio is unity
resulting in $\dfrac{\partial k}{\partial P} = 0$. From this, (3.29) is reduced to (3.30) below.

$$G_{cr,HEM}^2 = -\frac{\partial P}{\partial v} \qquad (3.30)$$

The right hand side of (3.30) can be expanded by introducing two thermodynamic relations for two-phase mixtures.

$$v = v_f + x v_{fg}$$
(3.31)

and

$$h = h_f + x h_{fg}$$
(3.32)

This leads to an expression for $\dfrac{\partial x}{\partial P}$ and the following expression for HEM (3.33) by assuming an isenthalpic path (Lahey, 1977).

$$G_{cr,HEM}^2 = \dfrac{-1}{\dfrac{dv_f}{dP} - \left(\dfrac{v_{fg}}{h_{fg}}\right)\dfrac{dh_f}{dP} + x\left[\dfrac{dv_{fg}}{dP} - \left(\dfrac{v_{fg}}{h_{fg}}\right)\dfrac{dh_{fg}}{dP}\right]}$$
(3.33)

The homogeneous frozen model (HFM) also assumes the flow is homogeneous and that the velocities of both phases are equal ($k=1$ and $\dfrac{\partial k}{\partial P} = 0$). Furthermore, HFM assumes that there is insufficient time for mass transfer between the liquid and vapor phase (Henry and Fauske, 1971). In other words, the quality remains constant throughout expansion or $\dfrac{\partial x}{\partial P} = 0$. These assumptions can be used to obtain an expression for the HFM (Wallis, 1969).

$$G_{cr,HFM}^2 = \dfrac{-1}{x\dfrac{\partial v_g}{\partial P} + (1-x)\dfrac{\partial v_f}{\partial P}}$$
(3.34)

RESULTS OF DEPRESSURIZATION MODEL CALCULATIONS

This section discusses the computations within the depressurization model and gives a qualitative discussion of the effect that changing test variables (orifice diameter, initial pressure, initial refrigerant amount, and vessel volume) had on model predictions.

Calculation of dP/dt from (3.27) required a relation for the mass flux. Three critical flow models were chosen for evaluation in the model. A computer program was written to calculate the depressurization rate and other related values including pressure and mass flux. Figure 3.2 provides the basic flow chart (or outline) of the computer program (Engineering Equation Solver, 1992) which contained internal algorithms for thermodynamic properties of R-22. Initial values of vessel volume, pressure, refrigerant mass, orifice diameter, and two-phase model quality were provided before running the program. The program solved the multiple equations iteratively before taking the next step forward in time. The value of dP/dt was used to calculate the next pressure (at the next time interval) which was used to begin the next calculation of dP/dt and other values like mass flux, instantaneous mass of refrigerant within the vessel, internal energies, specific volumes, etc. The program ended after the internal vessel pressure was well below the downstream reservoir pressure (120 kPa) or after completing timesteps equivalent to 60 seconds. Typical timesteps ranged between 0.1 and 1.0 seconds.

```
┌─────────────────────────────┐
│Set initial values:          │
│Pres, refrig. mass, orifice diam.,│
│vessel volume, outlet pressure,│
│HFM quality, & timestep.     │
└─────────────────────────────┘
            │
         ( START )
            │
┌─────────────────────────────┐
│Calculate lumped parameter   │
│properties based on initial setting.│
└─────────────────────────────┘
            │
┌─────────────────────────────┐
│Iteratively solve all equations:│
│dP/dt, G, Pres, specific volumes,│
│internal energies, vessel quality,│
│enthalpies, etc..            │
└─────────────────────────────┘
            │
┌─────────────────────────────┐
│Determine new value of internal│
│vessel pressure based on new dP/dt│
│and the timestep.            │
└─────────────────────────────┘
            │
```

YES

Is total time less than desired length and vessel pressure > 120 kPa?

NO

(END)

Figure 3.2. Flow chart of depressurization model predictions.

Effects of Varied Test Parameters on Model Predictions

Initially all three critical flow models were used in the depressurization model. Henry and Fauske (1971) stated that the HFM tends to yield good predictions of the critical mass flux, while the HEM tends to underpredict the flow rate. Furthermore, the HFM was developed for flows through short pipes or nozzles where it is assumed the fluid travels through the nozzle without time for a change in quality (i.e., no mass transfer between liquid and vapor phases). Therefore, the HEM was not used in the discussion of effects of test variables. The model using the HEM predicted lower mass flux values as compared to the HEM (shown in Figures 3.3). For comparisons purposes, a quality of 0.6 (for the refrigerant entering the orifice) was used in the two-phase model predictions, while the single phase model assumed a quality of 1.0. Of the three flow models, shown in Figure 3.3, the HFM predicted the highest initial mass flux and the single phase model (SPM) had the lowest initial value for critical mass flux. The two-phase models predicted within 0.2% of each other at 2 seconds.

Figure 3.4 and 3.5 show the pressure and mass flux profiles for varied orifice diameters (1.59 mm and 3.18 mm) from the depressurization model using both the HFM and SPM. Other initial test conditions were set at 0.68 kg R-22, 710 kPa, and Vessel I. The pressure drop was more rapid for the tests using the larger area orifice which agrees with the findings of Guhler et al. (1979) and Hanaoka (1990) who found the internal vessel pressure fell more quickly for larger orifice areas. The model predictions with the smaller orifice (1.59 mm diameter) maintained a higher exiting mass flux (Figure 3.5). The depressurization rate, dP/dt, had lower values for the small orifice (1.59 mm) condition since the orifice area is in the numerator of the prediction equation (6.27). In both cases, the HFM predicted a higher mass flux as compared with the SPM at the same
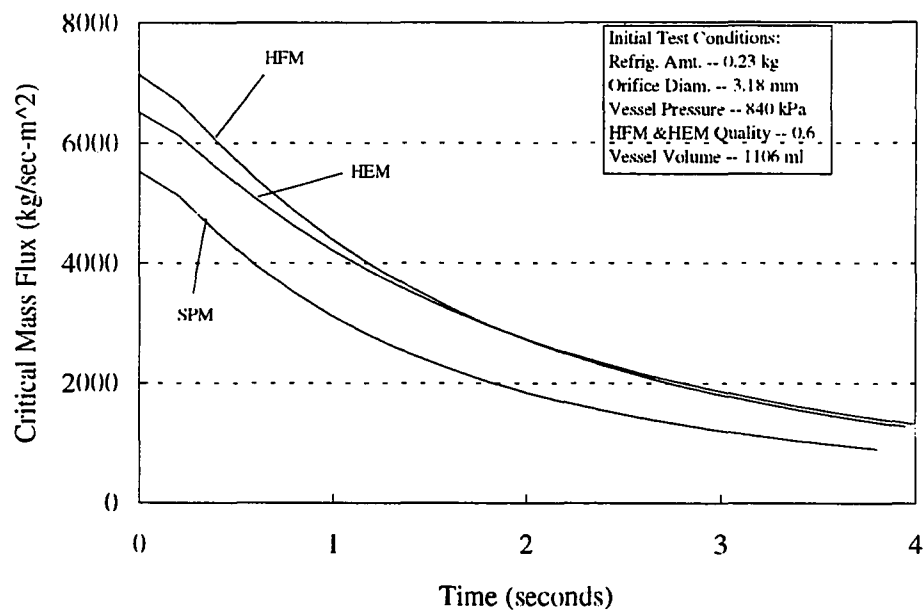
Figure 3.3. Predicted mass flux vs. time for each critical flow model.
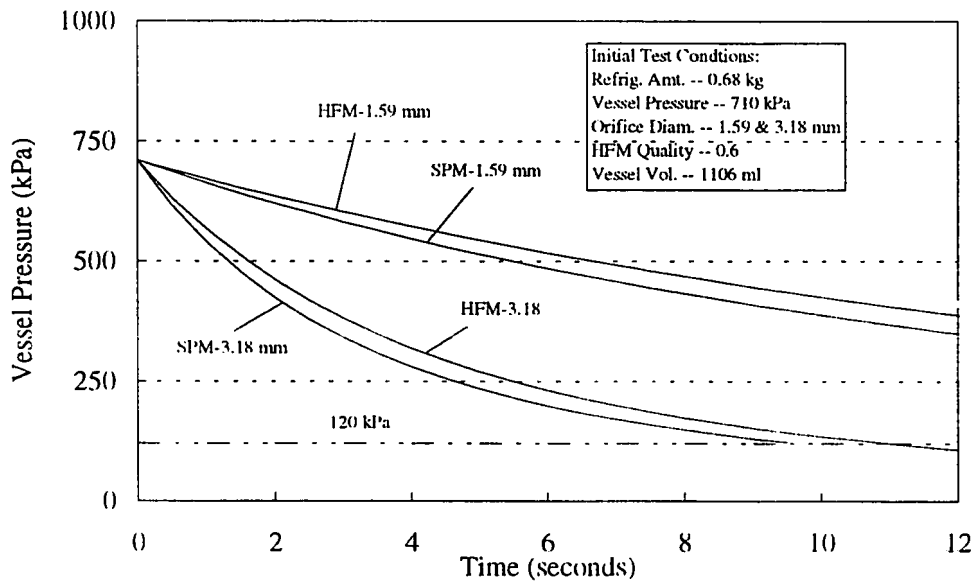
Figure 3.4. Predicted pressure vs. time for varied orifice sizes.
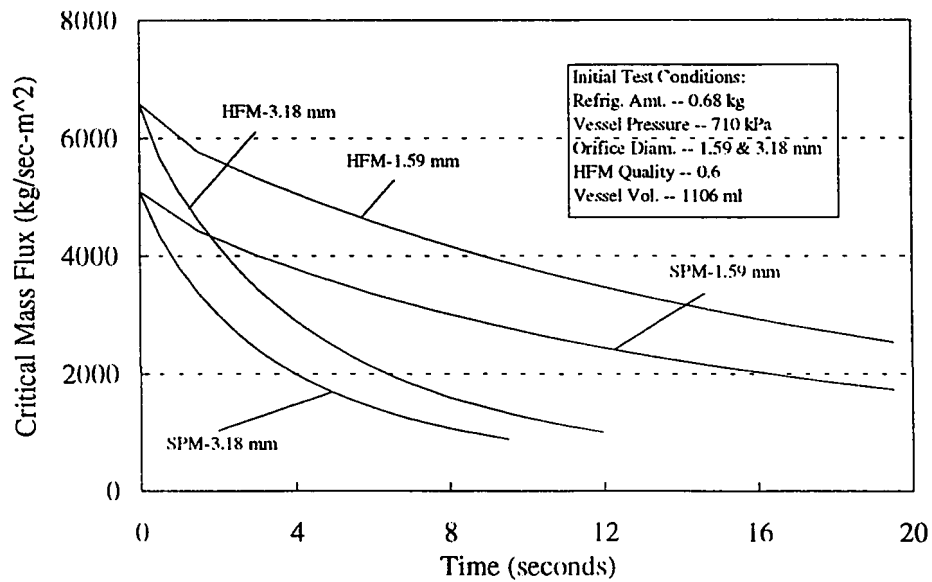
Figure 3.5. Predicted critical mass flux vs. time for varied orifice diameters.

condition, which would be expected since the HFM prediction had a higher quality (0.6 vs. 1.0).

The initial internal vessel pressure also had an impact on the mass flow. Figure 3.6 gives predicted mass flux tests for two pressure settings (575 kPa and 840 kPa) and other initial settings of 0.23 kg of refrigerant, 3.18 mm diameter orifice, and Vessel I. Mass flux for the HFM was less for the lower initial pressure (575 kPa) as compared to the higher initial pressure (840 kPa). Similarly the single-phase model predicted lower mass flux values, but with the same general trends as the HFM. The pressure profiles, shown in Figure 3.7, dropped quickly and approached the same value within 4 to 5 seconds.

The initial refrigerant amount had a significant influence on the predicted pressure profiles. Figure 3.8 shows a comparison between tests with two initial refrigerant amounts (0.23 kg and 0.68 kg) and other initial settings remaining the same (3.18 mm diameter orifice, 840 kPa initial pressure, and Vessel I). Pressure showed a more rapid decrease for the lesser initial refrigerant amount as did the predicted mass flux (Figure 3.9). With a quality of 0.6, predicted mass fluxes were higher for the HFM as compared to the single-phase model predictions.

Finally, the vessel volume had a smaller impact on the mass flux and pressure profiles as compared to the other test variables (orifice diameter, initial refrigerant amount, and initial pressure). Model predictions for both vessels were run with the initial refrigerant amount of 0.23 kg, initial pressure setting of 840 kPa, and the orifice diameter of 3.18 mm. Predicted pressures (Figure 3.10) and mass flux (Figure 3.11) had less of a difference for the single-phase model with predictions staying within 5% of each other at all times for the given test conditions. Vessel II predictions were generally lower than those of Vessel I for both mass flux models. Predictions for varied vessel
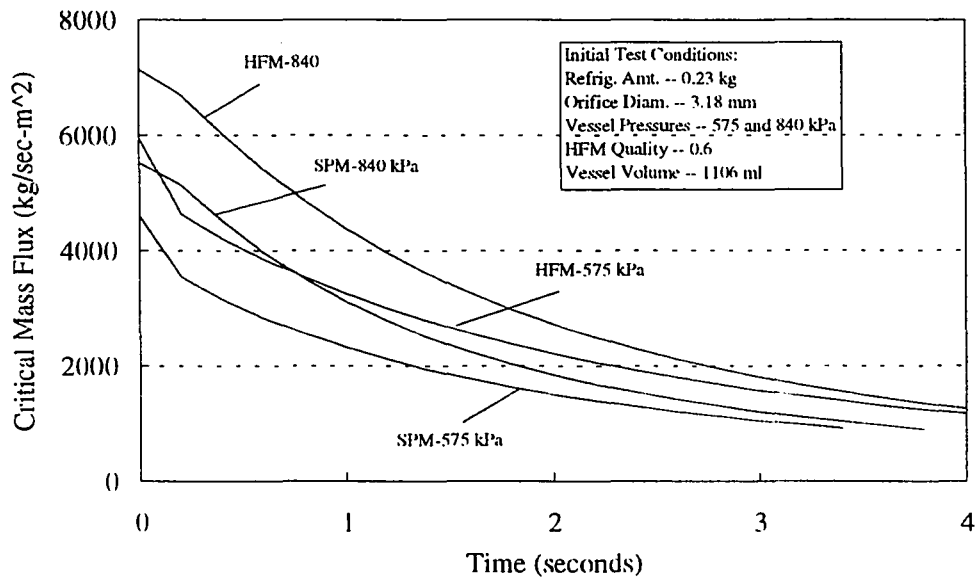
Figure 3.6. Predicted critical mass flux vs. time for varied initial pressures.
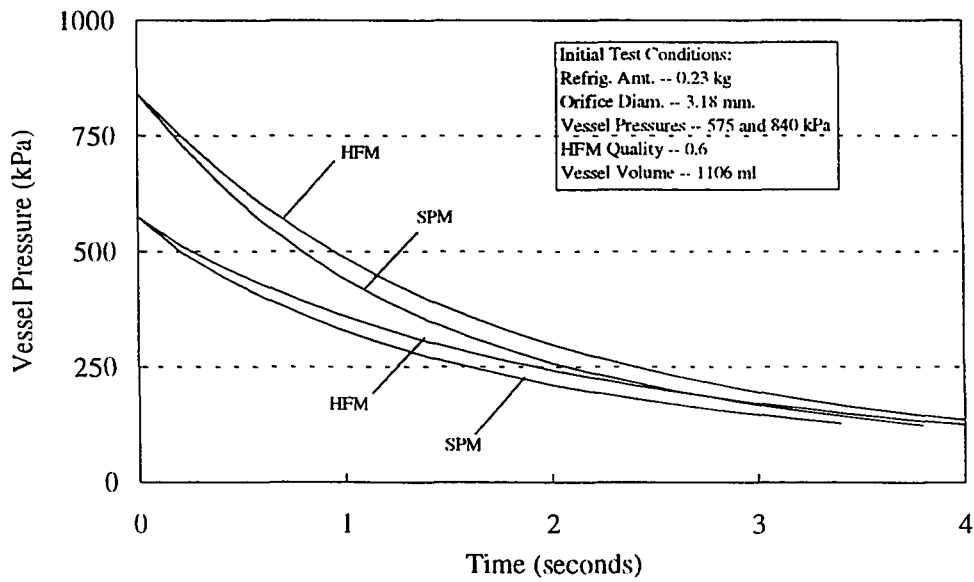
Figure 3.7. Predicted pressure vs. time for varied initial pressures.
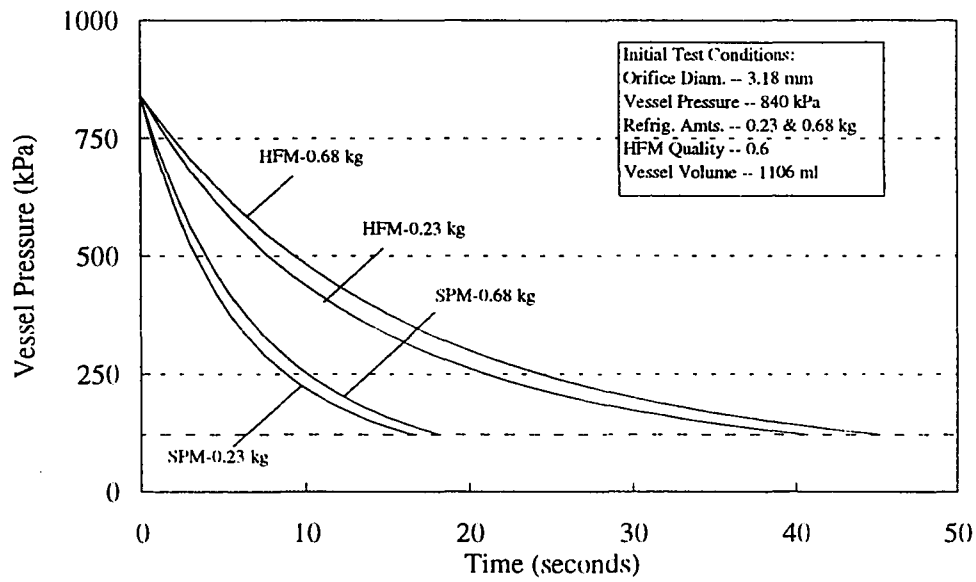
Figure 3.8. Predicted pressure for varied initial refrigerant amounts.
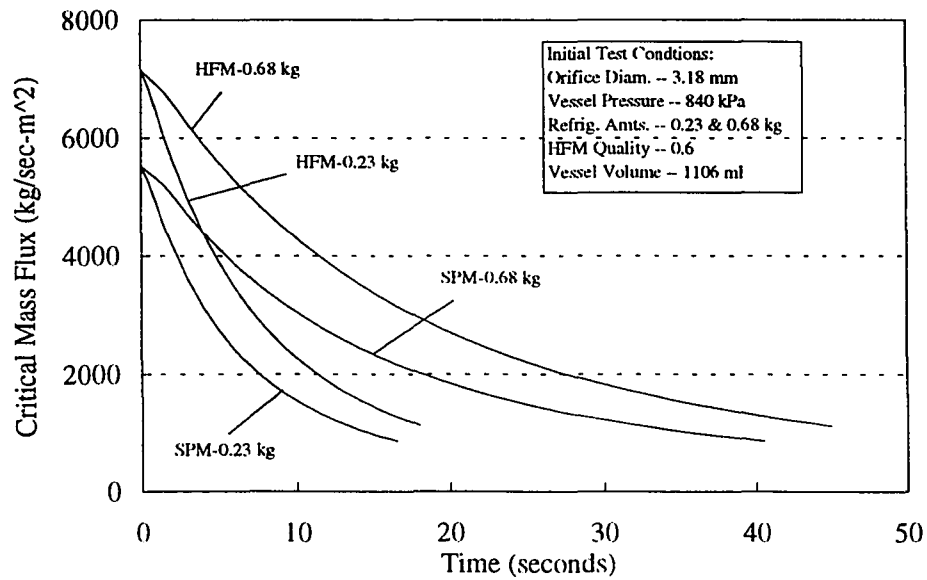
Figure 3.9. Predicted critical mass flux for varied initial refrigerant amount.
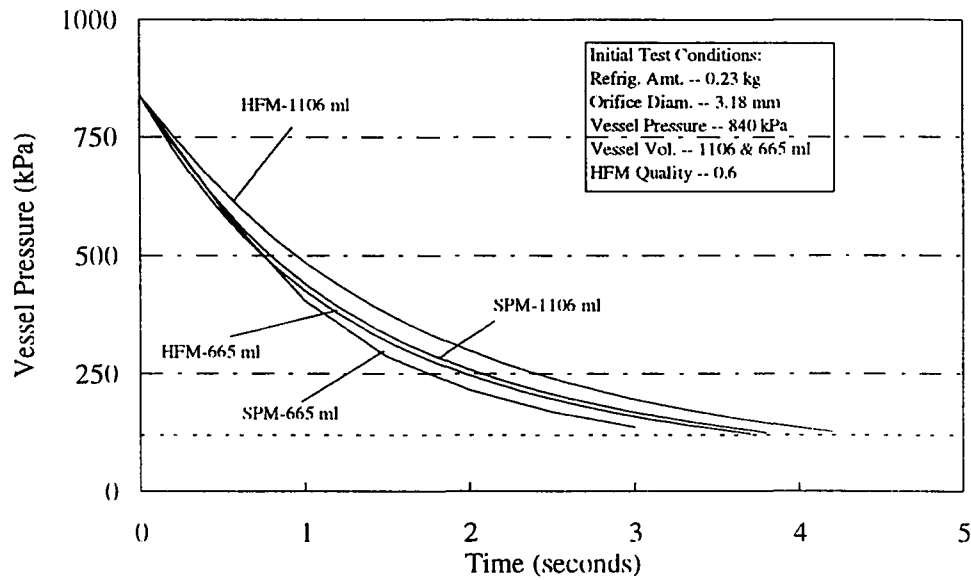
Figure 3.10. Predicted pressure vs. time for varied vessel volumes.
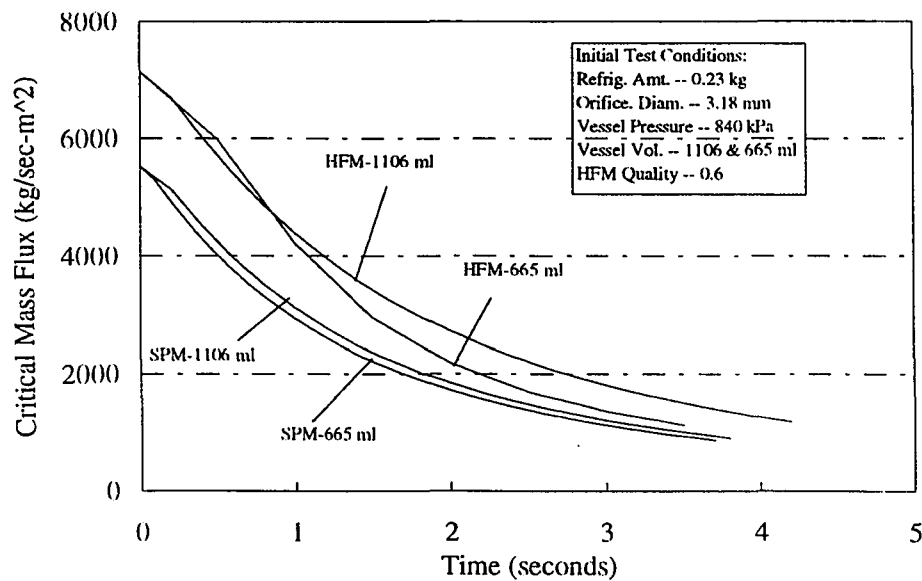
Figure 3.11. Predicted critical mass flux for varied vessel volumes.

45

volume showed more of an effect on the pressure and mass flux difference when the HFM was used in the depressurization model.

SUMMARY OF ANALYTICAL MODEL DEVELOPMENT

A model for predicting the vessel's internal rate of depressurization (dP/dt) was derived from basic thermodynamic principles for comparison against the experimental results. The primary assumptions used in the derivation were that the vessel was adiabatic, that there was no shaft work into or out of the vessel, that kinetic and potential energy effects were negligible, that the vessel was constant volume, the fluid withing the vessel was saturated, and that the liquid and vapor phase velocities through orifice were equal. The model requires an additional relation for the exiting mass flux. Three critical flow models (single-phase choked flow, homogeneous equilibrium model, and homogeneous frozen model) were used. Theoretical development of the depressurization model and the critical flow models were shown. A computer program was written to calculate the depressurization rate and other values like pressure, mass flux, internal energies, etc.

Results from the depressurization model calculations were discussed with regard to the effects of varied test parameters (orifice diameter, initial vessel pressure, initial refrigerant amount, and total vessel volume). Results reflected the same general trends discussed in the literature. Varied orifice area influenced the mass flux and pressure. A smaller orifice diameter resulted in a pressure drop and higher mass flux profiles. The HFM consistently predicted a higher mass flux as compared with the SPM at the same condition, which would be expected since the HFM prediction had a higher quality (0.6 vs. 1.0). The initial internal pressure also had an impact on the mass flow. Higher initial pressures resulted in greater mass flux values. After several seconds, pressures for both

vessel volumes began to approach the same values. The initial refrigerant amount had a significant influence on the pressure and mass flux profiles. Higher initial refrigerant amounts had slower pressure drops and higher mass flux values. Finally, varied vessel volume showed that the smaller volume maintained slightly higher pressures and mass flux values while the single-phase flow model predictions stayed within 5% of each other.

CHAPTER IV

EXPERIMENTAL SETUP AND PROCEDURE

Schematics of the experimental apparatus and the flashing vessel constructed for the flashing experiments are shown in Figures 4.1 and 4.2, respectively. The apparatus had interchangeable Pyrex heavy-walled glass vessels, allowing for visualization studies. The apparatus was equipped with a flashing vessel, refrigerant receiver, heat exchanger, refrigerant pump, vapor reservoir, transducers, controlling equipment, and a data acquisition system.

Refrigerant-22 was stored in a liquid refrigerant tank, which was an ASME rated liquid receiver with a working pressure up to 2760 kPa. The receiver held a maximum of 17.3 kg of R-22 with outside dimensions of 16.7 cm diameter by 108 cm in length. The liquid receiver was mounted vertically and had a 1.6 cm diameter and 43.2 cm tall site glass; a 0-1825 kPa Model 207 Setra pressure transducer; a 30-gauge type-T thermocouple; a 1.6 cm diameter by 12.7 cm long, 750-watt Watlow cartridge (immersion) heater; and two, 1.6 cm service valves with hose connections. The pressure transducer was powered by a 24 Volt DC power supply. The transducer output was 0-5.0 Volts DC. An Omega DWT 1305D deadweight tester was used to calibrate each pressure transducer used in the experiments. A linear relationship (DC output voltage vs. pressure) was determined based on 172 kPa increments. The thermocouple

Figure 4.1. Drawing of flashing apparatus.
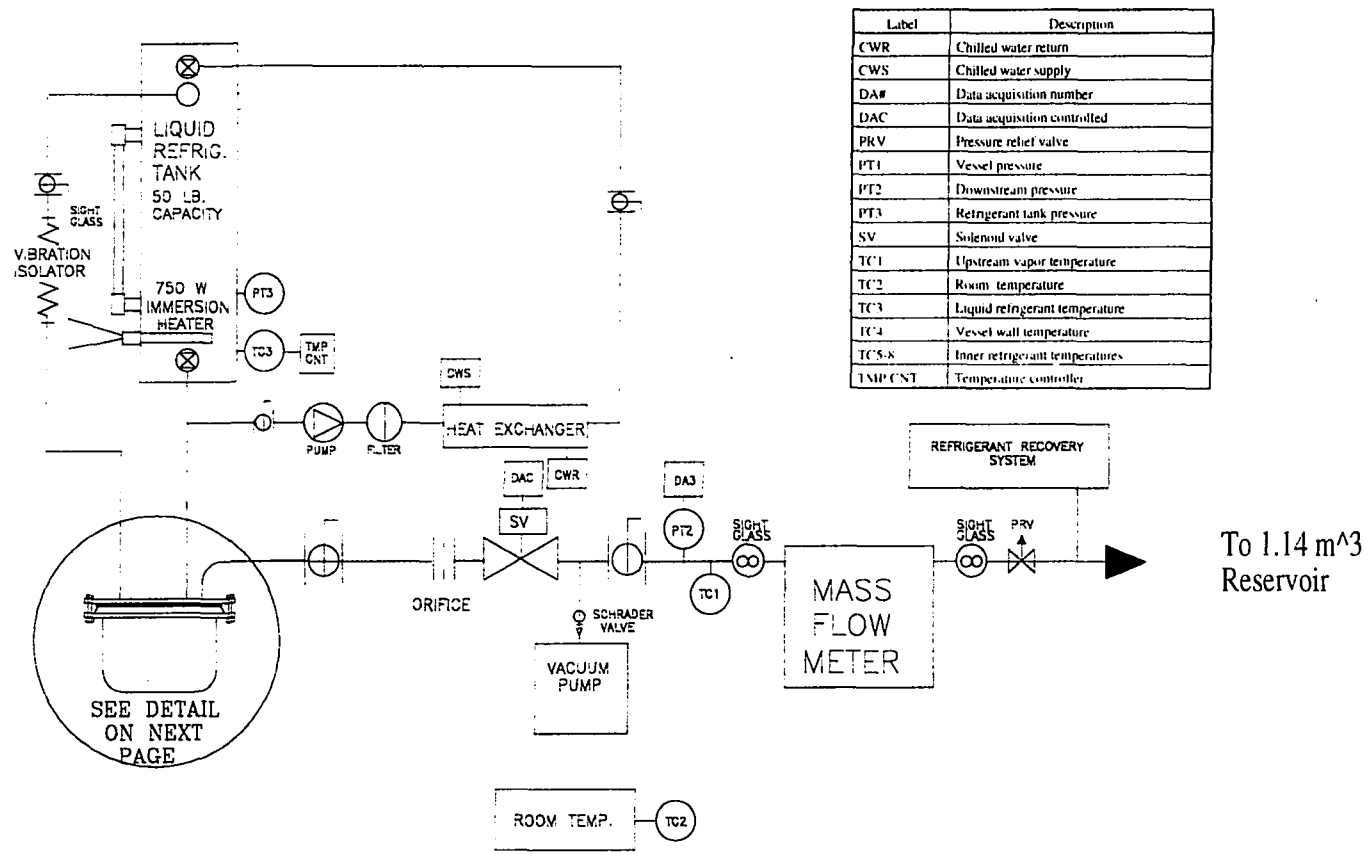
Label	Description
CWR	Chilled water return
CWS	Chilled water supply
DA#	Data acquisition number
DAC	Data acquisition controlled
PRV	Pressure relief valve
PT1	Vessel pressure
PT2	Downstream pressure
PT3	Refrigerant tank pressure
SV	Solenoid valve
TC1	Upstream vapor temperature
TC2	Room temperature
TC3	Liquid refrigerant temperature
TC4	Vessel wall temperature
TC5-8	Inner refrigerant temperatures
TMP CNT	Temperature controller

Figure 4.2. Detail of flashing vessel.

was wired to the temperature controller which activated a relay connected to the 230-volt, 750-watt immersion heater.

The temperature controller maintained a constant temperature (and pressure) within the closed-loop refrigerant system. A 5700 ml/min 0.15 kW Micromotion model 000-605 pump circulated the refrigerant from the liquid receiver, through the heat exchanger, and back to the top of the liquid receiver. The pump had Ryton gears and Teflon seals. The coolant side of the heat exchanger was supplied with a glycol-water solution from a 8.8 kW chiller. The heat exchanger had a maximum cooling capacity of 7 kW. The refrigerant was circulated through a liquid-line filter and then through the refrigerant-side of the heat exchanger. This heat exchanger was designed to over cool the refrigerant and have the temperature controller maintain the setpoint temperature by activating the immersion heater's relay and adding electric resistant heat to refrigerant.

New R-22, over 99.9 % pure[1], was added to the closed-loop system through the top service valve. Canisters containing 22.7 kg of R-22 were at room temperature and a higher pressure than the refrigerant tank. During the refilling, the refrigerant was continually circulated through the heat exchanger so it would migrate into the receiver. The site glass was used to visually check the refrigerant level in the liquid receiver.

Prior to a test, refrigerant was added to the glass vessel. Two 9.5 mm copper lines were connected to the flashing vessel from the liquid receiver. Several 9.5 mm quarter-turn ball valves were in-line between the liquid receiver and the flashing vessel.

---

[1]Based on conversations with Don Bivens of the Dupont Company.

Also in-line were two liquid-line filters, and a pressure relief valve. The pressure relief

valve was set at 997 kPa. This prevented the possibility of the glass bursting from

overpressurization. Heavy-walled glass tubing with conical-formed ends was used to

make each flashing vessel. The conical ends fit an aluminum flange and seal assembly

(Ace Glass, Inc., model 8864).

The dimensions of the Pyrex flashing vessels are given in Table 4.1. The vessels

are pictured in Figures 4.3 and 4.4. A 3.2 mm gasket was placed between the glass

vessel and the 12.7 mm aluminum top. The gasket was included in the height of each

vessel. Each aluminum top was tapped with five threaded holes for connecting a

pressure transducer, thermocouple rod (or immersion heater), the two copper lines from

the receiver, and the 0.7 mm inside diameter copper line leaving the vessel. Type-L

ACR copper tubing ranging from 7.9 mm to 14.3 mm inside diameter was used to

connect all the different pieces of equipment. Silver alloy solder and brass Swagelok

fittings were used to make some of the copper-to-copper connections.

Table 4.1 Flashing vessel dimensions

Vessel Number	Inside Diameter cm	Total Height cm	Vessel Volume ml
I	10.2	13.65	1106
II	7.6	14.6	665
III	7.6	22.5	1027
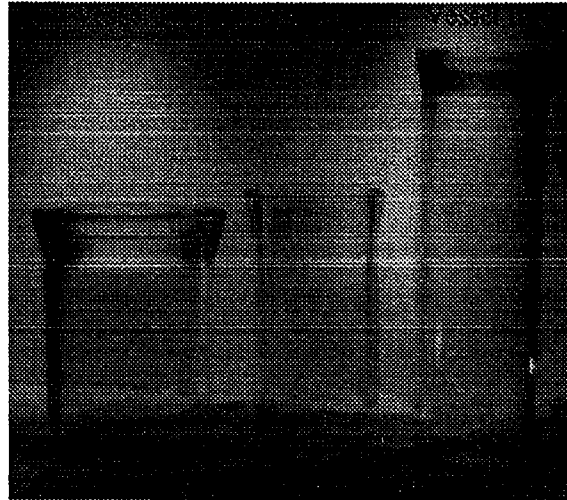
Figure 4.3. Picture of the three different vessels used during flashing experiments.

Pressure
Transducer

Solenoid Valve
not shown.
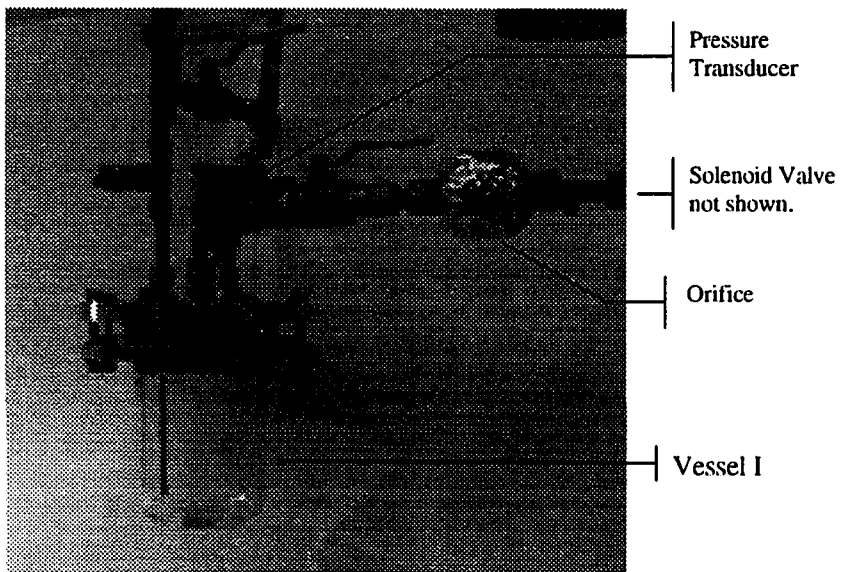
Orifice

Vessel I

Figure 4.4. Picture of Vessel I, pressure transducer and insulated orifice.

The pressure transducer mounted on top of the glass vessel was a 0-1725 Setra Model 204 pressure transducer. This pressure transducer had a 2 millisecond response time and an accuracy of ±0.1 % of full scale. A similar pressure transducer measured the outlet pressure and was located downstream 122 cm from the glass flashing vessel. Both pressure transducers were purchased new and included a calibration certificate. The calibration points were verified with a dead weight tester and were within an estimated 0.5 % of full scale. A thermocouple rod containing four 44-gauge type-T thermocouples also entered the flashing vessel through the aluminum top. When used, the thermocouple rod measured the temperature profile during flashing. The small thermocouples (0.13 mm thermocouple bead diameter) were chosen because of their fast response time, calculated at 12 ms. Each thermocouple was independently calibrated using a single-point ice bath. Type-T thermocouples have rated limits of error of ±0.6 ° C. A few tests had thermocouples that were attached to the bottom exterior of the glass vessel, interior glass wall, and on the surface of the immersion heater. The immersion heater used in the experiments was a flat spiral cable electric heater rated at 215-watts and powered by 120 Volts AC.

The refrigerant left the vessel through a 9.5 mm inside diameter copper line and traveled through a 1.6 cm quarter-turn valve, a fixed diameter orifice, a solenoid valve, another 1.6 cm quarter-turn valve, two site glasses, a mass flow meter, and into a 1.14 cubic meter reservoir maintained at 120 kPa. The refrigerant also passed by the outlet pressure transducer mentioned above, a schrader valve connection, and another 30-

gauge type-T thermocouple. A self-contained Sercon model 9000 refrigerant reclaim system was used to withdraw the refrigerant from the large reservoir. The quarter-turn valves were used to isolate the solenoid valve and the orifice. The solenoid valve occasionally needed servicing and the orifices were replaced on a regular basis. The orifices were fixed diameter aluminum orifices with the following inside diameters: 1.59±0.013 mm, 3.18±0.013 mm, and 5.56±0.013 mm, and were 7.6±0.5 mm in length.

The fast acting solenoid valve was a Burkett model 280-A-1/2 brass valve. It was connected to the data acquisition system via a 5 Volts DC relay and powered by 120 Volts AC. The Strawberry Tree data acquisition system was programmed to activate the solenoid valve using an external trigger (computer mouse). The mass flow meter was a coriolis-type Micro Motion model DS040S119. The mass flow meter was calibrated using water. The flow meter's output signal (4-20 milliamp) was averaged over two minutes and the total mass of the water was measured. Several readings were taken for each flow condition. The linear relationship (milliamp vs. mass flow rate) for mass flow rate was then computed. The flow meter had a manufacturer's rated accuracy of ±0.4% of flow rate and a response time of 0.1 seconds.

The control panel and data acquisition system utilized several relays and toggle switches to control the electrical components of the flashing apparatus. A toggle switch for manual on/off capabilities was installed for the temperature controller, the refrigerant pump, the solenoid valve, and both the 750-watt receiver heater and the flat spiral cable immersion heater. Each toggle switch had two positions, either power on or power off.

The data acquisition system used in all the experiments was Strawberry Tree version 2.03. It had one terminal panel (type T21) with eight analog channels and 12 digital input/output channels. The terminal panel was connected to an IBM compatible 386-40 MHz personal computer via an analog card (SN5020) installed inside the computer. The computer had 4 megabytes of random access memory (RAM) and two hard drives, one 80 megabytes and one 170 megabytes. The data acquisition system was programmed to power relays and begin logging data to the hard disk by triggering one icon with the computer's mouse.

A detailed uncertainty analysis for both measured mass flow and predicted mass flow was performed and the overall systematic uncertainties were ±8.1% and ±9.3%, respectively. Pressure transducers, orifice diameter, mass flow meter, and data acquisition system bias and precision limits were included. See Appendix A for detailed calculations.

EXPERIMENTAL PROCEDURE

A preliminary schedule of flashing experiments was developed prior to the first test. Five factors with three levels were created. The factors were initial vessel pressure, orifice size, refrigerant mass, vessel geometry, and boiling enhancement technique.

The three pressures were 575 kPa, 710 kPa, 840 kPa with corresponding saturation temperatures at 4.5 °C, 11.4 °C, and 17.8 °C, respectively. The three orifice sizes were 1.59 mm, 3.18 mm, and 5.56 mm with each having an overall length of 7.6

sizes were 1.59 mm, 3.18 mm, and 5.56 mm with each having an overall length of 7.6

mm. The three refrigerant mass amounts were 0.23 kg, 0.45 kg, and 0.68 kg. Finally.

basecase boiling tests along with enhancement techniques were run for many of the

possible combinations of experiments. The boiling enhancement techniques included a

passive technique using a 10 mm high layer of 3.6 mm diameter steel balls to promote

nucleation, an active boiling technique using immersion heaters with a power rating of

215-watts, and small amounts of oil were also added to the refrigerant to determine its

influence on the flashing process. A listing of the experimental matrix is given in Table

4.2.

Table 4.2 Listing of experiment matrix.

Test	Refrigerant pressure kPa	Orifice diameter mm	Vessel Geometry	Refrigerant amount kg
Baseline test	575 710 840	1.59 3.18 5.56	I II III	0.23 0.45 0.68
Steel Balls	575 840	1.59 5.56	I II	0.23 0.45, 0.68
Immersion heaters	575 840	1.59 5.56	I II	0.23 0.45, 0.68
Oil mixture	575 840	1.59 5.56	I II	0.45 0.68

(pressure, orifice size, refrigerant mass, and vessel geometry). Analysis of variance

(ANOVA) statistical tests were performed to determine the significance of each factor in

regards to the mass flow rate. This information was used to reduce the number of total

experiments and eliminate unnecessary factors and levels. A more detailed discussion of

the statistical analysis is presented in Chapter V.

Each experiment records the instantaneous mass flow rate, pressures, and

temperatures as shown in Figure 3.1. A sample rate of 100 milliseconds was used for

most of the tests. Data were recorded by the data acquisition system for a 60 second

period. The following is a list of initial actions taken prior to any experiments:

1.   Open the closed valves within the glycol loop.
2.   Turn on the chiller and bring glycol down to setpoint temperature.
3.   Clean and install proper glass flashing vessel and orifice.
4.   Evacuate glass vessel and orifice sections.
5.   Open closed valves within the refrigerant circulation loop.
6.   Turn on computer and activate data acquisition system.
7.   Turn on control panel toggle switches powering temperature controller, power supply, pressure transducers, solenoid valve, refrigerant pump, and relays.
8.   Set temperature controller to proper setpoint.
9.   Wait until refrigerant within the liquid receiver is down to the appropriate temperature and pressure.
10.   Check 1.14 cubic meter (300 gallon) reservoir for proper 120 kPa (17.4 psia) downstream pressure.
11.   Pressurize flashing vessel by slowly opening vent line running from top of liquid receiver to the flashing vessel.
12.   Check data acquisition displayed readings for proper and reasonable values.
13.   Open and close valve to fill flashing vessel to a preset preliminary level.

14. Open solenoid valve though data acquisition system for initial cooling and steadying of flashing vessel.

15. Repeat two previous steps until glass vessel is at required exterior wall temperature.

16. Reclaim refrigerant from 1.14 cubic meter (300 gallon) downstream reservoir until proper 120 kPa (17.4 psia) pressure is reached.

After the initialization steps were taken, the following step-by-step procedures were used

for each experiment:

1. Close orifice section valves and change orifice, if required.

2. Evacuate orifice section.

3. Open orifice section valves.

4. Check for proper downstream pressure and exterior vessel temperature.

5. Pressurize flashing vessel by slowly opening vent line running from top of liquid receiver to the flashing vessel.

6. Open and close valve to fill flashing vessel to a required level.

7. Name data file for specific experiment.

8. Close vent line.

9. Check data acquisition displayed readings for proper and reasonable values.

10. Open solenoid valve, power flat spiral immersion heater (if required), and activate data recording through data acquisition system.

11. Reclaim refrigerant from 1.14 cubic meter (300 gallon) reservoir.

12. Wait until exterior of flashing vessel reaches proper value

13. Repeat process above for next experiment.

CHAPTER V

EXPERIMENTAL BASELINE RESULTS

Baseline flash boiling experiments were run for a wide range of experimental conditions. Three levels of initial orifice diameter, initial refrigerant amount, initial pressure, and vessel geometry were used. Visualization studies and experimental data were used to characterize the different boiling phenomena taking place during the flashing process from a small vessel. Pressure, temperature, and mass flow rate data from all the baseline experiments along with calculated data such as saturation temperature, amount of superheat, mass flux, and total mass flashed were used to determine the influence that each of these variables had on the mass flow during a sixty second test. Results from the baseline experiments were used for comparison with enhanced boiling methods and model predictions. Results of visualization study experiments are also discussed in this chapter.

VISUALIZATION STUDY OF BASELINE EXPERIMENTS

Approximately half of the experiments were video taped, and the tapes were used repeatedly to observe and analyze the flashing phenomena prior to a detailed analysis of the quantitative results. Two extreme test cases were considered for presentation in this section. One test (called the minimum case) used the smallest orifice (1.59 mm) and least amount of initial refrigerant (0.23 kg) at the lowest initial pressure setting (579

kPa). The other test (called the maximum case) used the largest orifice (5.56 mm) and

greatest amount of initial refrigerant (0.68 kg) at the highest initial pressure setting (842

kPa). Both used the four inch inside diameter vessel (Vessel I). Pressure trends and

mass flow rates were also studied for each case. Digital images at time zero, one

second, two seconds, and 20 seconds were presented for the two test cases. Difference

in boiling and bubble formation were also discussed.

Figures 5.1 through 5.4 are pictures of the minimum case at 0, 1, 2, and 20

seconds. Figure 5.5 shows the pressures and mass flow rates throughout the same time

period with their range of uncertainty marked with uncertainty bars. Individual root-sum

squared uncertainties were found to be 7.8% of flow for the mass flow meter and 0.35%

of full scale for the pressure transducer. As can be seen in Figure 5.5, the uncertainty of

both measurements was small. Therefore, uncertainty bars were not placed on each plot

throughout this treatment.

The liquid temperature was initially near saturated conditions (5°C) and the rapid

depressurization caused the liquid to be superheated immediately after the solenoid valve

was opened. One second after the solenoid valve was opened, the vapor that existed

above the liquid before opening the valve began exiting the vessel as the pressure

continued to drop and a cloud of vapor and minuscule droplets rose from the liquid

surface. At two seconds, the newly formed vapor and small droplets filled the vessel. At

this point, no other type of bubble formation was visible. Even though the flow was

choked for the first seven seconds, the mass flow rate was greatest during this time.
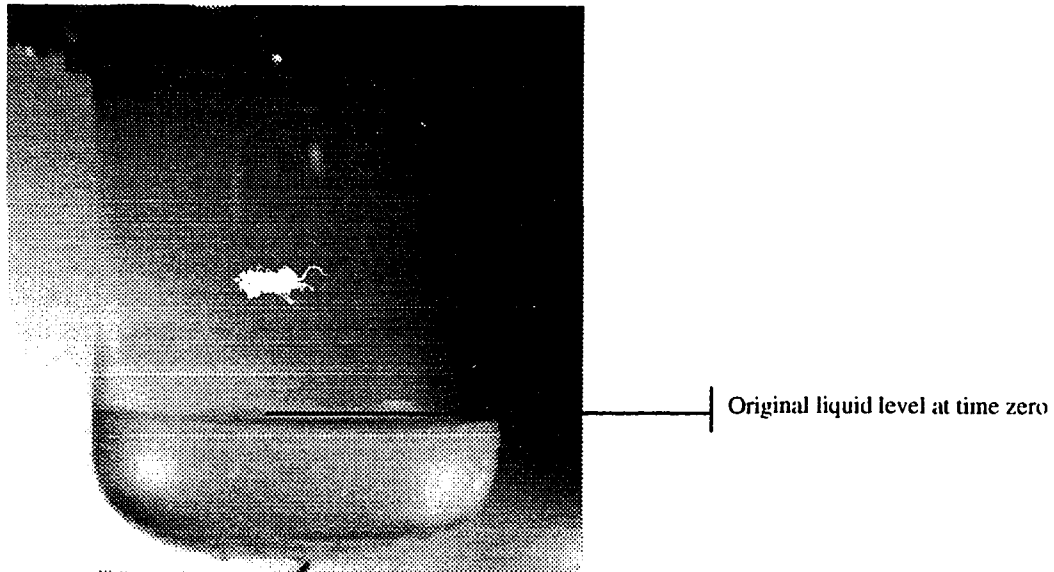
Figure 5.1. Picture of Vessel I prior to activation of solenoid valve. Initial test conditions were: 580 kPa pressure, 1.59 mm orifice diameter, 0.23 kg refrigerant amount.
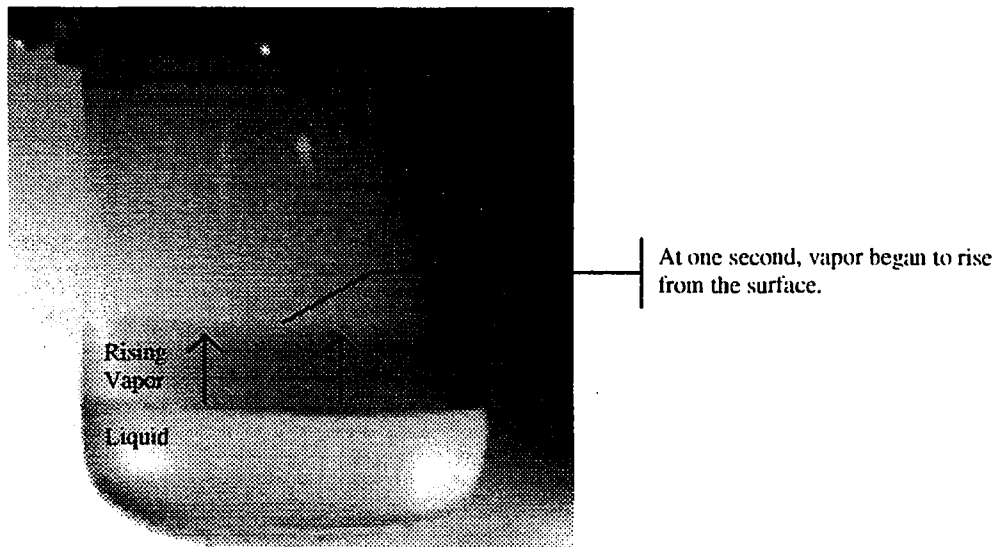
Figure 5.2. Picture of flash boiling in Vessel I one second after activation of solenoid valve. Test conditions at one second were: 479 kPa, 1.59 mm orifice, 0.004 kg of R-22 flashed.

Figure 5.3. Picture of flash boiling in Vessel I two seconds after activation of solenoid valve. Test conditions at two seconds were: 391 kPa, 1.59 mm orifice, 0.007 kg of R-22 flashed.
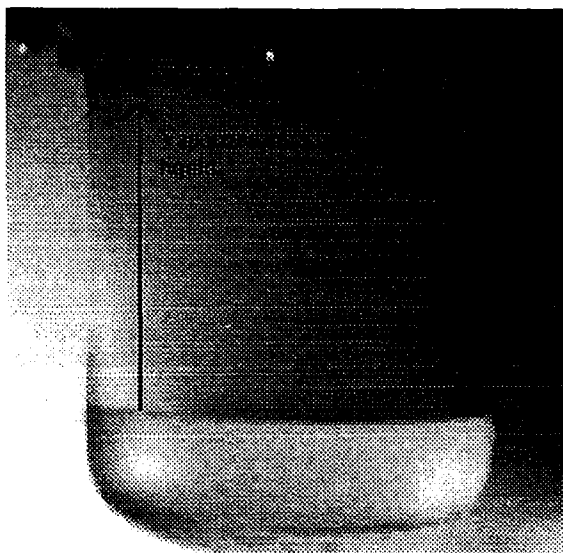
At two seconds, vaporized liquid refrigerant began to exit vessel.

Figure 5.4. Picture of flash boiling in Vessel I twenty seconds after activation of solenoid valve. Test conditions at twenty seconds were: 162 kPa, 1.59 mm orifice, 0.032 kg of R-22 flashed.
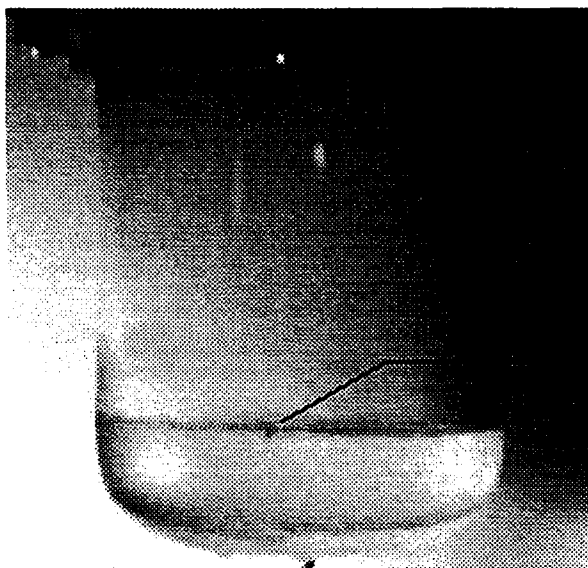
At 20 seconds, only a few specific nucleation sites occur on vessel perimeter.
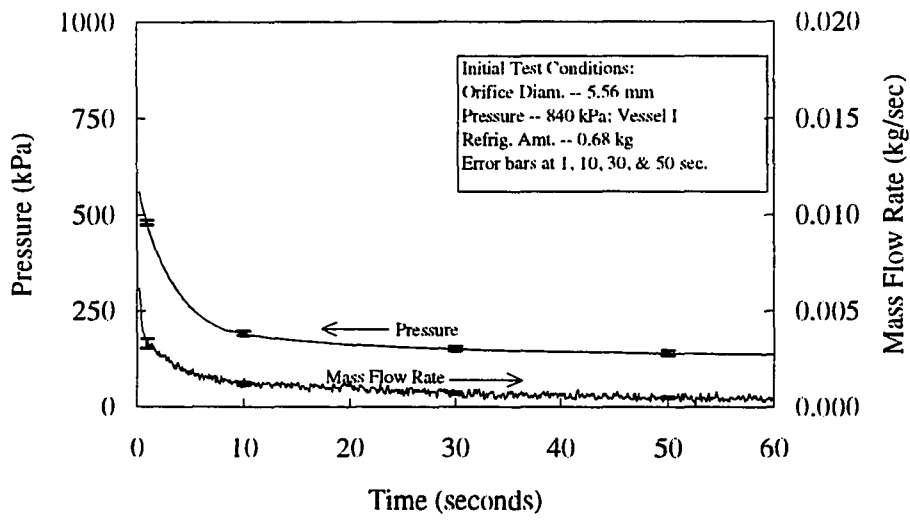
Figure 5.5. Mass flow rate and pressure profiles for minimum case.

Three to four seconds later, the bulk liquid began to cool and the initial vaporization

process was no longer visible as heterogeneous bubble nucleation began at the solid-

liquid-vapor interface. No visible bubble formation occurred below the liquid surface for

this test which using the small orifice. Approximately 10 to 20 different nucleation sites

generated vapor at the wall and that number slowly decreased to three or four (at 20

seconds) as time continued and as the pressure within the vessel dropped to within 15

kPa of the downstream reservoir pressure.

Figures 5.6 through 5.9 show pictures of the maximum test case at 0, 1, 2, and

20 seconds. Figure 5.10 provides the corresponding pressures and mass flow rates

throughout the same time period. The initial pressure drop occurred about six times

more rapidly with the larger orifice and flow was only choked for about 0.2 seconds. A

cloud of vapor and minuscule liquid droplets were formed across the entire liquid surface

and rose toward the top of the vessel during the first second. After the first second,

vigorous vapor formation began at the liquid surface, primarily near the wall (Figure

5.6). The pressure increased within the vessel with more vapor being generated than

could leave. The pressure decreased and reached a minimum at 0.7 seconds (194 kPa).

It then rose, with the vapor generation, to local maximum at 1.2 seconds (240 kPa) and

2.7 seconds (247 kPa) as seen in Figure 5.10. Cooling at the surface due to the heat of

vaporization during the phase change caused circulation downward within the vessel as

shown in Figure 5.7, which also shows how large liquid droplets were accelerated

upward as vapor bubbles burst at the surface. Observations found that few if any of the
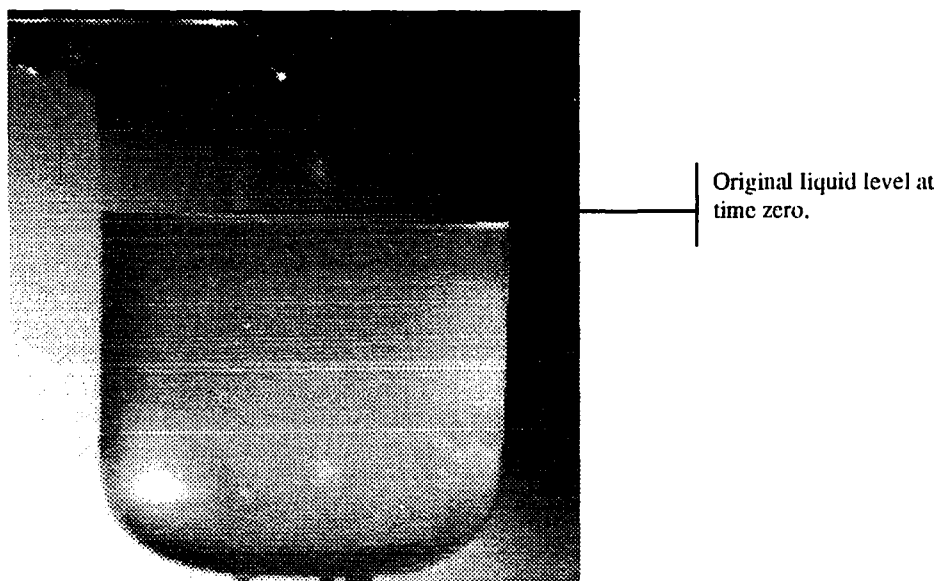
Figure 5.6. Picture of Vessel I just prior to activation of solenoid valve. Initial test conditions were: 843 kPa, 5.56 mm orifice, 0.68 kg R-22.
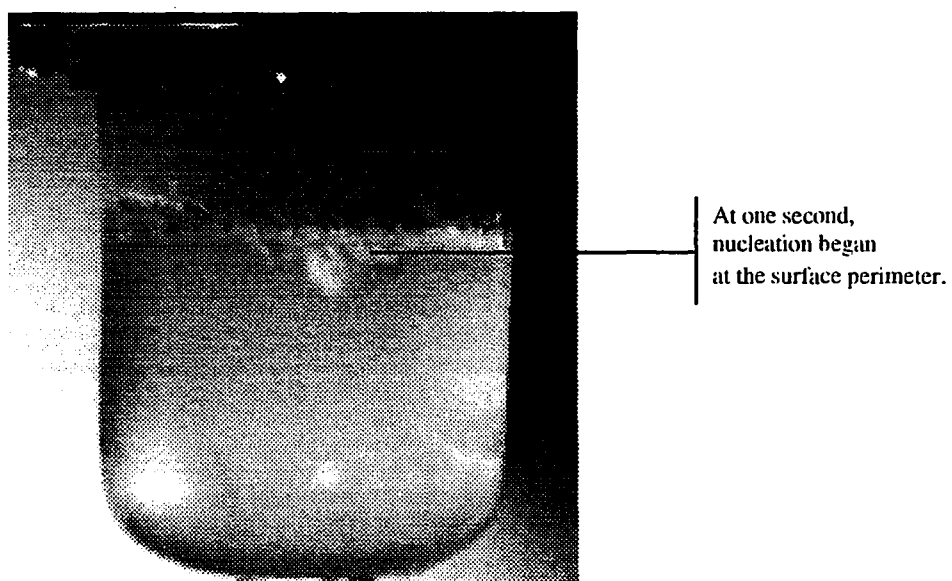
Figure 5.7. Picture of flash boiling in Vessel I one second after activation of solenoid valve. Test conditions at one second were: 239 kPa, 5.56 mm orifice, 0.02 kg of R-22 flashed.

At 2 seconds, liquid droplets were propelled upward as vapor escaped out the top.

Some nucleation occurred on the liquid-wall interface while most occurred at the liquid surface.

Circulation
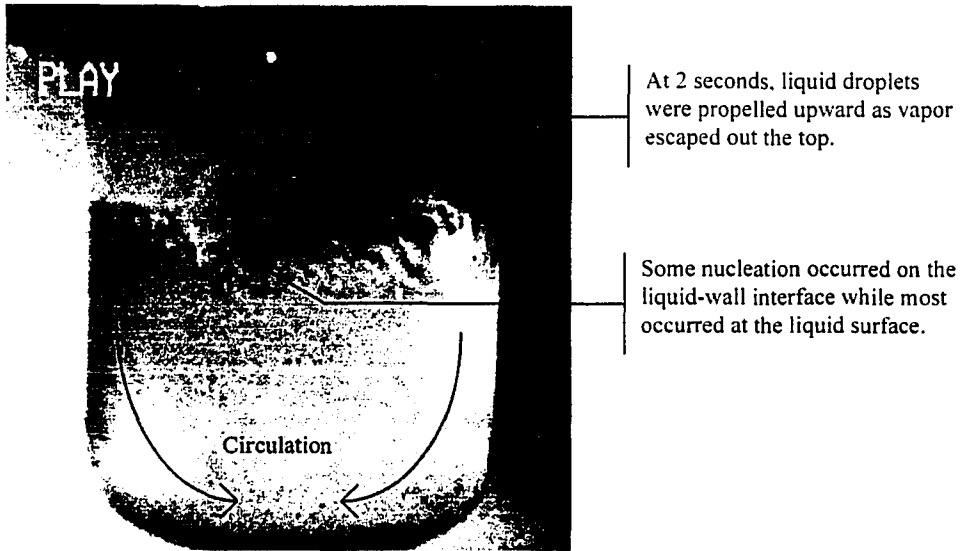
Figure 5.8. Picture of flash boiling in Vessel I two seconds after activation of solenoid valve. Test conditions at two seconds were: 222 kPa, 5.56 mm orifice, 0.03 kg of R-22 flashed.

Approximate original liquid level.

At 20 seconds, some suface and wall nucleation was still ocurring.
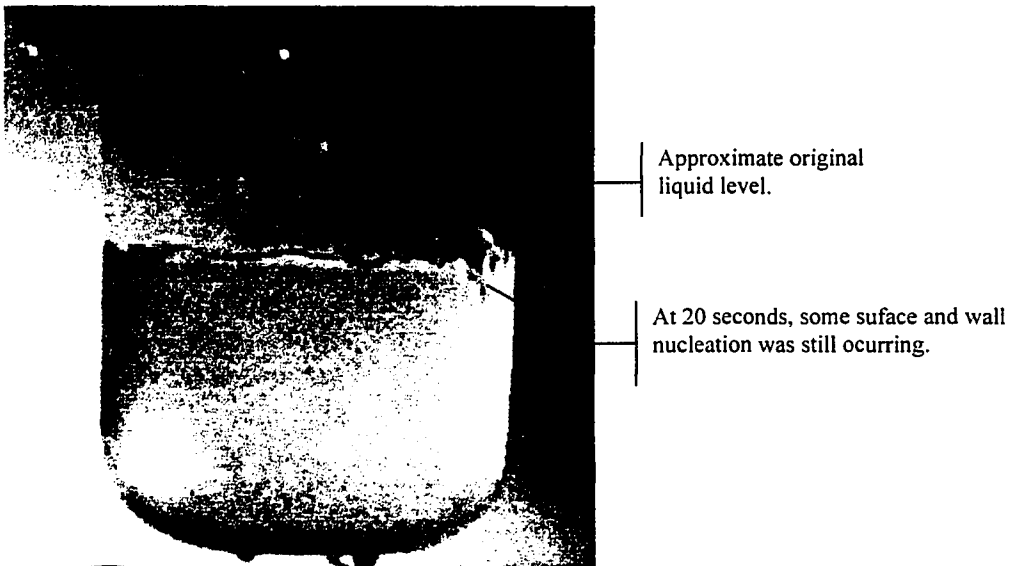
Figure 5.9. Picture of flash boiling in Vessel I twenty seconds after activation of solenoid valve. Test conditions at twenty seconds were: 135 kPa, 5.56 mm orifice, 0.12 kg of R-22 flashed.
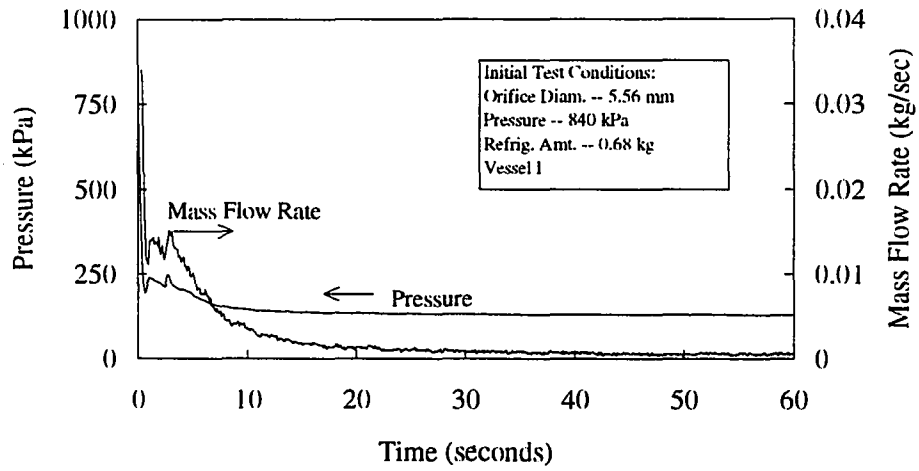
Figure 5.10. Mass flow rate and pressure profiles for maximum case.

droplets, however, had enough momentum to leave the vessel. As compared to the minimum case, a few more bubbles were formed below the liquid surface. The more violent vapor generation had subsided by twenty seconds, but bubbles were still being formed at the surface and at the wall. Finally, as compared to the minimum case, an obvious loss in liquid had occurred after twenty seconds. After sixty seconds, the maximum case flashed 0.15 kg (or 22% of the initial refrigerant amount) of R-22 as compared to the minimum case which flashed 0.057 kg (or 25% of the original amount).

ANALYSIS AND RESULTS OF BASELINE EXPERIMENTAL DATA

Each experiment was run for sixty seconds with pressures, temperatures, and the mass flow rate recorded for each test. Temperature profiles were not available for each test condition, but a representative number were obtained for analysis. The temperature probes became nucleation sites whenever they were placed in the liquid refrigerant. The added nucleation skewed the mass flow results. A comparison between tests with and without the temperature probe placed in the vessel showed the probe caused additional vapor generation that ranged between 15 to 24%. Only experiments that utilized a clean vessel, without any added nucleation sites, were included as valid baseline tests. In addition to the measured data, other calculated properties such as saturation temperature, amount of superheat, mass flux and total mass flashed were included in the analysis. The effects of orifice diameter, initial refrigerant amount, initial pressure, and

vessel geometry were investigated. Comprehensive results from representative tests for each condition considered are presented.

Effects of Orifice Diameter on the Mass Flow

Figure 5.11 shows the pressure profiles for three tests with varying orifice diameters. The tests had the same initial conditions except for the orifice size. Table 5.1 gives the diameter and related area of each orifice used. The experiment with the 1.59 mm diameter orifice had the slowest depressurization rate followed by the 3.18 mm and 5.56 mm orifices. Choked flow conditions, based on the measured vessel pressure, existed for a portion of the tests for each discharge orifice. Flow was choked for 6.6 seconds, 0.9 seconds, and 0.1 seconds for the 1.59 mm, 3.18 mm, and 5.56 mm diameter orifices, respectively.

Table 5.1. Selected orifice area and diameter for flashing experiments.

Orifice Description	Diameter (mm)	Area (m^2)
small	1.59	1.98×10^{-6}
medium	3.18	7.92×10^{-6}
large	5.56	2.43×10^{-5}

Pressures for the tests using the two larger orifices reached a brief minimum before they increased because large amounts of vapor bubbles were bursting at the surface. Based
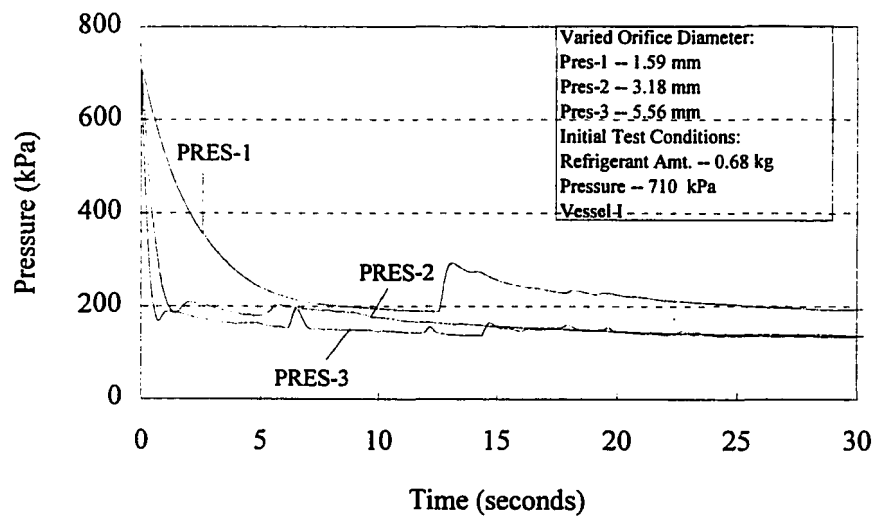
Figure 5.11. Baseline pressure (PRES) profiles for three tests with different orifice sizes.

on the two local minimum pressures, the liquid reached a maximum of 38 °C (3.18 mm

diameter) and 41 °C (5.56 mm) superheated before vaporization at the liquid surface

caused cooling of the bulk liquid. The minimum pressures reached during the tests that

used the two larger orifices appeared to be related to the size of the orifice. The larger

orifice typically reached a lower minimum pressure. It was hypothesized that the larger

orifice allowed the initial cloud of vapor to exit the vessel more quickly and the pressure

to drop to a lower value (and a greater amount of superheat) before vapor bubbles began

bursting at the liquid-vapor interface. Some of the pressure spikes in Figure 5.11 (those

after five seconds) represent individual bursts of a large bubble.

For a selected few tests, a site glass was placed just before to the entrance of the

orifice in an effort to determine the phase characteristics of the fluid entering the orifice.

No liquid was observed to enter the orifice for the combination of tests run, including

tests using the smallest and largest orifices. Previous researchers have observed two-

phase flow through the orifice during flashing from a small vessel. Hanaoka, et al.

(1990) observed that both liquid and vapor (R-11 and R-113) were discharged from the

vessel while the flow was choked. They placed a test rod within their test vessel to

provide nucleation sites for greater vapor formation and encourage the two-phase region

of the fluid to reach the top of the vessel. Guhler, et al. (1979) also had entrained liquid

entering the orifice for the larger of two orifices (4.76 mm vs. 1.59 mm) while flashing

R-12. Their tests with the smaller orifice (1.59 mm) had only vapor entering the orifice.

They also mounted thermocouples from the metallic bottom of the vessel which also added artificial nucleation sites that promoted nucleation.

Figures 5.12 and 5.13 show the mass flow rate and the mass flux for varying orifice sizes. The mass flow rate was initially over three times greater (0.030 vs. 0.009 kg/sec) for the larger orifice. The more rapid depressurization led to more refrigerant being released during the initial stages of flashing as more vigorous boiling took place (Figure 5.12). Similar to the maximum case in the visualization study (Figure 5.8), abundant amounts of vapor were generated at the perimeter of the liquid surface. For the test which used the larger orifice, the spikes in the mass flow rate corresponded to large bubbles nucleating below the liquid surface (primarily off the wall) rising to the surface and bursting. More energy was released during the first few seconds of flashing for the test that used the 5.56 mm diameter orifice. The higher mass flow rates meant more energy was released from the liquid due to the heat of vaporization. During the first 20 seconds of the tests, the mass flow rate for the 1.59 mm diameter orifice was consistently lower, averaging 0.002 kg/sec. Small vapor bubbles formed only at the wall. Since the flow was choked for nearly seven seconds, vaporization was essentially suppressed as the mass flow rate was limited to that of single-phase choked flow during the time the vessel had the highest internal pressure and the liquid had the greatest potential for boiling.

While the largest orifice had the highest flow rate, it had the smallest mass flux (Figure 5.13). Because the smaller orifice was at maximum (or choked) flow conditions
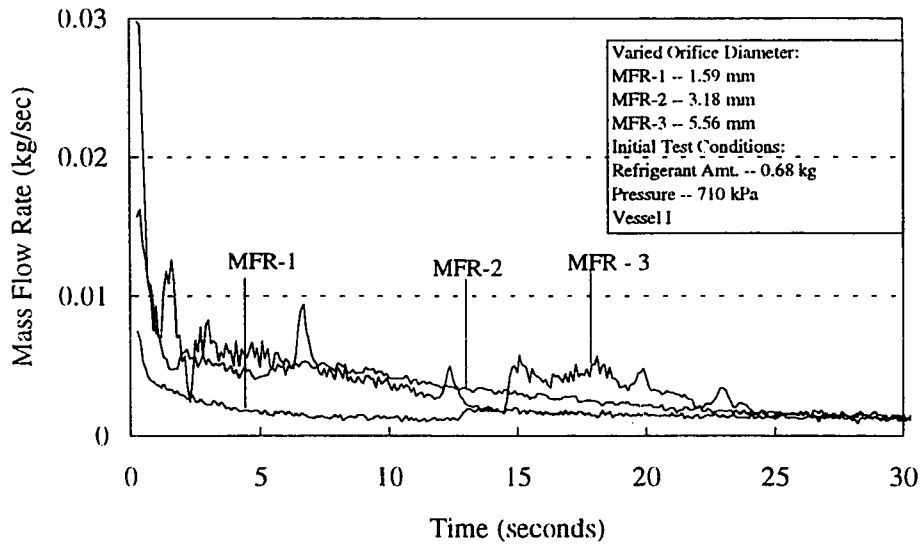
Figure 5.12. Baseline mass flow rate (MFR) profiles for three tests with different orifice sizes.
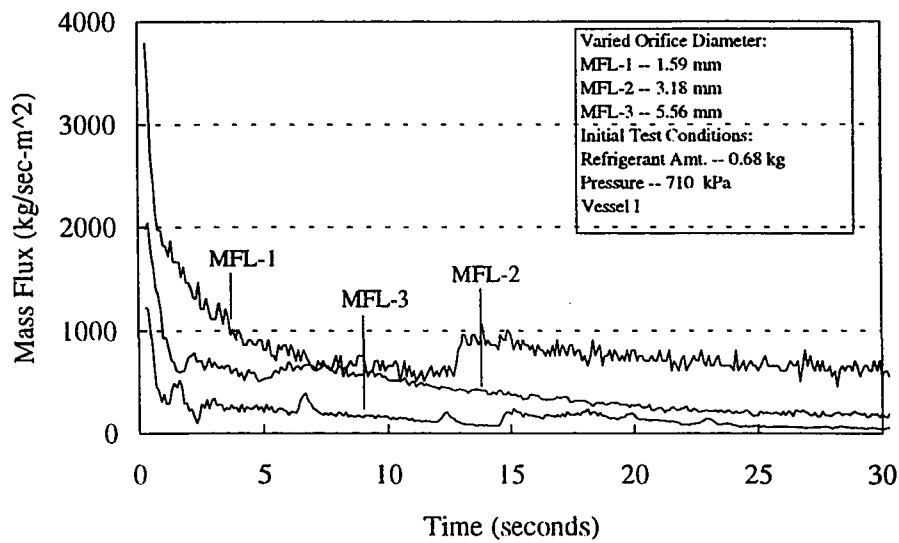
Figure 5.13. Baseline mass flux (MFL) profiles for three tests with different orifice sizes.

longer than the two larger orifices, it had a higher mass flux than the other two. The initial mass flux for the three tests were 3790, 2050, and 1230 kg/sec-m^2 from the smallest orifice to largest, respectively.

A plot of the total mass flashed during each sixty second test is provided in Figure 5.14. Mass flow rates were greater for the larger orifices and correspondingly, the total mass flashed was greater. A larger orifice allowed more vapor to be generated and to exit the vessel. For example, a total of 0.139 kg of R-22 was flashed from the vessel for the experiment using the larger 5.56 mm diameter orifice, 0.129 kg for the 3.18 mm orifice, and 0.078 kg for the 1.59 mm orifice.

Effects of Initial Refrigerant Amount on Mass Flow

Figure 5.15 shows the mass flow rate for three different experiments using the same test conditions (Vessel 1, 710 kPa initial pressure, and 5.56 mm orifice diameter) except for the initial amount of refrigerant in the vessel. Three arbitrary amounts were chosen for the experiments. They were 0.23 kg, 0.45 kg, and 0.68 kg. The mass flow rate was essentially the same for the first second as the initial vapor rose from the surface of the liquid. After one second, the mass flow rate for the 0.23 kg initial refrigerant amount continued to slowly decline. Both the 0.45 kg and the 0.68 kg test had increases in the mass flow rate. At 1.6 seconds, the 0.68 kg test had a mass flow rate of 0.013 kg/sec after dropping to 0.007 kg/sec at 1.1 seconds. This was due to the more agitated boiling caused by greater initial refrigerant amount. Observations of the boiling showed
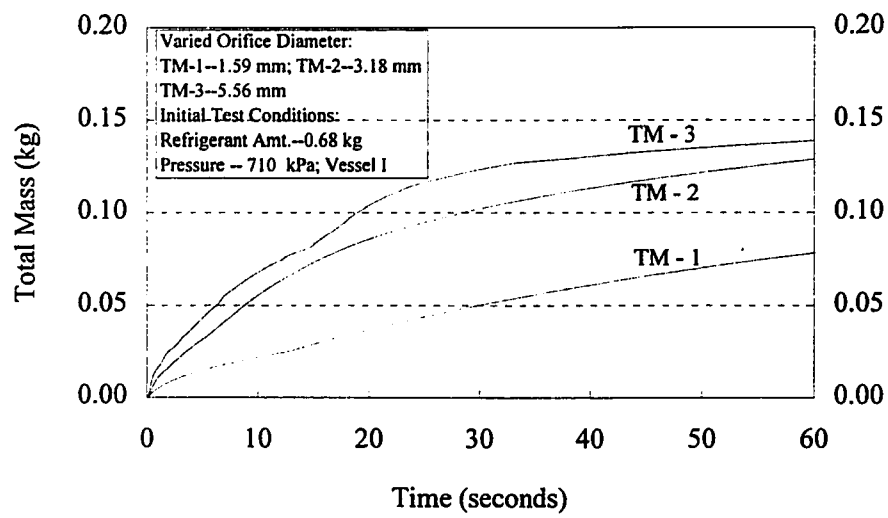
Figure 5.14. Baseline total mass (TM) flashed for three tests with different orifice sizes.
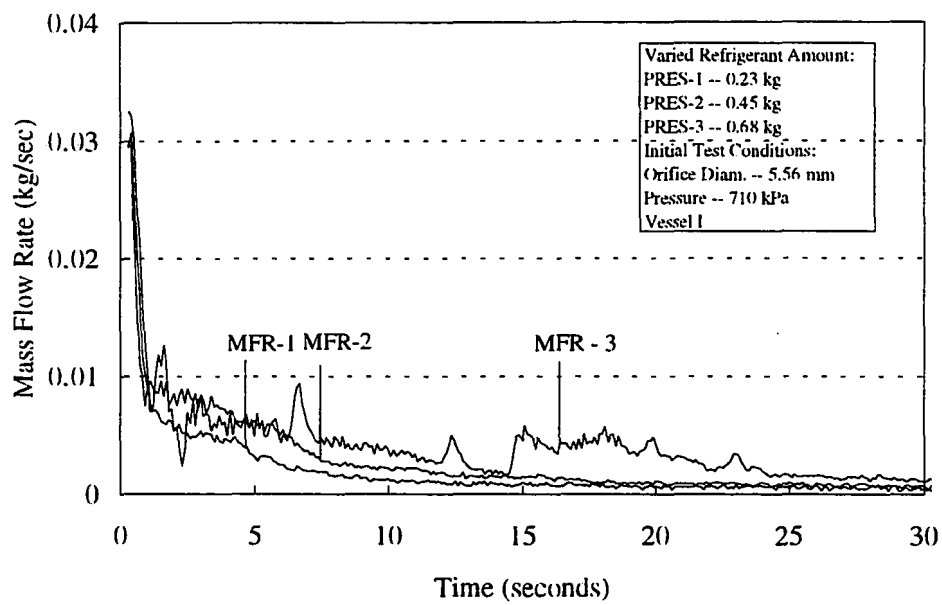
Figure 5.15. Baseline mass flow rates (MFR) for tests with different initial refrigerant amounts.

that vapor bubbles were larger with larger orifices, and a slightly larger two-phase region was generated. Nakamura et al., (1985) reported similar findings when they observed that a higher initial liquid level caused a higher liquid swell during first few seconds of flashing.

If vapor bubble growth is great enough to promote two-phase "swelling" of the fluid within (an increased void fraction), then the interface of the fluid will rise higher than the initial liquid level. The entire vessel can become a two-phase mixture as was shown by Guhler, et al. (1979) who flashed R-12 from a similarly sized vessel (1230 ml), but with the vessel completely full before flashing. With no room for the two-phase region to rise, entrained liquid was forced out through the orifice. They showed pictures of liquid R-12 leaving the vessel and the data showed mass flow rates over twice as high (0.07 kg/sec) as that in Figure 5.15. In other words, even relatively small amounts of entrained liquid greatly impact the mass flow rate. Moreover, Guhler had thermocouples placed in the refrigerant which caused nucleation and bubble growth below the liquid surface and swelling while flashing. Later stages of their boiling looked much more like the enhanced flash boiling discussed in the next chapter.

The pressure profiles in Figure 5.16 are typical of the data which show that the pressure drop after opening the solenoid valve was nearly the same for all three liquid levels. The only noticeable difference between the three occurred at one second. The test that had the lowest initial amount of refrigerant did not develop a local pressure minimum and subsequent increase before continuing to decline, but had a continual and
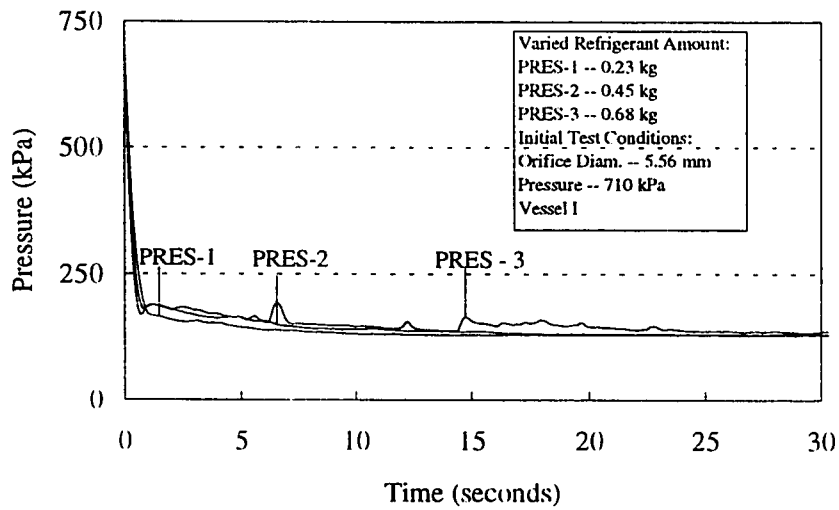
Figure 5.16. Baseline pressure (PRES) profiles for tests with different initial refrigerant amounts.
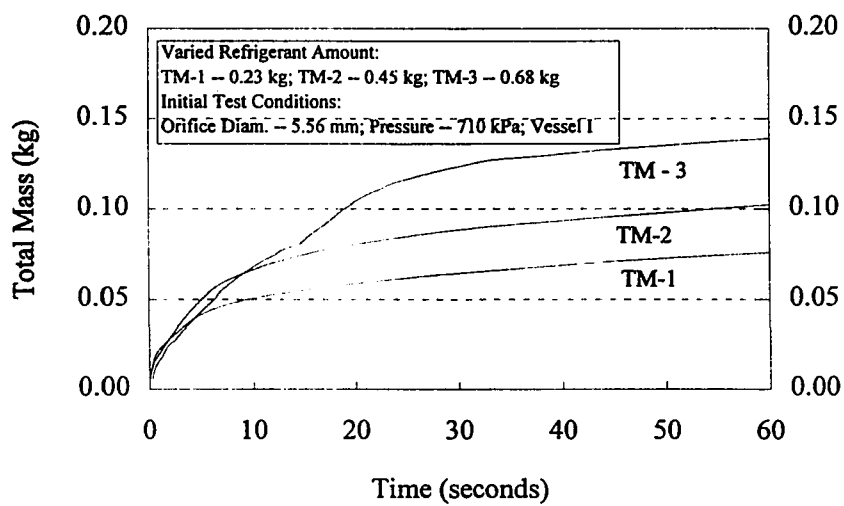
Figure 5.17. Baseline total mass (TM) flashed for tests with different initial refrigerant amounts.

less steep rate of depressurization. The average rates of depressurization for the first 0.7 seconds were 690, 740, and 775 kPa/sec for initial refrigerant amounts of 0.23, 0.45, and 0.68 kg, respectively. It was hypothesized that the amount of vapor above the liquid, that existed prior to opening the solenoid valve, influenced the initial depressurization rate. Larger amounts of vapor above the liquid slowed the rate of depressurization because it took a longer period of time to empty the vapor for the lesser refrigerant amount (0.23 kg). Only the bursting of larger bubbles after five seconds caused increases in the internal vessel pressure. This was confirmed by Nakamura, et al. (1985) who observed a slower rate of pressure drop for the higher liquid levels.

Figure 5.17 shows the total mass summed during the sixty second tests. The differences between the three experiments are significant with the greater initial refrigerant amount flashing more refrigerant. The test with 0.68 kg initial amount flashed a total of 0.14 kg (21% of total), as compared to 0.10 kg (23% of total) and 0.076 (33% of total) for initial refrigerant amounts of 0.45 kg and 0.23 kg, respectively. It was hypothesized that the additional mass flow for the test that used higher initial amounts was partially due to lower minimum pressures reached before one second by the 0.45 and 0.68 kg initial refrigerant amounts. This resulted in the liquid being more highly superheated (39 °C and 41 °C, respectively) which caused a greater amount of vapor bubble production and a subsequent increase in internal vessel pressure. The higher internal pressures (0.23 kg -- 131 kPa, 0.45 -- 140 kPa, and 0.68 kg -- 146 kPa at 10 seconds), in turn, resulted in greater potential for more vapor bubble growth and,

therefore, higher mass flow rates (0.23 kg -- 0.0013 kg/sec, 0.45 kg -- 0.0022 kg/sec,

and 0.68 kg -- 0.0037 kg/sec at 10 seconds).

Effects of Initial Pressure on Mass Flow

Internal vessel pressures of 840 kPa, 710 kPa, and 575 kPa were run to

determine the influence of pressure on the mass flow. Figure 5.18 is a plot of the

pressure versus time for three experiments with the only difference being the initial

pressure in the vessel. All tests were run in Vessel I using the 3.18 mm diameter orifice,

and 0.23 kg initial amount of Refrigerant-22. The internal vessel pressure for all three

cases reached essentially the same pressure after 6 seconds. It was hypothesized that it

took the first 6 seconds for the additional flashed refrigerant (as compared to the 575

kPa test) to exit the vessel. The higher initial pressures provided more internal energy

(575 kPa -- 47.2 kJ, 710 kPa -- 49.1 kJ, and 840 kPa -- 50.6 kJ) which was used as heat

of vaporization during the first six seconds and therefore, higher mass flow rates during

that time. Calculations showed the energy remaining in the vessel after six seconds was

highest for the test initially at the lowest internal pressure of 575 kPa (575 kPa -- 32.6

kJ, 710 kPa -- 31.6, and 840 kPa -- 31.3 kJ).

The data showed that an increased pressure setting had some influence on the

mass flow during the first five seconds (Figures 5.19 and 5.20), but it was not as

dramatic as the influence of the orifice or initial refrigerant amount. The experiments

using higher initial pressure settings had higher mass flow rates and flashed more
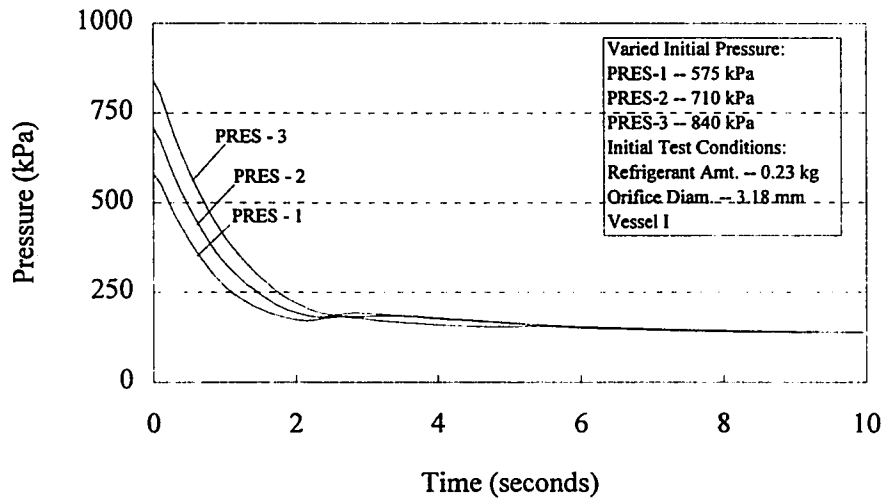
Figure 5.18. Baseline pressure (PRES) profiles for tests with different initial pressures.
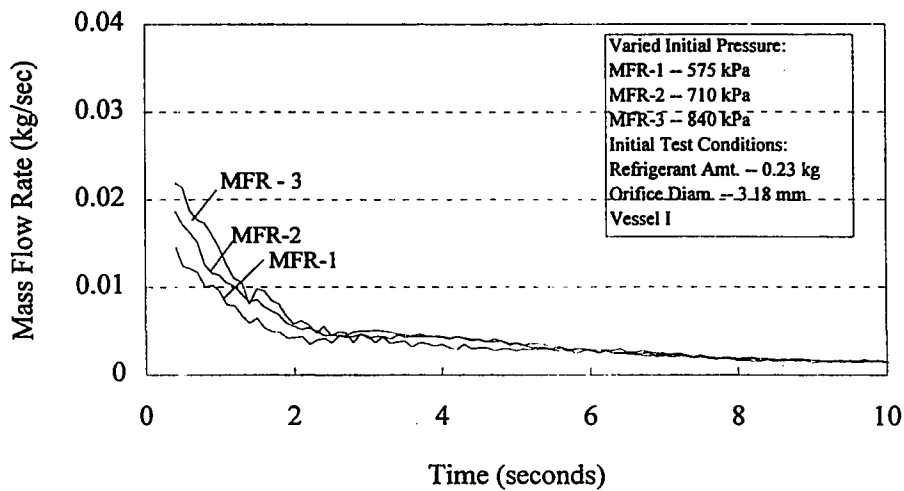
Figure 5.19. Baseline mass flow rates (MFR) for tests with different initial pressures.
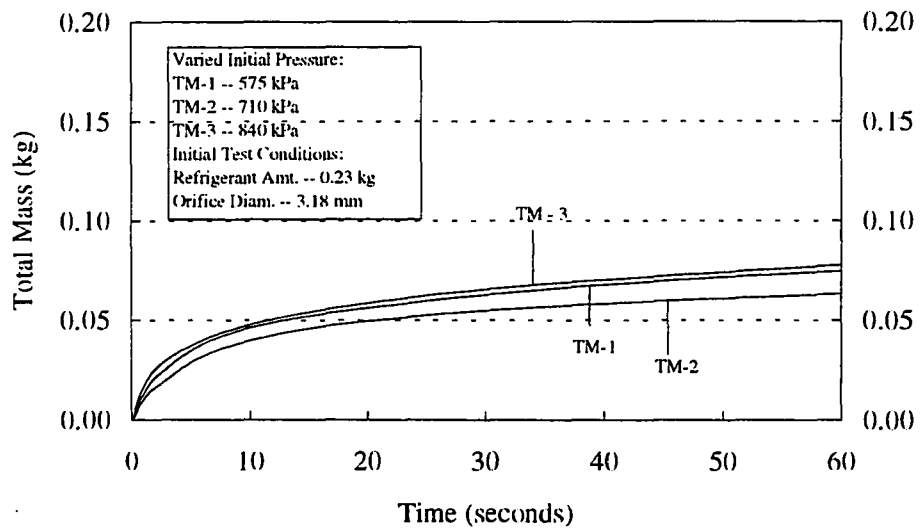
Figure 5.20. Baseline total mass (TM) for tests with different initial pressures.

refrigerant which agreed with Nakamura, et al. (1985) who found that higher initial pressure settings caused more flash steam to be generated. It was hypothesized that if greater initial pressure differences were used (500 kPa, 1000 kPa, and 2000 kPa, for example), the pressure would have had a greater impact on the mass flow and it would have taken longer before the vessels reached the same pressure. Initial refrigerant pressure settings were chosen based on the observation that the pressure within an accumulator of a heat pump only sees pressures of up to approximately 1000 kPa (145 psia). A second criterion used in determining the maximum initial pressure was the calculated pressure for failure of the glass vessels (1035 kPa or 150 psia).

Effects of Vessel Geometry on the Mass Flow

Three glass pyrex vessels were constructed to evaluate the effect of vessel geometry on flash boiling. Two vessels were constructed having the same volume (Vessels I and III) and two had the same height (Vessels I and II). Overall dimensions are listed in Chapter 4, Table 4.1. Inspection of individual experiments revealed varied results with regard to the total mass flashed during each sixty second experiment. In general, vessel geometry produced only limited differences in the mass flow from the vessel. For example, Figure 5.21 shows the mass flow rate and the total mass flashed for the test condition where the initial pressure was 840 kPa, the orifice size was 3.18 mm, and the initial amount of refrigerant was 0.23 kg. Mass flow rates were 35% higher at the same moment in time (0.9 seconds) for Vessel I until Vessel II's mass flow rate became 50% higher at 4.5 seconds. After 10 seconds, both cases had mass flow rates
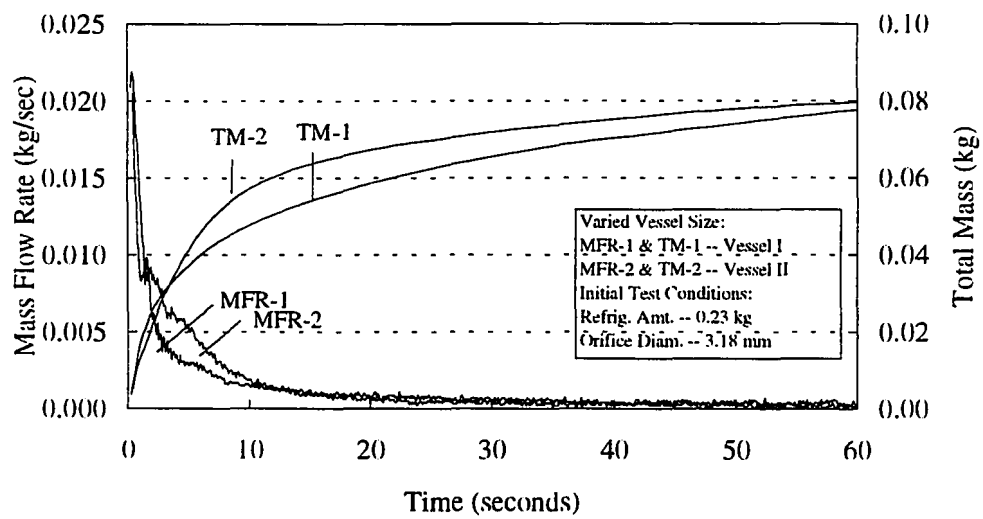
Figure 5.21. Baseline mass flow rates and pressures for tests with different vessel sizes.

within 10% of each other, with Vessel I being slightly higher and coming close to equaling the total mass flashed of Vessel II (0.0797 kg for Vessel I vs. 0.0777 kg for Vessel II).

Since the impact of the vessel geometry on the mass flow appeared to be small, three statistical studies were performed to ensure that each of the identified factors (initial vessel pressure, P; initial refrigerant mass, RM; orifice size, OR; and vessel geometry, VL) had significant influence on the flashing process primarily with regard to the mass flow. For the first analysis, 67 experiments were run at maximum and minimum (two levels) test conditions. Initial pressure settings of 575 kPa and 840 kPa, initial refrigerant amounts of 0.227 kg and 0.680 kg, and orifice diameters of 1.588 and 5.56 mm were used for tests with the two vessels (I and III) having the same internal volume (1075 ml ±5%, but with different geometric configuration. A minimum of four replications were performed for each test condition. The ANOVA test used total mass during each 60 second test as the dependent variable. Pressure, vessel, orifice, and refrigerant amount were used as the factors. A confidence level of 95% was used for each study. Detailed results are shown in Table 5.2.

With an F-Ratio of 124.8, the amount of refrigerant initially placed in the vessel had the greatest influence on the flashing process. Next, the orifice size, with an F-Ratio of 35.8, was also found to be statistically significant. The initial pressure setting showed some importance as well with an F-Ratio of 16.8. However, the vessel geometry had very little

influence on the total mass during flash boiling. It had a low F-Ratio of 0.02. Further

basecase experiments were run using only Vessels I and II. Vessel III, having the same

volume as Vessel I, was not used after the preliminary test. Furthermore, more

importance was given to the orifice and initial refrigerant amount which showed a

greater impact on the flashing process than the initial pressure setting within the given

range of test conditions.

Table 5.2. Results from ANOVA test checking the influence of test variables on the total mass removed from each vessel during a 60 second test using Vessels I and III.

Source	F-Ratio	P
Initial Refrig. Amount	124.78	0.000
Orifice Diameter	35.80	0.000
Pressure	16.82	0.000
Vessel Geometry	**0.02**	**0.877**

After running baseline tests with both Vessels I and II, a second statistical

analysis was performed. Results from 46 experiments where the initial refrigerant

amount (RA), orifice diameter (OR), and vessel (VL) were varied. The initial pressure

for each test was set at 840 kPa. Data were taken at each condition for Vessels I and II.

Both vessels had the same height, but Vessel I had a 101.6 mm inside diameter and

Vessel II had a 76.2 mm inside diameter. Three levels of orifice size were used (1.59

mm, 3.18 mm, and 5.56 mm) and two levels of initial refrigerant amount were used (0.23

kg and 0.45 kg). The larger 0.68 kg refrigerant amount was not included because Vessel

II did not have the capacity to hold that amount of liquid. The ANOVA test used the

total mass flashed during each 60 second experiment as the dependent variable. The

results are shown below in Table 5.3.

Results from the second ANOVA test revealed that the vessel volume made very

little statistical difference to the amount of flashed refrigerant. The initial refrigerant

amount and the orifice diameter were shown to have an influence on the flashing process

and had F-Ratios of 71.1 and 18.4, respectively. A similar ANOVA test was run on data

from the steel shot enhancement method. Results were the same as both the initial

refrigerant mass and orifice diameter had a significant impact on the flashed amount and

the vessel (either Vessel I or II) did not impact the amount flashed.

Table 5.3. Results from ANOVA test checking the influence of test variables on the
total mass removed from each vessel during a 60 second test using Vessels I and II.
Initial pressure for all tests were at the 840 kPa condition.

Source	F-Ratio	P
Initial Refrigerant Amount	71.131	0.000
Orifice Diameter	18.357	0.000
Vessel Geometry	**1.387**	**0.247**

Other subtle differences existed between the performance of the two vessels.

These became apparent after reviewing the pressure profile for each vessel. Vessel I

had a smooth curved pressure decline without any noticeable pressure increases (Figure

5.22). Vessel II tests, however, consistently developed a pressure dip and rise before

declining near the reservoir pressure. The pressure drop was faster for Vessel II because

there was less vapor (initially) above the liquid which left the vessel more quickly. This
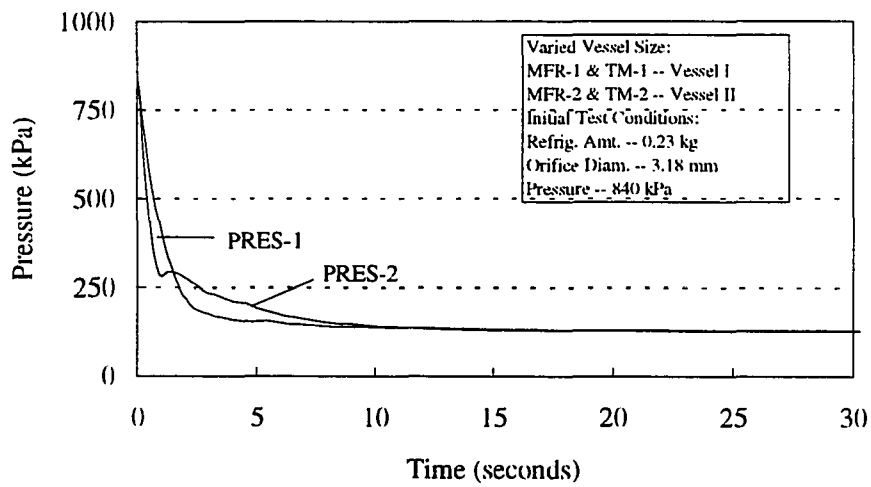
Figure 5.22. Baseline pressures (PRES) for tests with different vessel sizes.

led to the identification of another difference between the two vessels. The total time

that the vessel was choked during the initial few seconds of each experiment was

consistently shorter for Vessel I (Table 5.4).

Table 5.4. Differences in choked flow duration and total amount of refrigerant flashed for three tests (A, B, and C) at like test conditions (840 kPa initial pressure, 3.18 mm orifice diameter, and 0.23 kg initial refrigerant amount) between Vessel I and II.

Test	Vessel	Choked Time (seconds)	Flashed Amount (kg)
A	I	1.9	0.078
B	I	2.0	0.086
C	I	1.9	0.078
A	II	3.6	0.084
B	II	2.9	0.080
C	II	3.4	0.079

It was hypothesized that the pressure increase (in Vessel II tests) was interrelated

with the length of time pressures were choked. Just prior to the pressure rise in Vessel

II, the difference between the two vessel's pressure was nearly two-fold (Vessel I -- 406

kPa and Vessel II -- 280 kPa). Vessel II's vapor generation was delayed momentarily

even though the liquid was approximately 10 °C more superheated at 1.0 seconds.

Vessel II's mass flow rate then surpassed that of Vessel I once vapor generation

increased because the liquid refrigerant was superheated. As Vessel II's pressure

increased and surpassed that of Vessel I (at 1.4 seconds), both tests were choked.

Temperature Characteristics within the Vessel during Flash Boiling

A temperature probe consisting of four, 44-gauge thermocouples mounted on a piece of glass tubing was used to measure the temperature within the vessel. The thermocouples were placed 30 mm apart from bottom to top. A diagram of the probe can be seen in Chapter 4, Figure 4.2. The tests that included temperature measurements were not included as baseline tests. The temperature probe added nucleation sites within the liquid which would have skewed the mass flow results. Two tests that included the probe showed an increase in the total amount flashed. Fore example, one test (with initial settings of Vessel II, 840 kPa, 5.56 mm diameter orifice, and 0.45 kg of R-22) flashed 0.151 kg as opposed to the baseline average of 0.122 kg. A problem with probe failure was also experienced. The glass tubing broke due to the thermal shock during flashing.

A large temperature gradient was found to exist before and during most of the flashing process that existed in the vapor region (above the liquid). The temperature gradient, prior to initiation of the test, was observed in a number of the temperature measuring tests. It was hypothesized that the differences in vapor temperature existed because of heat transfer through the top half of the glass vessel. The vessel did not reach complete equilibrium because the ambient temperature was maintained above the saturation temperature at the vessel's internal pressure. The liquid temperature, however, consistently corresponded to the saturation temperature. With the liquid initially at saturated conditions, the solenoid valve was opened and the pressure quickly

dropped below the liquid's saturation pressure. This caused the liquid as well as the

vapor above the liquid to become superheated. Figure 5.23 is a plot of the four

measured refrigerant temperatures and the corresponding saturation temperature based

on the measured vessel pressure for the first two seconds of the experiment. The initial

pressure was 575 kPa, orifice size was 5.56 mm, and initial refrigerant amount was 0.23

kg. Only the bottom thermocouple was immersed in the liquid. The remaining three

thermocouples were located in the vapor for the entire experiment. A temperature

gradient existed within the vapor prior to opening the valve. The second thermocouple,

approximately 20 mm above the liquid, was 10°C warmer than the liquid. The vapor

within the vessel gradually cooled down to the saturation temperature (approximately -

25°C). On the other hand, the liquid temperature dropped quickly to the saturation

temperature at one second.

Figure 5.24 shows the amount of superheat measured by each thermocouple

based on the saturation temperature corresponding to the measured vessel pressure. All

three vapor temperatures approached the same amount of superheat (23°C) at 0.5

seconds, but became saturated within the next second. The liquid remained at the same

initial temperature and reached a maximum amount of superheat (34°C) at one second.

Vapor production began within the liquid and rapidly reduced the superheat.

Calculations found that the maximum amount of superheat possible (or the kinetic limit

of superheat) was 57.4 °C for pure R-22 at 575 kPa.
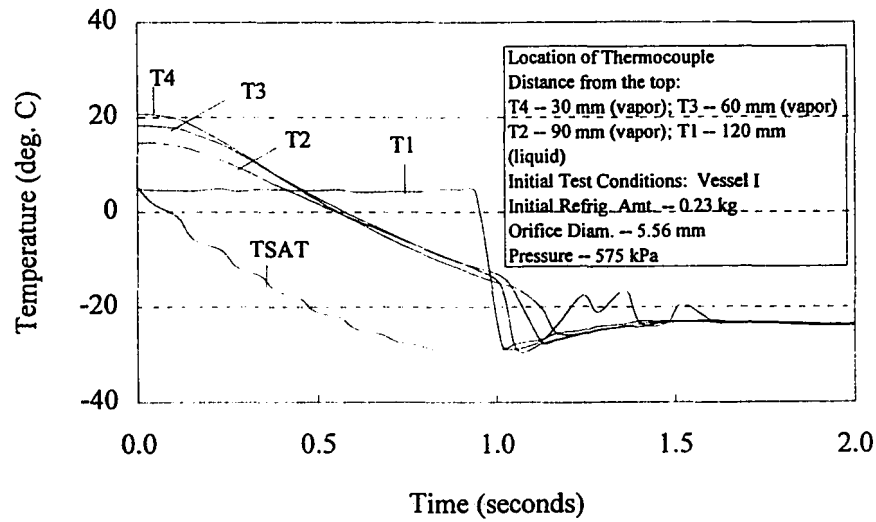
Figure 5.23. Saturation temp. (TSAT) and measured temps. (T) within test vessel.
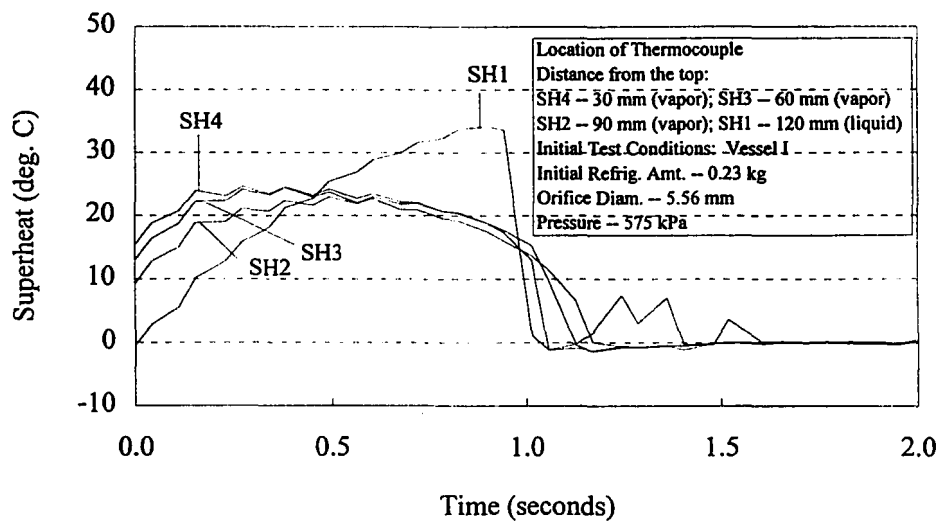
Figure 5.24. Amount of superheat (SH) at each thermocouple within the vessel.

As shown in Figures 5.25 and 5.26, both the vapor and liquid remained at

saturated conditions until the vapor near the top two thermocouples became increasingly

warmer and superheated. It was hypothesized that as the pressure and liquid

temperature dropped, the newly formed vapor rose toward the surface at the

temperature which corresponded to surrounding liquid pressure as the vapor bubble

burst. The vapor continued to increase in temperature because the temperature of the

inner vessel wall was superheated throughout most of the test (Figure 5.21). The

temperature gradient within the vapor indicated that the vapor did not thoroughly mix

before exiting through the orifice (Guhler, et al., 1979). The liquid temperature

maintained a more constant temperature because of convective churning and mixing.

The observed temperature profiles (Figure 5.25) were consistent with those presented in

the literature. Hanaoka, et al. (1990) showed similar data for three thermocouples

placed within a vessel flashing R-113. The temperatures within the liquid remained

steady until vapor nucleation began. Figure 5.27 shows the temperature profile of R-12

measured by Guhler, et al. (1979) during flashing from an initially full vessel. The same

temperature increases and significant temperature gradients within the vapor region were

observed in their data.
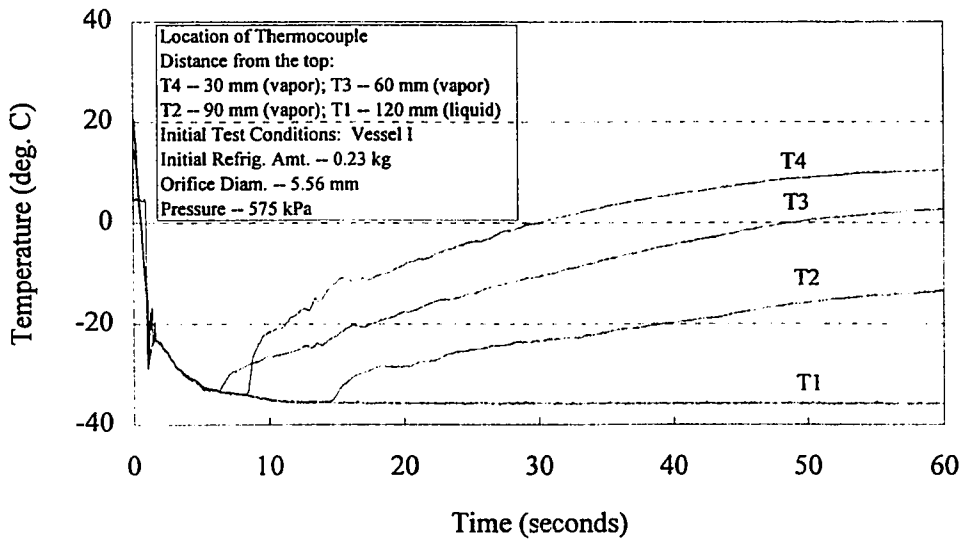
Figure 5.25. Measured temperatures (T) within the test vessel.
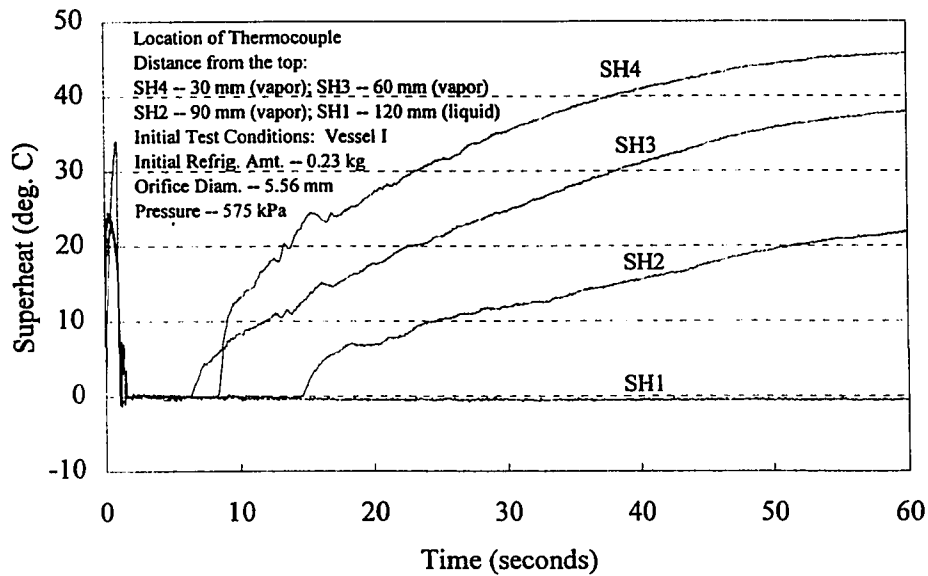
Figure 5.26. Amount of superheat (SH) at each thermocouple within the vessel.
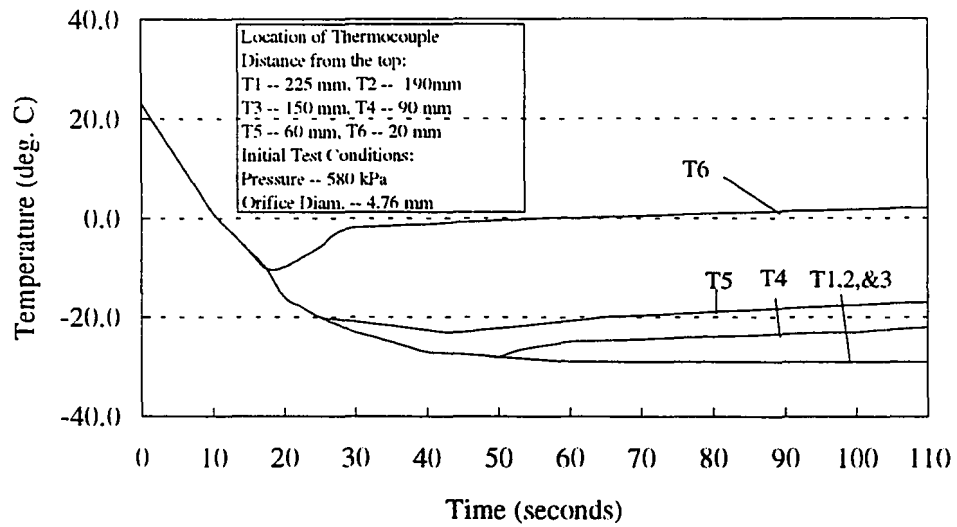
Figure 5.27. Measured temps. (T) within a vessel initially full of R-12 (Guhler et al., 1979).

SUMMARY OF RESULTS FOR BASELINE EXPERIMENTS

Mass flow experiments were run establishing a baseline to compare against the enhanced boiling techniques and to use in predictions. A literature review led to the introduction of four variables that could affect the mass flow during flash boiling. The four variables were initial orifice diameter, initial refrigerant amount, initial pressure, and vessel geometry. Three levels of each variable were studied. The influence of each variable was investigated and discussed.

A visualization study showed that tests run at the lowest conditions (575 kPa, 1.59 mm orifice diameter, and 0.23 kg refrigerant) had a cloud of vapor and minuscule droplets rise from the liquid surface just after opening the solenoid valve. Next, larger vapor bubbles appeared at the surface of the liquid primarily around the perimeter. After 20 seconds, only three or four nucleation sites were seen in the vessel. Mass flow leaving the orifice was choked for seven seconds for this particular experiment. Pictures of an experiment at the upper bound test conditions (840 kPa, 5.56 mm orifice diameter, and 0.68 kg refrigerant) revealed similar results but with a greater magnitude. The major difference was an increased amount of vapor formation and vigorous bubble bursting.

The orifice size was found to directly impact the mass flow. A smaller orifice caused a slower depressurization rate within the vessel and reduced mass flow rates. Tests using a smaller orifice experienced choked flow conditions for a longer duration. Tests that used a larger orifice allowed more energy to be released during the initial stages of the flashing process and more vigorous vapor bubble growth. It was

hypothesized that a larger orifice allowed the initial cloud of vapor to exit the vessel more quickly and the pressure to drop to lower value and a greater amount of superheat (which resulted in more vapor production). Furthermore, the mass flux was inversely influenced by the orifice size. The mass flux for test conditions using a smaller orifice had higher mass fluxes due to the flow being at, or closer to, critical (or maximum) conditions for longer periods of time.

The initial refrigerant amount was found to influence the mass flow rate as well. A higher initial refrigerant amount caused increased two-phase mixture swelling and increased the overall amount of refrigerant that was flashed. Three tests with identical initial conditions, except for initial liquid level amount, flashed different quantities of refrigerant. The higher refrigerant amount (0.68 kg) flashed 0.14 kg, versus 0.10 kg and 0.076 kg for the 0.45 kg and 0.23 kg initial amounts. It was hypothesized that this was caused by the steeper initial depressurization rates for the higher initial refrigerant amount tests. This was caused by the vapor above the liquid emptying more quickly and reaching a lower local minimum pressure.

The initial pressure setting of the refrigerant within the vessel was changed to determine its impact on the mass flow. The data showed that an increased initial pressure only changed the mass flow during the initial few seconds of the test, but did slightly increase the total mass flashed over a 60 second experiment. It was shown that the higher pressure tests contained more internal energy and it was hypothesized that this additional energy was transferred to additional vaporization of liquid during the first six

seconds of the tests. Relative to the orifice diameter and the initial refrigerant amount, the impact of the initial pressure setting was minor.

The fourth variable investigated was the vessel's geometric configuration. Three glass vessels were constructed. Two had approximately the same volume (Vessels I and III) and two had the same height (Vessels I and II). A review of the experiments found varied results with respect to the total mass flashed. Therefore, three statistical studies of the data were performed to determine the importance of each varied parameter (initial orifice diameter, initial refrigerant amount, initial pressure, and vessel geometry). The statistical analysis found that the vessel geometry was not significant when compared against the other parameters. The dependent factor used in the ANOVA test was the total amount of refrigerant flashed during each experiment.

Differences in the pressure characteristics between Vessels I and II did exist. Vessel I had a smooth pressure drop while Vessel II developed a pressure dip and rise before declining toward the outlet reservoir pressure. Choked flow conditions for the vessel with a smaller volume (Vessel II) occurred for a shorter period of time because the rate of depressurization for this vessel was steeper. This caused the liquid within Vessel II to be 10°C more superheated than that in Vessel I. This resulted in the vaporization of more refrigerant during the first 10 seconds of the test and also caused a pressure rise at two seconds.

Refrigerant temperatures were measured to determine the temperature characteristics within the vessel. A large temperature gradient was found to exist in the

vapor region. After the solenoid valve was opened, the pressure quickly dropped below

the saturation pressure causing the liquid to be superheated. The liquid was superheated

as much as 34°C before vaporization quickly cooled the bulk liquid near the saturation

temperature. Between one and seven seconds, the measured temperatures were the

same as the saturated temperature. Afterwards, a temperature gradient developed in the

vapor region with cooler temperatures near the liquid surface and increased temperatures

as the vapor approached the orifice. The vapor was superheated as much as 46°C at the

top of the vessel near the end of the test. The temperature gradient formed due to the

lack of mixing within the vapor region and the poor heat transfer characteristics of the

Pyrex glass vessel. Results agreed quite well with those presented by Guhler, et al.

(1979).

CHAPTER VI

EXPERIMENTAL ENHANCED BOILING RESULTS

Flash boiling experiments were conducted using three additions to the vessel as potential flash boiling enhancements. The data from these flash boiling experiments were compared with the baseline experimental results with primary regard to the mass flow. Classically, enhanced boiling techniques have been classified into two general categories: 1) passive -- which require no direct application of external power and 2) active -- which use external power. Experiments were run using two passive and one active enhancement methods. One of the passive enhanced boiling techniques used small steel balls (or steel shot), 3.6 mm in diameter. The decision to use steel shot was based the hypothesis that the steel would provide nucleation enhancement (Carey, 1992 and Thome, 1991). In addition, previous researchers (Chuah and Carey, 1987) used a layer of small copper beads at the bottom of a pool of water. They found the heat transfer coefficients increased up to two times over that of an ordinary pool of water at the same heat flux. The second passive technique included the addition of small amounts of mineral oil (4% by volume) to the refrigerant. The interest in this stemmed from the fact that the compressors in heat pumps require oil as a lubricant. The lubricant is mixed with the refrigerant. Experiments were performed to see if a small amount of mineral oil changed the mass flow characteristics during flash boiling from a small vessel. Finally, a nominal 215-watt immersion heater was chosen for the active

enhanced boiling technique. The immersion heater was specially constructed to fit

within both Vessels I and II. Some literature is available discussing heat flux

characteristics of an electric resistance element (Sakurai, et al., 1978 and Kung, et al.,

1981), but nothing was found on how electric resistance heat addition changes the mass

flow characteristics during flash boiling. Experimental results of the three techniques

were compared against baseline results and an analytical model. A visualization study

along with the analysis and discussion of the comparisons of using each potential

enhancement method and baseline experiments are discussed in this chapter.

ANALYSIS AND RESULTS OF STEEL BALL PASSIVE ENHANCEMENT EXPERIMENTS

A layer of 3.6 mm diameter steel balls was added to the bottom of the vessel

during some of the flash boiling experiments. The visualization study showed, as

expected, that the 10 mm high layer of steel balls added numerous nucleation sites

within the liquid and promoted abundant vapor growth during depressurization. The

steel spheres were in contact with each other and the interior of the glass vessel.

Theoretically, this added potential heterogeneous nucleation sites throughout the entire

base of the vessel (Carey, 1992). As with the baseline experiments, each test was run

for sixty seconds using varied orifice diameters (1.59 and 5.56 mm), initial refrigerant

amounts (0.23, 0.45, and 0.68 kg), initial pressures (575 and 840 kPa), and vessel

geometries (I and II). Pressures, temperatures, and mass flow rates, along with

calculated saturation temperatures, amount of superheat, mass flux, and total mass

flashed were used to compare the baseline experiments with the enhance boiling

method. The visualization study included pictures of the flash boiling process at time 0,

1, 2, and 20 seconds. Plots of the mass flow rates, pressures, and total mass are also

presented.

Visualization Study of Steel Ball Passive Enhancement Method

Videos of the passive enhancement experiments were used to observe and study

the flash boiling process prior to analyzing the detailed quantitative results. One

representative test is presented in this section. This test used Vessel I (see Table 4.1 for

descriptions) and had initial conditions set at 837 kPa, 5.56 mm orifice diameter, and

0.68 kg of refrigerant. Figure 6.1 shows the vessel at the initial conditions prior to

opening the solenoid valve, and Figures 6.2 through 6.4 are pictures of the passive

enhanced flash boiling experiment at 1, 2, and 20 seconds. At one second, vigorous

boiling had begun within the steel shot as the pressure dropped from 837 to 495 kPa.

Compared to the baseline experiments where primary bubble formation was at the

surface, the majority of vapor was generated from bubbles formed below the surface

within the steel shot. Pictures of the baseline tests at the same initial conditions are

shown in Figures 5.5 through 5.9. Finally, entrained liquid reached the top of the

vessel as the vessel was momentarily filled with a liquid-vapor swell (or two-phase

mixture). Consequently, both vapor and liquid were leaving the vessel through the

orifice.

Initial liquid level.

Layer of 3.6 mm steel balls placed approximately 10 mm high.
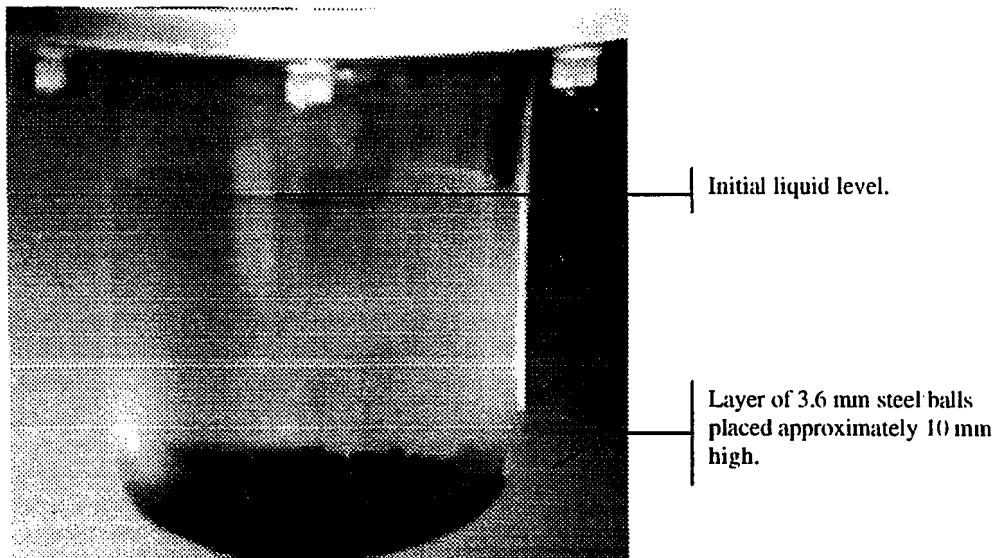
Figure 6.1. Picture of Vessel I with 3 mm diameter steel shot prior to activation of solenoid valve. Initial test conditions were: 837 kPa, 5.56 mm orifice diameter, 0.68 kg refrigerant amount.

Vessel fills with two-phase mixture of refrigerant. Some liquid was entrained in the vapor.

Slug shaped bubbles depart from the layer of steel balls.
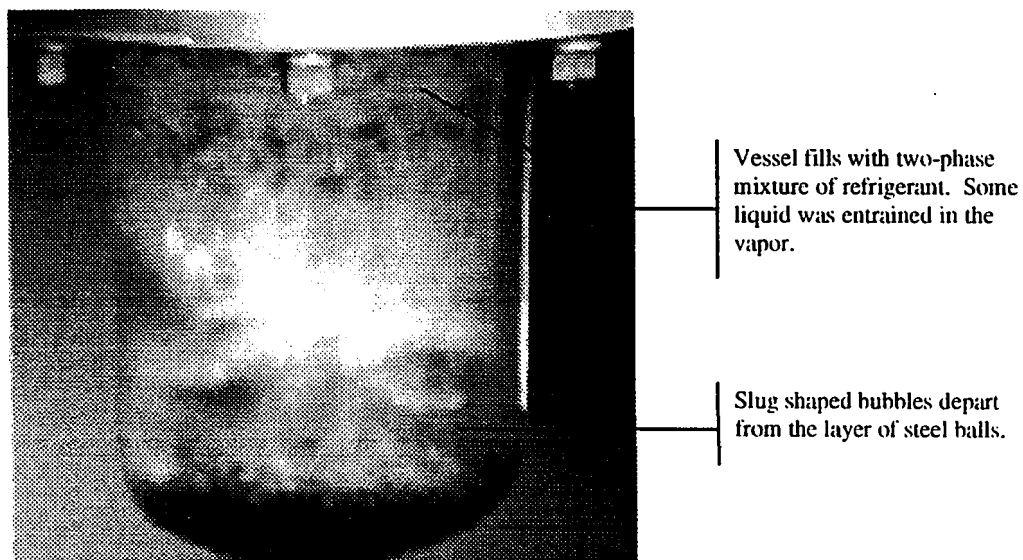
Figure 6.2. Picture of Vessel I with 3 mm diameter steel shot one second after activation of solenoid valve. Measured conditions at one second were: 495 kPa, 5.56 mm orifice diameter, 0.028 kg of R-22 flashed.

Figure 6.3. Picture of Vessel I with 3 mm diameter steel shot two seconds after activation of solenoid valve. Measured conditions at two seconds were: 374 kPa, 5.56 mm orifice diameter, 0.060 kg of R-22 flashed.
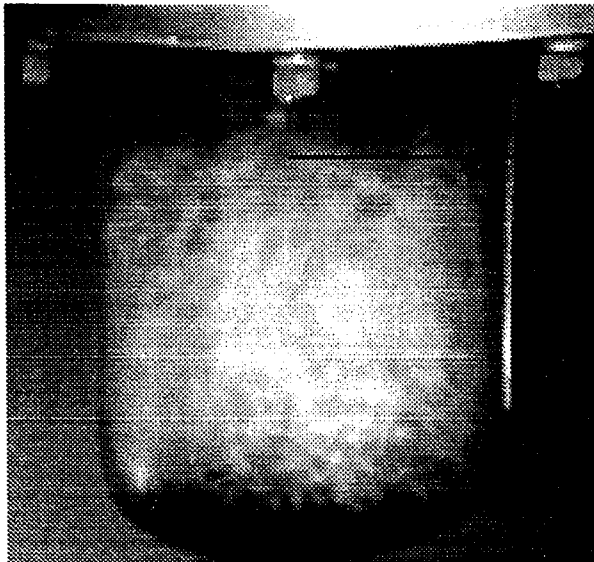
The two-phase liquid swell began receding.

Figure 6.4. Picture of Vessel I with 3 mm diameter steel shot twenty seconds after activation of solenoid valve. Measured conditions at twenty seconds were: 137 kPa, 5.56 mm orifice diameter, 0.20 kg of R-22 flashed.

Individual vapor bubbles were still being formed from within the layer of steel balls at 20 seconds.

At two seconds (Figure 6.3), a continuous flow of bubbles was rising to the liquid surface and bursting. The bubbles were departing uniformly across the whole layer of steel balls and completely overwhelmed any wall or surface bubble formation that may have been occurring. The fluid within the vessel was agitated and the liquid-vapor swell receded approximately 30 mm as a vapor region formed at the top. The pressure dropped to 374 kPa and over 25% (0.06 kg) of the refrigerant leaving leave the vessel during the 60 second experiment already had exited. After the first five seconds, bubbles formed and flowed upward as small bubbles coalesced into oblong shaped, nonuniform bubbles before reaching the surface. Observations of the experiment showed that most of the bubble formation within the steel shot appeared to begin at the intersection of each steel ball and the bottom of the vessel. It was hypothesized that the bubble shape may have been altered while traveling through the gaps within the layer of steel shot. Due to interference from surrounding steel balls, the original form of the bubble before departing from the surface may have been irregular as well. Figure 6.4 shows the boiling process 20 seconds after opening the solenoid valve. Only distinct areas within the bed of steel balls were creating vapor bubbles. The vessel pressure had dropped to within 17 kPa of the downstream reservoir pressure (120 kPa), and 88% of the flashed R-22 had left the vessel.

Comparison of Steel Ball Passive Enhancement and Baseline Experiments

Table 6.1 gives a comparison of the baseline experiments and the corresponding

experiments using steel balls as an enhanced boiling method. Results showed an

increase in the total mass flashed at each test condition ranging from an average of 22%

to 81% with respect to the baseline experiments. Furthermore, no clear correlations

between percent increase and the controlled parameters (initial refrigerant amount,

orifice diameter, vessel size, or initial pressure) were found.

Table 6.1. Percent increase of refrigerant flashed for the passive enhanced boiling
method (steel balls) compared to corresponding baseline tests

Initial Pressure (kPa)	Vessel Used (I or II)	Orifice Diameter (mm)	Initial Refrig. Amount (kg)	Percent Increase (%)
840	II	5.56	0.45	51±2
840	II	5.56	0.23	41±13
840	II	1.59	0.45	32±1
840	II	1.59	0.23	49±5
840	I	5.56	0.68	27±11
840	I	5.56	0.45	81±5
840	I	5.56	0.23	26±15
840	I	1.59	0.68	44±21
840	I	1.59	0.45	70±5
840	I	1.59	0.23	22±13
575	I	5.56	0.68	28±13
575	I	5.56	0.45	78±2
575	I	5.56	0.23	36±15
575	I	1.59	0.68	28±23
575	I	1.59	0.45	58±3
575	I	1.59	0.23	50±15

Two test conditions were chosen to compare passive method enhanced flash boiling test cases with the corresponding baseline tests. The detailed analysis and comparison is presented in the remainder of this section. The second test condition corresponds to the one discussed in the visualization study. The first test condition used the smallest orifice

(1.56 mm) and least amount of initial refrigerant (0.23 kg) at the initial pressure setting of 840 kPa. The experiment utilized Vessel I. Figure 6.5 shows the mass flow rate for both the baseline and steel shot enhanced tests. The mass flow rates differed in two areas. First, the peak initial mass flow rate was higher for the baseline test (0.009 vs. 0.0078 kg/sec). The small difference between the two tests appearred to be insignificant because a review of other tests at the same conditions found that the peak initial mass flow rate was not dependent on whether it was a baseline or enhancement test. Second, the passive enhanced test had a steep increase in the mass flow rate at 9.3 seconds. The mass flow rate more than doubled as it increased from 0.0017 to 0.0037 kg/sec in 1.1 seconds. This peak corresponded to the initiation of vapor generation from within the layer of steel shot.

The pressure within the vessel, Figure 6.6, had the same general trends as the mass flow rates. The pressure for the enhanced test reached a minimum of 242 kPa at 9.3 seconds and rose to 499 kPa at 9.7 seconds. The initial cloud of vapor rose from the surface and subsided at about 8.0 seconds. Next, two small bubbles formed on the vessel wall just below the surface of the liquid (Figure 6.7). Less than 0.2 seconds after
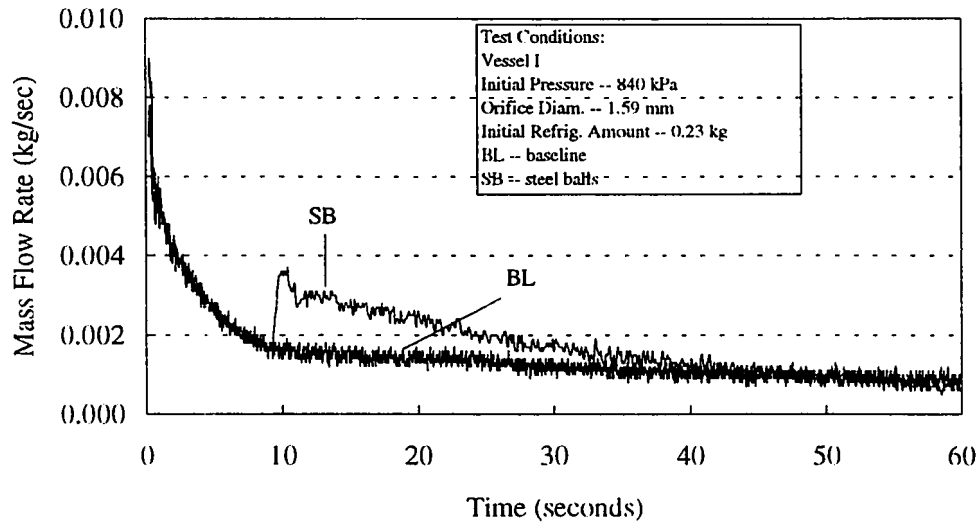
Figure 6.5. Mass flow rate vs. time for baseline and steel ball tests.
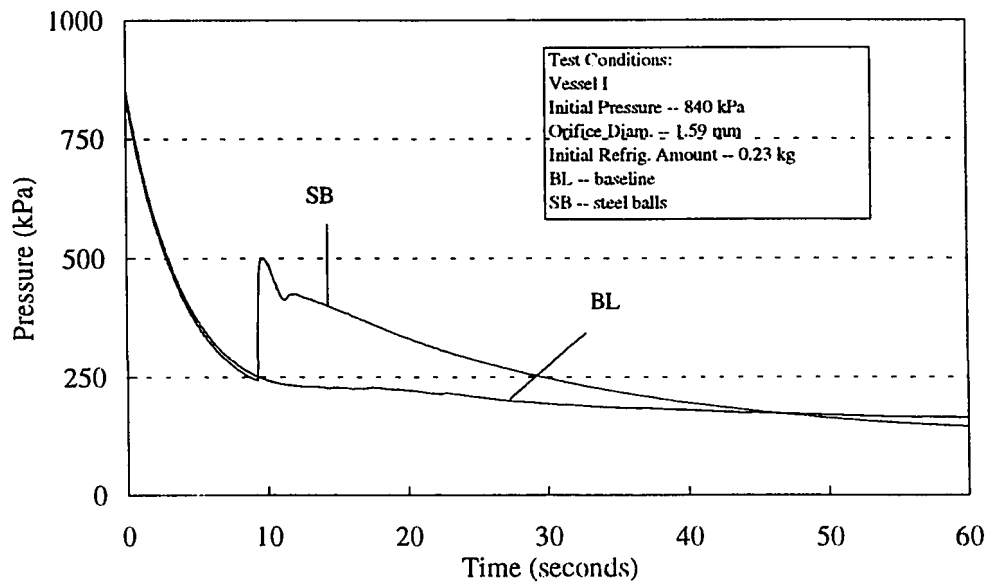
Figure 6.6. Pressure vs. time for baseline and steel ball tests.
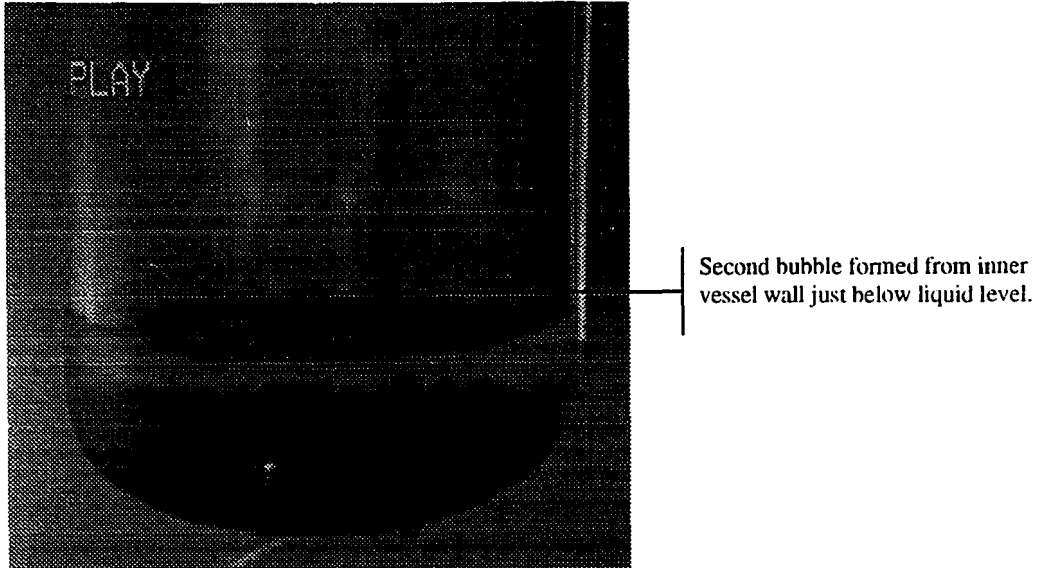
Figure 6.7. Picture of bubble formed on wall 0.2 seconds before boiling began within the layer of steel balls (9.3 seconds).

Second bubble formed from inner vessel wall just below liquid level.
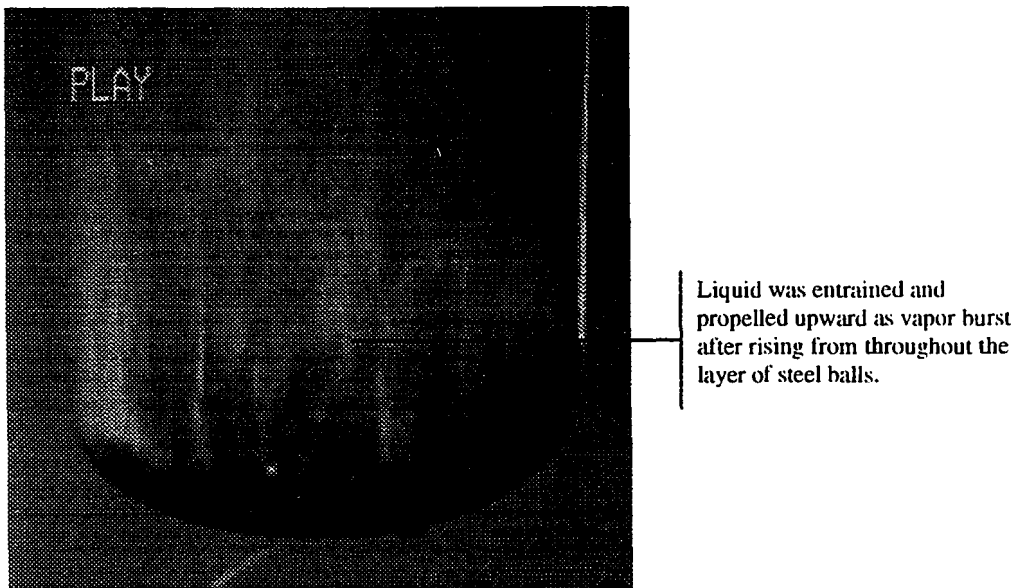
Figure 6.8. Picture of bubbles bursting simultaneously after forming from within the layer of steel shot (9.5 seconds).

Liquid was entrained and propelled upward as vapor burst after rising from throughout the layer of steel balls.
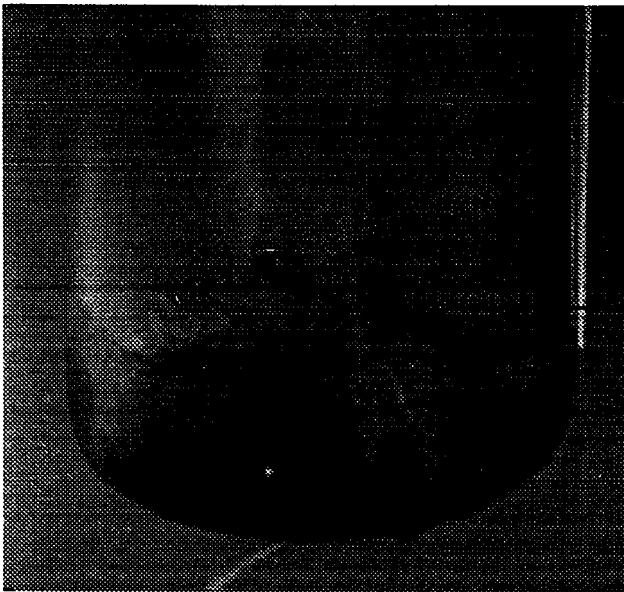
Liquid entrainment had subsided as liquid sloshed around and a continuous flow of bubbles begin forming from within the layer of steel balls.

Figure 6.9. Picture of vessel one second after large burst (10.5 seconds).

the second bubble burst, a wall of bubbles rose from the layer of steel shot to the surface, bursting almost simultaneously. As the bubbles burst, liquid was entrained with the vapor causing the vessel to be filled with a two-phase mixture (Figure 6.8). The liquid fell back to the bottom of the vessel and bubbles began forming from within the steel balls continuously traveling upward to the surface (Figure 6.9). It was hypothesized that the liquid was initially in a metastable state requiring a perturbation large enough to initiate boiling. The bursting of the second vapor bubble formed on the vessel wall may have been the perturbation needed to activate bubble growth from within the steel shot. Based on the measured pressure, the liquid had become superheated by 37 °C. This was followed by a steady generation of vapor bubbles as the pressure and mass flow rate declined and reached approximately the same value as the baseline case at 45 seconds. The baseline experiment for this test did not have a similar pressure or mass flow spike. It was hypothesized that the liquid was highly superheated as in the test that used the steel shot, but very few potential nucleation sites existed below the liquid level. After several seconds, a few vapor bubbles had been produced on the surface and at the vessel wall, but none below the liquid surface. As the pressure profile began to flatten, the potential for the liquid to have an increased amount of superheat diminished as convective cooling took place within the liquid. In other words, if boiling within the liquid did not occur quickly, the downward circulation would cool the bulk liquid, which reduced to potential for boiling. The circulation of liquid was observed in several of the baseline experiments.

Flow was choked in both cases. The baseline test ceased to be choked at 21.5 seconds. The large pressure spike for the enhanced case prolonged the choked flow condition by increasing the pressure differential between the vessel and downstream reservoir. It was hypothesized that the increase in vapor production from within the added steel shot probably forced an increase in vessel pressure when the newly formed vapor could not escape as quickly as it was produced. The mass flow of the refrigerant during the enhanced flash boiling test was choked for 35.5 seconds. Mass flux had the same profiles as the mass flow rates, different only in magnitude with the baseline test peaking at 4550 kg/sec-m^2 and the enhanced peaking at 3940 kg/sec-m^2.

Figure 6.10 shows the summed totals of the mass flashed throughout each 60 second test. The two test cases diverged at the 9.3 second mark when the mass flow rate of the enhanced experiment increased dramatically. For these two tests, the steel ball passive enhancement test ultimately flashed 27% more R-22 (0.112 vs. 0.0883 kg) than the baseline.

The second test used the largest orifice (5.6 mm) and maximum amount of initial refrigerant (0.68 kg) at an initial pressure setting of 840 kPa. The four inch inside diameter vessel (Vessel I) was used in this test as well. These "higher" settings encouraged maximum mass flow within the range of experiments. At these conditions, the baseline experiments flashed an average of 0.165 kg and the steel shot passive enhanced method flashed an average of 0.210 kg.
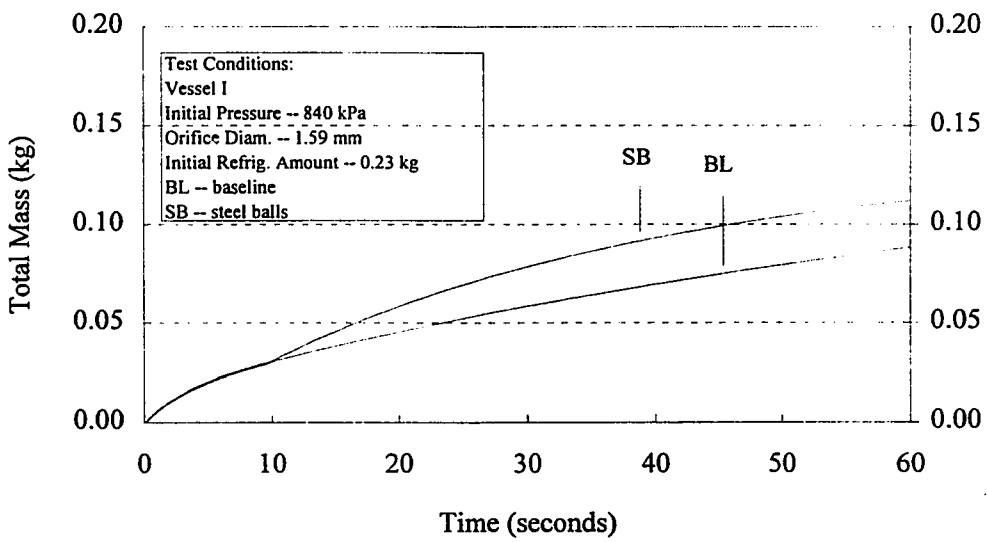
Figure 6.10. Total mass flashed vs. time for baseline and steel ball tests.

Figure 6.11 shows the mass flow rate over time for both the baseline and the steel shot passive enhanced method. For the first 0.4 seconds, both cases had similar mass flow rates. At 0.4 seconds, both pressures (Figure 6.12) dropped to 290 kPa and were superheated by 32 °C. At that moment, boiling began within the layer of steel balls. The baseline pressure continued to drop for another 0.3 seconds to 194 kPa and 43 °C of superheat before boiling began at the surface. The initial mass flow rate came from the vapor held above the liquid before the solenoid valve was opened and from the initial mist that formed at the beginning of each experiment. The baseline case required 11 °C more superheat before vapor generation occurred primarily on the vessel wall, while the steel shot enhancement test needed less superheat before boiling began within the layer of steel balls.

After boiling began in the layer of steel balls, the pressure and mass flow rate for the enhanced test quickly increased to 527 kPa (at 0.8 seconds) and 0.037 kg/sec (at 1.0 seconds), respectively. The pressure and mass flow rate for the baseline test increased by a lesser amount because vapor production was less for the baseline experiments. Pressure increased by 53 kPa and the mass flow rate increased from a local minimum of 0.011 kg/sec at 1.0 seconds to a maximum of 0.015 kg/sec at 3.0 seconds. After peaking, the mass flow and pressure gradually declined.

The mass flux for the baseline case had a maximum value of 1400 kg/sec-m^2, while the enhanced flux peaked at 1340 kg/sec-m^2. As in the baseline tests, the mass flux was higher for the cases with smaller orifices because they approached maximum
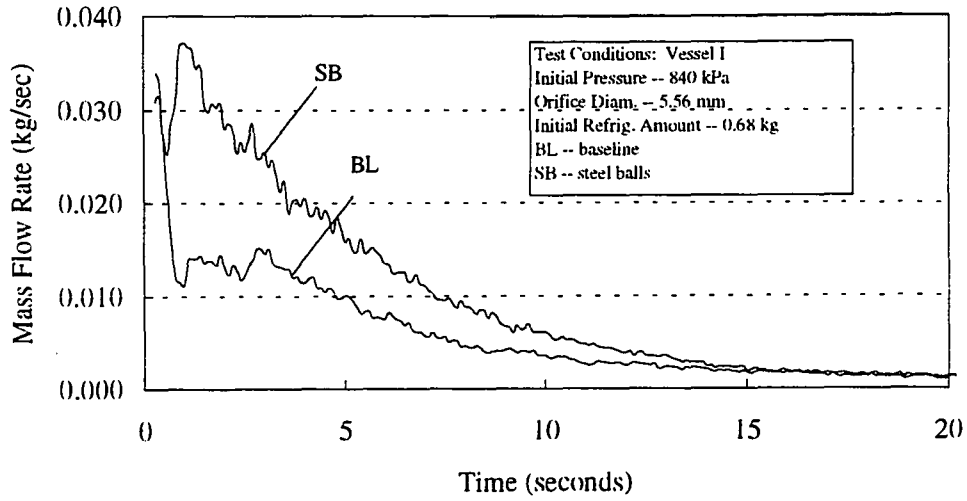
Figure 6.11. Mass flow rate vs. time for the baseline and steel ball tests.
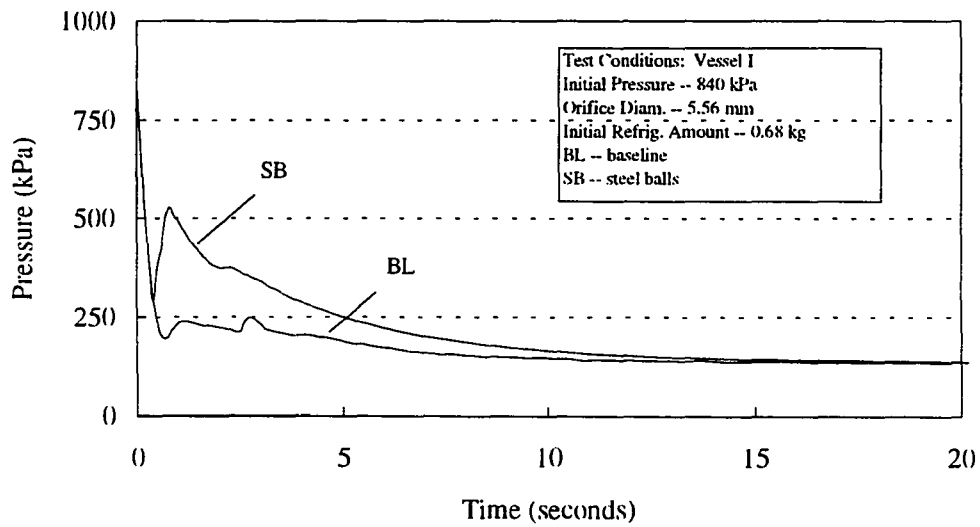
Figure 6.12. Pressure vs. time for baseline and steel ball tests.

flow (choked) for several seconds during each test. Figure 6.13 shows the total mass that exited the vessel during each 60 second test. The steel ball passive method test flashed as much refrigerant (0.147 kg) in the first 6.5 seconds as the baseline case did in 60 seconds. This was due to greater vapor production rates, and therefore greater mass flow rates, for the enhanced case during the first few seconds after boiling began at the base of the vessel. The case flashed 55% more than the baseline by the end of the test.

For the same initial conditions, the refrigerant plus the steel balls would have a greater internal energy than when the vessel only had refrigerant alone in it. It was hypothesized that energy from the steel balls was transferred to the refrigerant during flashing. In both cases discussed above, an additional 3.5 to 4.5 KJ of energy was initially stored in the vessel prior to the flashing process as compared to the baseline tests. This additional energy corresponded to 11% and 6% of calculated total energy released from the liquid for the "lower" setting test (first discussed above) and "higher" setting test, respectively. Figure 6.13 also shows a curve for the refrigerent that was vaporized because of the added energy. Calculation of the curve was based on the assumption that the balls were at a temperature equal to the saturation temperatures of the liquid refrigerant for the given measured pressure. The steel balls were also assumed to have constant specific heat. Since more refrigerant was flashed than was provided by the energy available from the steel, it is reasonable to conclude that the steel balls created additional nucleation sites and promoted vapor bubble growth. To also support this hypothesis, conduction calculations were performed and found that a
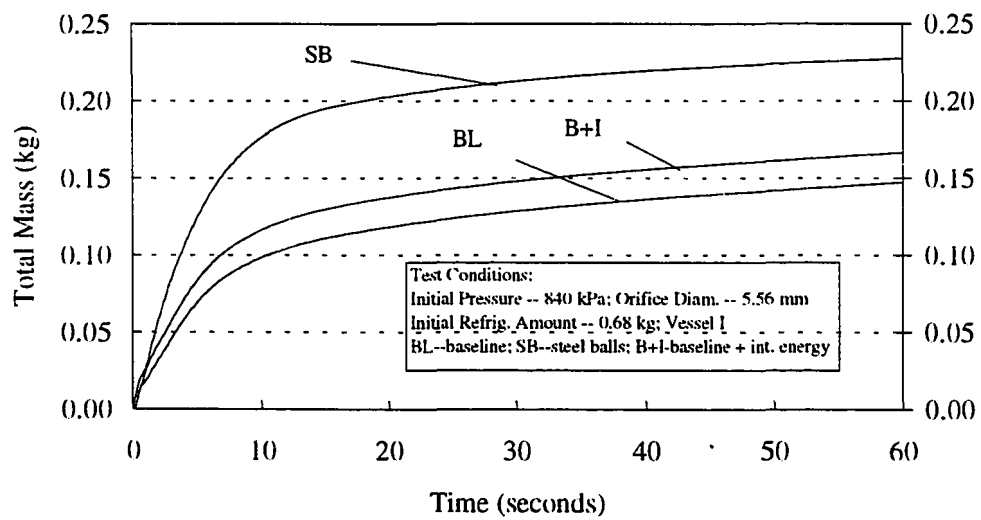
Figure 6.13. Total mass flashed for baseline test, baseline plus steel ball internal energy, and steel ball tests.

steel sphere (3.6 mm diameter) approaches within 1°C of the surrounding liquid temperature in less than one second as the energy is transferred from a single steel ball into an assumed surrounding liquid maintained at 25°C (Incopera and DeWitt, 1990). This meant the additional energy was supplied to the liquid and that the nucleation that occurred around the steel balls was not caused by the balls maintaining a high level of superheat, but because the steel balls provided enhanced nucleation.

Measurements of the inner wall temperature indicated that the wall may be superheated (i.e., higher than the refrigerant's saturation temperature) during most of the test. A thermocouple was placed on the wall about 10 mm from the bottom of the vessel. As shown in Figure 6.14, the wall was slightly subcooled as the solenoid valve was opened, but quickly became superheated within two seconds after the start of the test. Data are shown for both a baseline test and a steel shot test. Because the glass had a relatively low thermal conductivity (1.4 W/m-K vs. 237 W/m-K for aluminum, for example), cooling of the glass wall was delayed resulting in a superheated wall temperature for all but the first two seconds of the test. The baseline test increased wall superheat for four seconds and maintained about 10 °C for the rest of the test. For the steel ball enhancement test, the inner wall superheat was 5.2°C at the end of the test. It was hypothesized that the wall superheat was lower for the steel shot test because the liquid was quite agitated as vapor bubbles rose from the steel balls. This increased the heat transfer coefficient resulting in lower wall temperatures. Furthermore, close observation of several steel shot enhancement experiments showed that the majority of
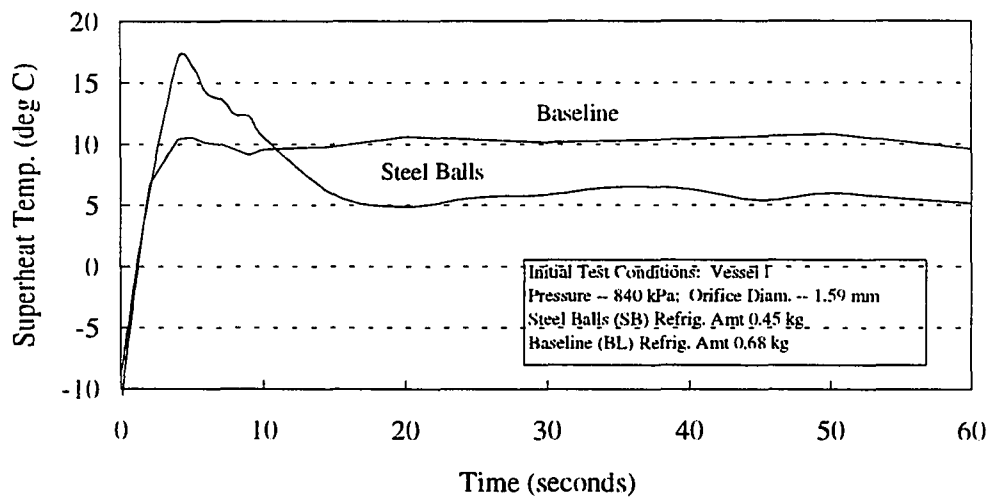
Figure 6.14. Amount of superheat for inner wall during a baseline and a steel shot test.

the vapor nucleation occurred at the intersection of the vessel bottom (and wall) and

each steel ball. Therefore, the delayed cooling of the vessel wall created a superheat

that promoted vapor bubble growth production at locations where the each steel ball was

in contact with the glass. This supported the findings of Chuah and Carey (1987) who

found that the layer height of small copper and glass beads had very little influence on

the heat flux since the majority of the boiling took place below the lowest layer of

spherical balls.

ANALYSIS AND RESULTS OF OIL MIXTURE FLASH BOILING EXPERIMENTS

A series of tests were run with a small percentage of oil mixed with the

refrigerant. The experiments were performed to see if a small amount of mineral oil

changed the mass flow characteristics during flash boiling. Refrigerant grade mineral

oil was added to the refrigerant reservoir used to supply liquid to the test vessel. The

mineral oil was injected into the pressurized refrigerant reservoir vessel which contained

a known amount of refrigerant. Mineral oil was added with an oil pump to four percent

concentration by volume. Experiments were run using varied orifice diameters (1.59

and 5.56 mm), two initial refrigerant amounts (0.23 and 0.68 kg), an initial pressure of

840 kPa, and two vessel geometries (I and II). Pressures, temperatures, and mass flow

rates, along with calculated saturation temperatures, amounts of superheat, mass flux,

and total mass flashed were used to compare the baseline experiments with the

enhanced boiling method. A visualization study shows pictures of the flash boiling

process at time 0, 1, 5, and 20 seconds. Plots of the mass flow rates, pressures, and total

mass are also presented.

Visualization Study of Oil Mixture Flash Boiling Experiments

Figures 6.15 through 6.18 show pictures of the flashing process with the 4% oil

mixture at times 0, 1, 5, and 20 seconds. The initial test conditions for this experiment

were set at 839 kPa, 5.56 mm orifice diameter, 0.68 kg of refrigerant and Vessel I.

Figure 6.15 shows the vessel just prior to opening the solenoid valve. The initial liquid

level is indicated. After the solenoid valve was energized, a cloud of vapor mist rose

from the surface, which stopped before one second had passed. Vapor bubbles then

formed at the liquid surface primarily at the perimeter. The surface then became

agitated. As the larger bubbles burst, an approximately 1 cm high layer of foam formed

on top of the liquid. The foam can be observed in Figure 6.16 which shows the vessel at

one second. The pressure had dropped to 280 kPa and 0.019 kg of the refrigerant had

been flashed. The cooling of the liquid surface caused a visible circular motion

downward along the wall and upward in the center. As was measured in the some of the

baseline tests, this mixing was expected to quickly bring the bulk liquid near the

saturation temperature. Vapor bubbles continued to form within the liquid and by 5

seconds (Figure 6.17), the layer of foam still existed as entrained liquid reached the top
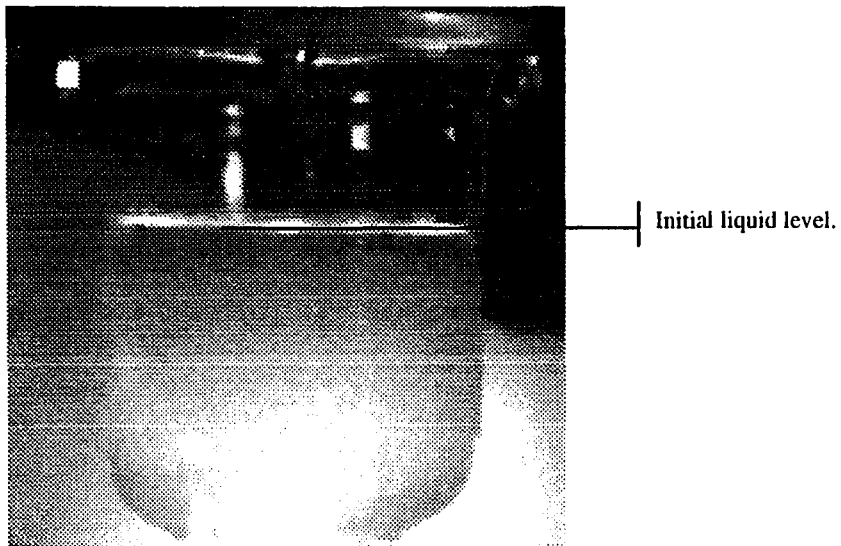
Figure 6.15. Picture of Vessel I with 4% oil added prior to activation of solenoid valve. Initial test conditions were: 839 kPa, 5.56 mm orifice diameter, 0.68 kg refrigerant amount.

Initial liquid level.

About 1 cm layer of foam developed on top of the liquid surface.
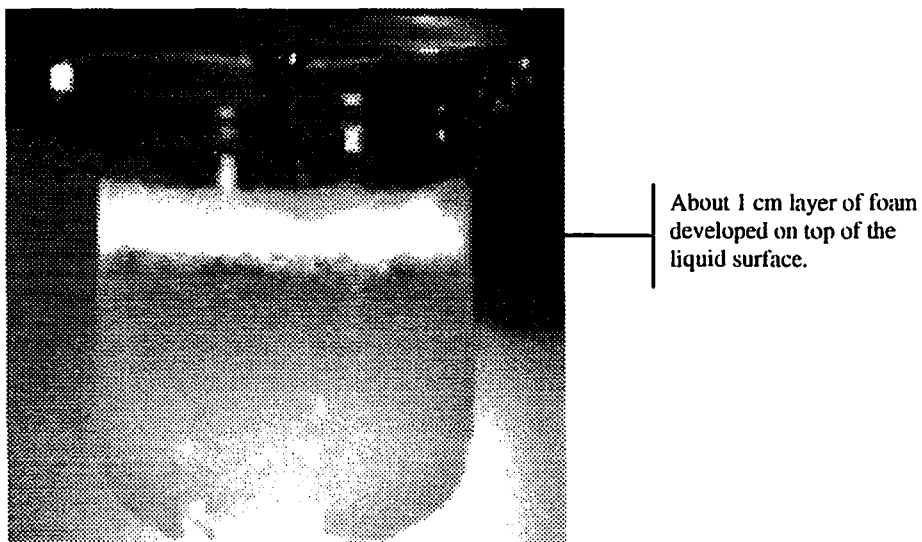
Figure 6.16. Picture of Vessel I with 4% oil added one second after activation of solenoid valve. Measured conditions at one second were: 280 kPa, 5.56 mm orifice diameter, 0.019 kg of R-22 flashed.
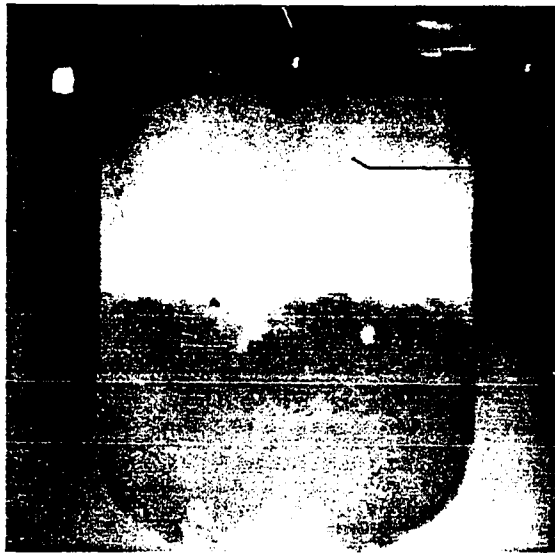
Bursting of multiple vapor
bubbles caused entrained liquid
to travel upward and the top half
of the vessel to fill with a two-
phase mixture.

Foam layer still existed at 5 seconds.

Figure 6.17. Picture of Vessel I with 4% oil added five seconds after activation of solenoid valve.
Measured conditions at five seconds were: 149 kPa, 5.56 mm orifice diameter, 0.040 kg of R-22 flashed.

Thinner layer of foam exists on
the surface of the liquid with
vapor exiting above the foam.

Figure 6.18. Picture of Vessel I with 4% oil added 20 seconds after activation of solenoid valve.
Measured conditions at twenty seconds were: 141 kPa, 5.56 mm orifice diameter, 0.11 kg of R-22
flashed.

of the vessel after large bubbles burst. The pressure had dropped to 149 kPa and 0.040 kg of refrigerant had been flashed.

Twenty seconds into the test, shown in Figure 6.18, the foam layer diminished as the number of observable vapor bubbles rising to the surface decreased. The pressure had dropped 8 kPa to 141 kPa and circulation of the liquid had slowed. Once the foam layer had diminished, a visible spider-web like pattern developed on the surface of the remaining liquid. This pattern moved around on the surface and change configuration. It was hypothesized this was caused by the cooling effect's downward circulation of the refrigerant-oil mixture. This pattern only appeared during the tests containing the added oil mixture. Furthermore, the circulation within the liquid (below the surface) was more visible during the oil mixture tests. This was probably due to the oil only being only partially miscible in R-22 (ASHRAE Refrigeration Handbook, 1994) and not completely mixing which caused it to leave a visible trail during its flow downward.

Comparison of Oil Mixture and Baseline Experiments

Table 6.2 gives a comparison of the baseline experiments and the corresponding experiments where the refrigerant contained 4% mineral oil by volume. Six tests showed a reduction in the total mass flashed while two showed an increase. Only one initial pressure setting was used (840 kPa) for these experiments. This was due to the earlier results that found initial pressure setting had less influence on the mass flow than initial mass of refrigerant and orifice size. Furthermore, no clear correlations between

percent difference and the controlled parameters (initial refrigerant amount, orifice

diameter, vessel size, or initial pressure) were found.

Table 6.2. Percent decrease (-) or increase (+) of total mass flashed for the 4% added
mineral oil mixture tests compared to corresponding baseline tests.

Initial Pressure (kPa)	Vessel Used (I or II)	Orifice Diameter (mm)	Initial Refrig. Amount (kg)	Percent Difference (%)
840	II	5.56	0.45	-27±3
840	II	5.56	0.23	21±4
840	II	1.59	0.45	-28±7
840	II	1.59	0.23	3±5
840	I	5.56	0.68	-18±2
840	I	5.56	0.23	-17±0
840	I	1.59	0.68	-9±4
840	I	1.59	0.23	-14±1

The small amount of oil changed the liquid properties compared to those of the

pure refrigerant. The ASHRAE Handbook of Refrigeration Systems (1994) discusses

the effect of oil on the viscosity of refrigerant. Refrigerant is much less viscous than

mineral oil. Also, mineral oil is only partially miscible in Refrigerant-22 at the lower

pressures seen in the flashing tests (Bosworth, 1952). It was hypothesized that both of

these factors played a role in changing the viscosity, surface tension and other boiling

related properties which changed the bubble growth characteristics during flash boiling.

Table 6.3 provides some property values for both pure R-22 and mineral oil at 20 °C

and 37.8 °C.

Table 6.3. Selected properties for Refrigerant-22 and paraffin-based mineral oil (150 SSU) at 20 °C and 37.8 °C.

Property (units)[1]	R- 22		Mineral Oil (150 SSU)	
	at 20 °C	at 37.8 °C	at 20 °C	at 37.8 °C
Absolute Viscosity (cP)	0.207	0.186	70	32
Density (kg/m³)	1214	1141	865	854
Heat of Vaporiz. (kJ/kg)	188	169	357	not available
surface tension (N/m)	0.0083	0.0062	0.014	not available

[1] References include CRC Handbook of Chemistry and Physics, 1976; CRC Handbook of Tables for Applied Engineering Science, 1976; ASHRAE Handbook of Refrigeration Systems, 1994; ASHRAE Handbook of Fundamentals, 1993: and Carey, 1992.

Two initial test conditions were used for presentation to compare the 4% oil mixture flash boiling test cases with the corresponding baseline tests. The second test condition presented corresponds to the one discussed in the visualization study. The first test used the smallest orifice (1.56 mm) and lowest initial refrigerant amount of 0.23 kg at the initial pressure setting of 840 kPa. Vessel I was used in this experiment. Figures 6.19 and 6.20 show the mass flow rates and pressures for both the pure refrigerant (baseline) and the refrigerant-oil mixture. Both tests started with the same initial conditions and maintained equal values for mass flow rates and pressures for almost 10 seconds before the values became different. After approximately 10 seconds, the baseline case maintained a mass flow rate that averaged 17% higher and a vessel pressure that averaged 18% higher than those of the refrigerant-oil mixture. The reduced internal vessel pressures caused the lower mass flow rates for the refrigerant-oil mixture test. The increased pressure that the baseline test maintained created a greater

Figure 6.19. Mass flow rate vs. time for baseline and oil mixture tests.
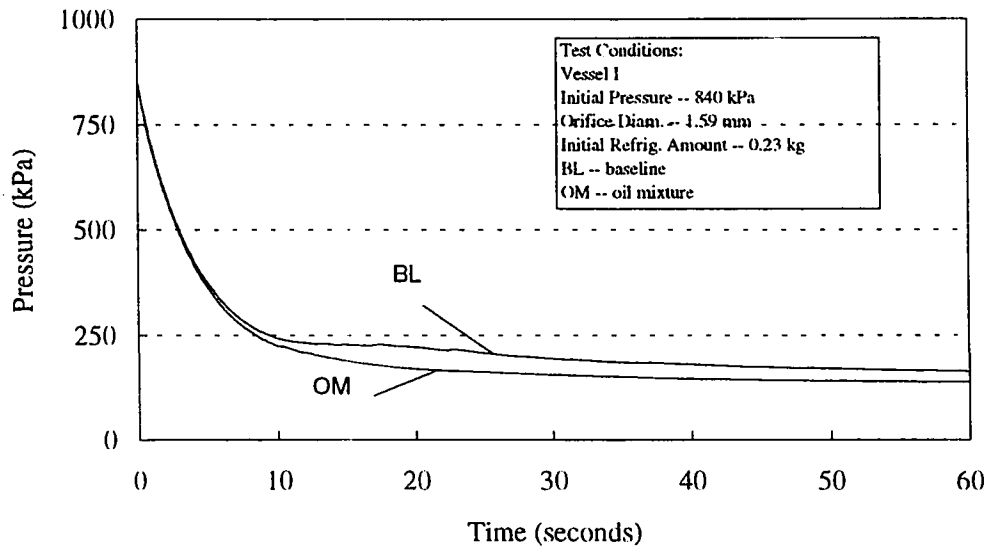
Figure 6.20. Pressure vs. time for baseline and oil mixture tests.

potential for higher evaporation rates during the last 50 seconds. It was hypothesized

that the differences in the pressure were caused from the foam that developed at the

surface of the liquid by suppressing, or condensing, the smaller vapor bubbles before

they burst. Furthermore, the vapor bubbles may have burst underneath the foam layer

which inhibited the flow into the vapor region.

The mass flux had identical profiles as the mass flow rate, differing only in

magnitude. The baseline test had a maximum mass flux of 4550 kg/sec-m^2, and the

refrigerant-oil mixture method peaked at 4140 kg/sec-m^2. As shown in Figure 6.21, the

end result was that the baseline case flashed 0.088 kg while the refrigerant-oil mixture

flashed 0.075 kg.

The second oil mixture test used the largest orifice (5.6 mm) and greatest amount

of initial refrigerant (0.68 kg) at an initial pressure setting of 840 kPa. The 102 mm

inside diameter vessel (Vessel I) was used. Figure 6.22 gives the mass flow rate for the

first 20 seconds of each test. The mass flow rates followed the same path until the

baseline case stopped declining at 1.0 second and rose to a local maximum, at 2.8

seconds, of 0.015 kg/sec before steadily declining. The mass flow rate for the

experiment with the refrigerant-oil mixture dropped for 1.7 seconds and maintained a

value of approximately 0.005 kg/sec until the large increase at 6.3 seconds. A large

single bubble rose from within the liquid, burst at the surface, and caused this spike and

the corresponding pressure increase shown in Figure 6.23. The mass flow rate

momentarily increased to a local maximum of 0.016 kg/sec, before dropping back down
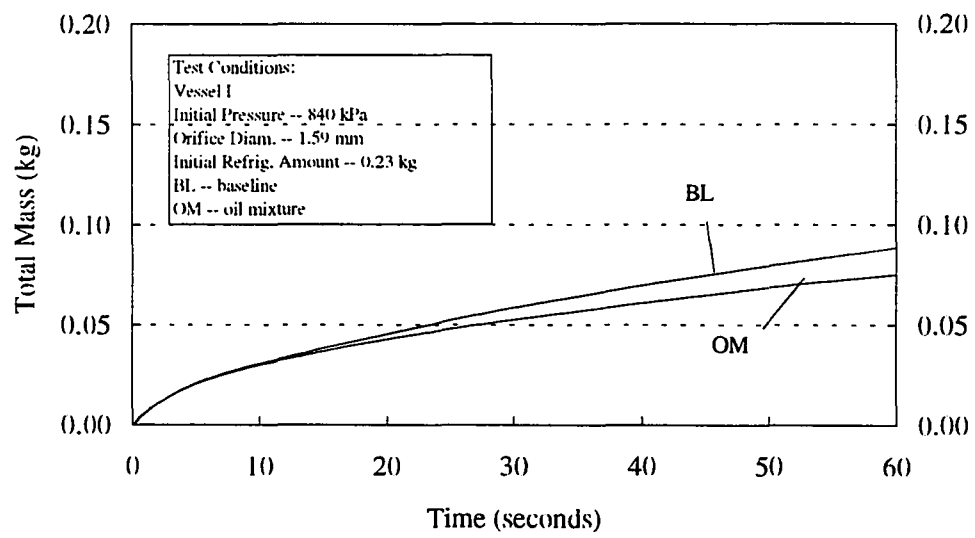
Figure 6.21. Total mass flashed for baseline and oil mixture tests.
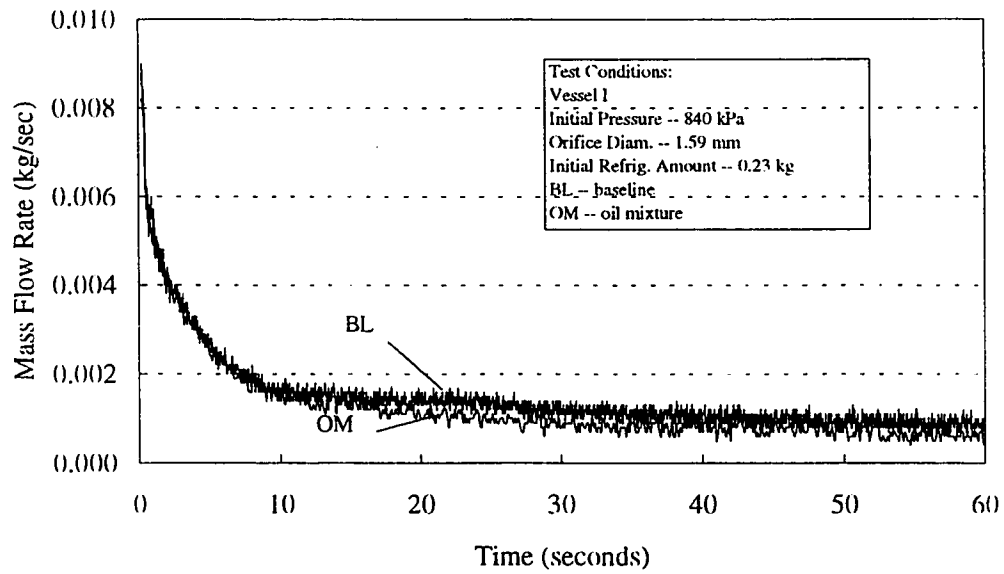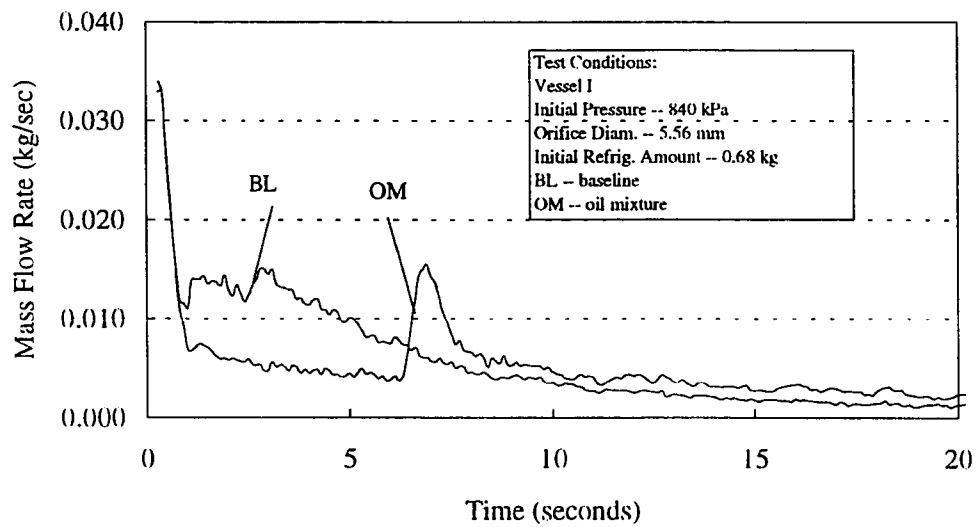
Figure 6.22. Mass flow rate for baseline and oil mixture tests.
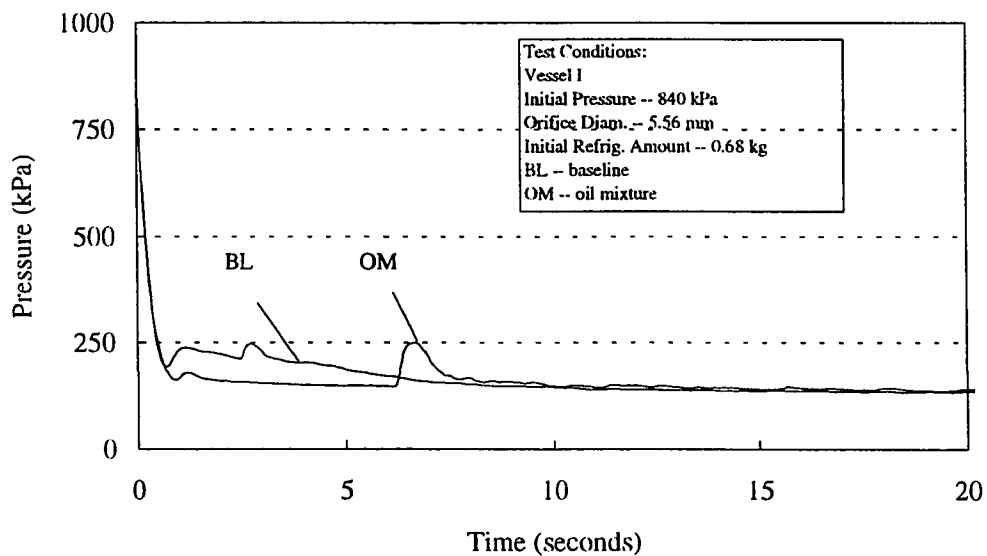
Figure 6.23. Pressure vs. time for baseline and oil mixture tests.

to 0.005 kg/sec at 8.4 seconds and declining at a lesser rate after that. It was

hypothesized that the refrigerant-oil mixture caused an increase in the surface tension of

the fluid. Pure paraffinic mineral oil has a higher surface tension than Refrigerant-22 at

the same temperature (Table 6.3). At low oil concentrations (4% in this case), the

mixture would be completely miscible until the temperature drops below about -15 °C

(Bosworth, 1952) and enters the partially miscible region. It was hypothesized that the

flashing characteristics were the same between the baseline and refrigerant-oil mixture

tests until the oil became partially miscible and changed the surface characteristics of the

liquid. Higher concentrations of oil may have formed at the surface which caused the

higher surface tensions and prevented the same rate of bubble growth (as the baseline

test) and vapor release. To demonstrate the impact of increased surface tension, the

Young-Laplace equation (6.1) can be used. The pressure inside the bubble, P_{inside}, is

greater than that on the inside by the amount of $2\sigma / r$. For example, assuming a bubble

radius of 1×10^{-6} m and a saturated fluid temperature of 20 °C, the surface tension of pure

R-22 would be 0.0083 N/m. If the added mineral oil caused an

$$P_{inside} = P_{outside} + \frac{2\sigma}{r_{bubble}} \qquad 6.1$$

increase in surface tension to 0.01 N/m, the pressure inside the bubble would increase

from 926.2 kPa to 929.6 kPa for each bubble. More energy would be required to form a

bubble with higher internal pressures than a bubble the same size and with the same

surrounding pressure, but with a lower liquid surface tension. Therefore, for the case

containing oil, each bubble maintained a higher internal energy level before bursting which resulted in less vapor production (i.e., total mass flashed) for the same energy input from the surroundings.

The baseline test had a maximum mass flux of 1400 kg/sec-m^2, and the refrigerant-oil mixture method peaked at essentially the same value (1360 kg/sec-m^2). The baseline pressure dropped to 194 kPa at 0.7 seconds and the refrigerant-oil mixture dropped to 162 kPa. This corresponded to 4.3 °C more superheat for the refrigerant-oil test before boiling began. Figure 6.24 is a plot of the total mass flashed for each test case. The reduction of bubble growth and vapor generation resulted in a net reduction of total mass flashed for the refrigerant-oil mixture test. The baseline case flashed 0.147 kg while the test with 4% oil flashed 0.139 kg.

ANALYSIS AND RESULTS OF ACTIVE ENHANCEMENT BOILING EXPERIMENTS

A 215-watt coiled immersion heater was mounted inside the vessel for some of the flash boiling experiments. As with the baseline experiments, each test was run for sixty seconds and were conducted using varied orifice diameters (1.59 and 5.56 mm), initial refrigerant amounts (0.45 and 0.68 kg), initial pressures (575 and 840 kPa), and vessel geometries (I and II). The smallest initial refrigerant amount was not used as an initial condition because the immersion heater was not mounted low enough in the vessel to be completely immersed in the liquid. Pressures, temperatures, and mass flow rates,
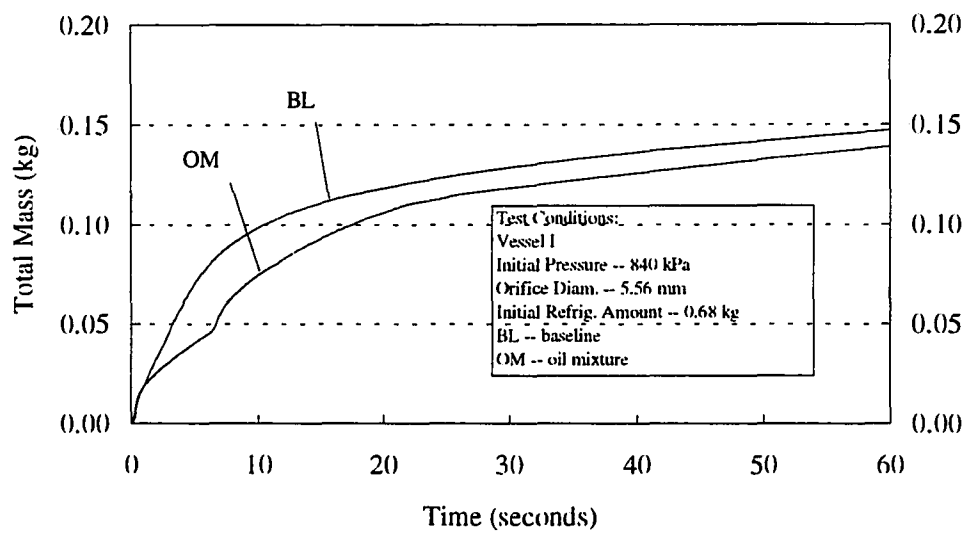
Figure 6.24. Total mass flashed for baseline and oil mixture tests.

along with calculated saturation temperatures, amounts of superheat, mass flux and total

mass flashed were used to compare the baseline experiments with the enhanced boiling

method. A visualization study shows pictures of the flash boiling process at time 0, 1, 2,

and 20 seconds. Plots of the mass flow rates, pressures, and total mass are also

presented.

Visualization Study of Active Enhancement Method

Videos of the active enhancement experiments were used to observe and study

the flash boiling process prior to analyzing the detailed quantitative results. One example

test condition was considered for presentation in this section. This test used Vessel I and

had initial conditions set at 841 kPa, 5.56 mm orifice diameter, and 0.68 kg of

refrigerant. Figures 6.25 through 6.28 show pictures of the flashing process with the

immersion heater at times 0, 1, 2, and 20 seconds.

Figure 6.25 shows the initial liquid level and the entire vessel with the immersion

heater just prior to opening the solenoid valve. Figure 6.26 shows the vessel one second

into the depressurization process. The pressure had dropped to 322 kPa and 9% of the

total flashed refrigerant had left the vessel. At one second, boiling had begun on the

lead wire that was the first part of the immersion heater to receive electrical current.

Bubbles first formed on the lead arm, and then, in a circular motion inward, began

forming on the coil heater with the center being the last area for bubbles to appear. At

two seconds, the entire heater was generating vapor bubbles and the pressure increased

Intial liquid level.
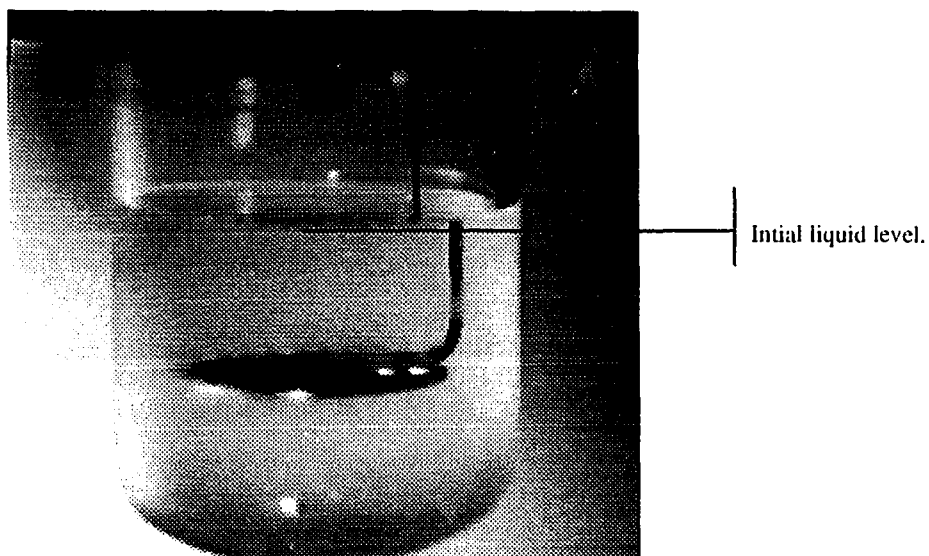
Figure 6.25. Picture of Vessel I with 215-watt immersion heater prior to activation of solenoid valve. Initial test conditions were: 841 kPa, 5.56 mm orifice diameter, 0.68 kg refrigerant amount.

Vapor bubble nucleation first began on the arm of the immersion heater which first received electrical current.
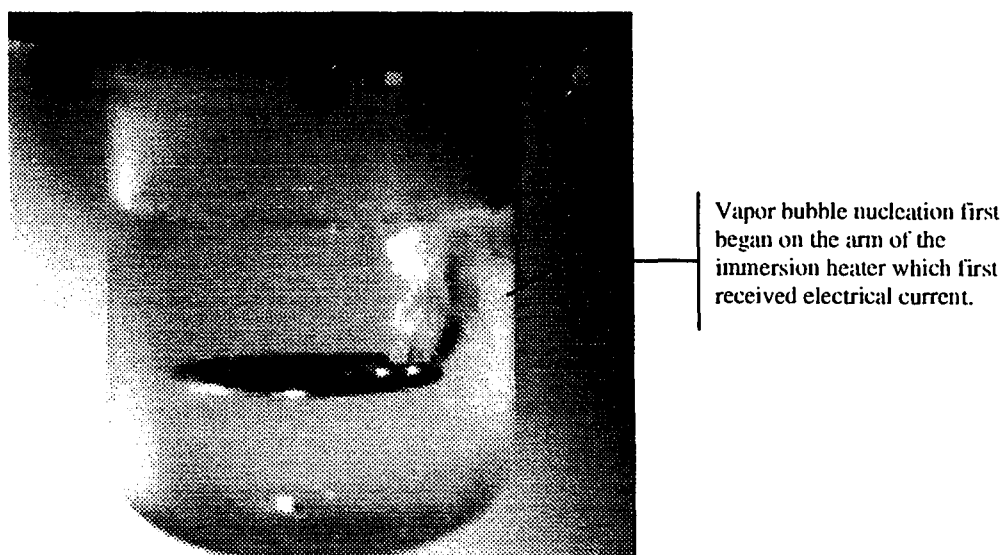
Figure 6.26. Picture of Vessel I with 215-watt immersion heater one second after activation of solenoid valve. Measured conditions at one second were: 322 kPa, 5.56 mm orifice diameter, 0.022 kg of R-22 flashed.

Vessel filled with two-phase mixture as the entire heater has vapor bubbles developing on it
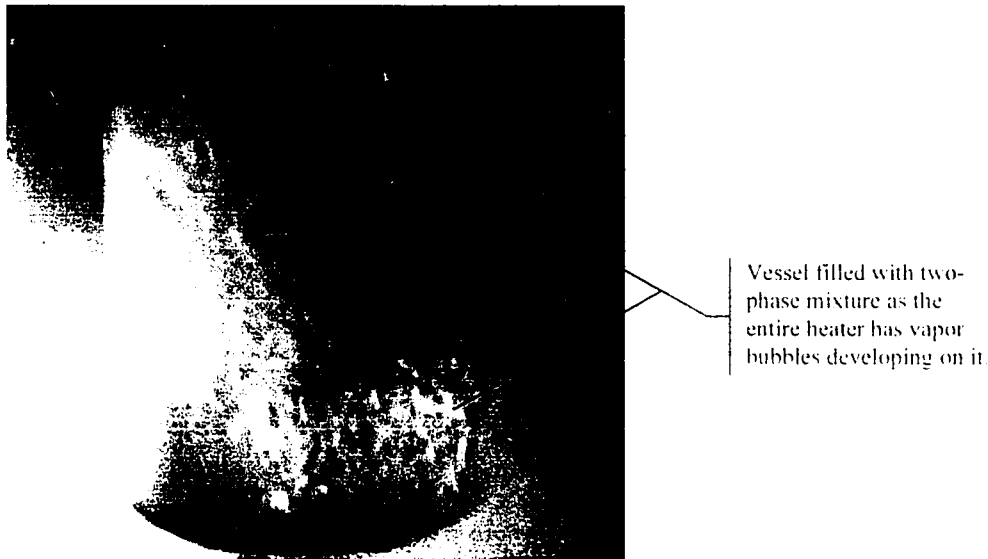
Figure 6.27. Picture of Vessel 1 with 215-watt immersion heater two seconds after activation of solenoid valve. Measured conditions at two seconds were: 390 kPa, 5.56 mm orifice diameter, 0.048 kg of R-22 flashed.

Bubble generation still occuring at 20 seconds. Heater wall superheat was approximately 2.3 °C
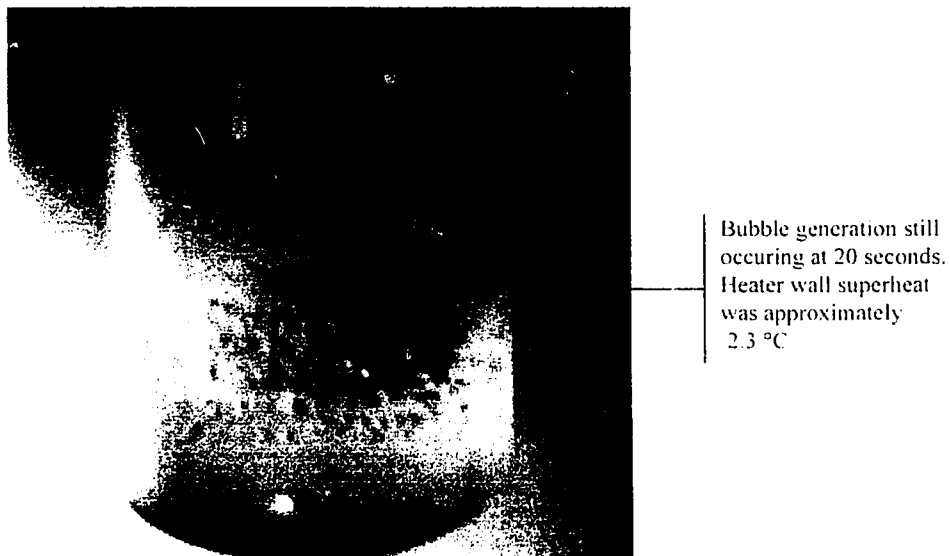
Figure 6.28. Picture of Vessel 1 with 215-watt immersion heater 20 seconds after activation of solenoid valve. Measured conditions at 20 seconds were: 141 kPa, 5.56 mm orifice diameter, 0.188 kg of R-22 flashed.

to 390 kPa (shown in Figure 6.27). It was hypothesized that the pressure increase occurred because the increased vapor production was momentarily greater than the total mass exiting the vessel through the orifice. As in the steel shot passive enhanced method, the vessel was momentarily filled with a two-phase mixture resulting in higher mass flow rates from entrained liquid exiting the vessel. Eighteen seconds later, as shown in Figure 6.28, the pressure had dropped to 141 kPa, and 77% of the total flashed refrigerant had left the vessel. Bubbles formed on the electric heater throughout the entire 60 second experiment. Based on observations, the bubbles had a different shape than the vapor bubbles formed within the steel shot, oil mixture and the baseline experiments. The bubbles formed on the immersion heater were spherical in shape and more consistent in size as compared to those formed within the layer of steel shot discussed earlier in the chapter.

Comparison of Active Enhancement and Baseline Experiments

Table 6.4 gives a comparison of the baseline experiments and the corresponding experiments using a 215-watt immersion heater as an active enhanced boiling method. Results showed an increase in the total mass flashed at each test condition ranging from an average 47% to 111% increase with respect to the baseline experiments. Initial test conditions using the minimum level of refrigerant (0.23 kg) were not considered because the immersion heater was not long enough to be completely immersed in the liquid. Furthermore, no clear correlations between percent increase and the controlled

parameters (initial refrigerant amount, orifice diameter, vessel size, or initial pressure)

were found.

Table 6.4. Percent increase of total mass flashed for the active enhanced boiling method (immersion heater) compared to corresponding baseline tests.

Initial Pressure (kPa)	Vessel Used (I or II)	Orifice Diameter (mm)	Initial Refrig. Amount (kg)	Percent Increase (%)
840	II	5.56	0.45	57±1
840	II	1.59	0.45	47±3
840	I	5.56	0.68	49±2
840	I	5.56	0.45	84±22
840	I	1.59	0.68	73±15
840	I	1.59	0.45	93±19
575	I	5.56	0.68	47±1
575	I	5.56	0.45	111±5
575	I	1.59	0.68	56±7
575	I	1.59	0.45	68±15

Two test conditions were used to compare the active method enhanced flash

boiling test cases with the corresponding baseline tests. The detailed analysis and

comparison is presented in this section. The second test condition presented

corresponded to the one discussed in the visualization study. The first test condition

used the smallest orifice (1.56 mm) and an initial refrigerant amount of 0.45 kg at the

initial pressure setting of 840 kPa. The experiment utilized Vessel I. Figures 6.29 and

6.30 show the mass flow rate and pressure profiles for both the baseline and electric

immersion heater enhanced tests. The baseline mass flow rates and pressures gradually

declined to minimum values while the electric immersion test departed from this trend

Figure 6.29. Mass flow rate vs. time for baseline and immersion heater test.
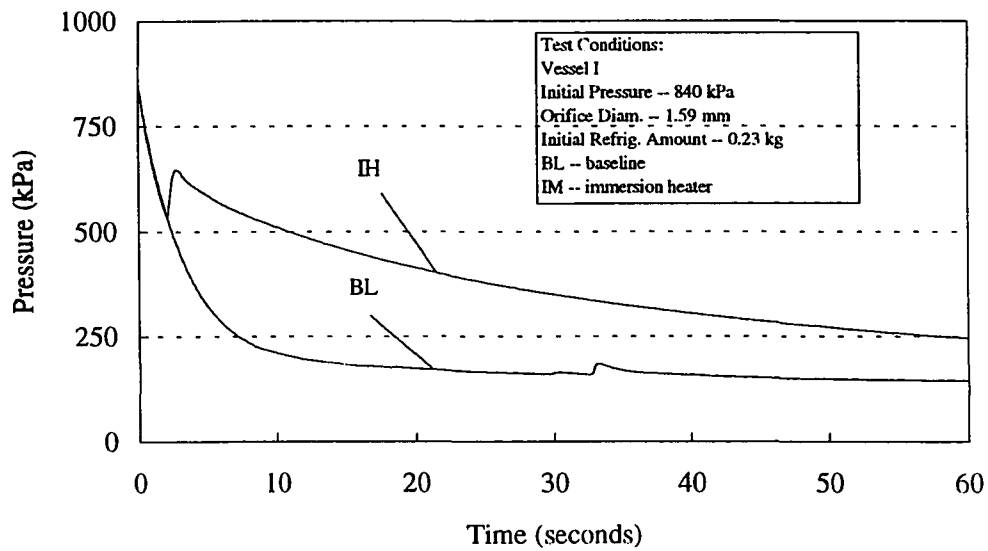
Figure 6.30. Pressure vs. time for baseline and immersion heater tests.

after two seconds as the entire heater generated vapor bubbles. The mass flow rate
increased 30% from 0.0037 kg/sec at 2.0 seconds to 0.0048 kg/sec at 3.2 seconds. The
pressure increased 20% from 538 kPa to 647 kPa in 0.7 seconds. The increases
corresponded to the same time boiling began on the immersion heater. The mass flux
had identical profiles as the mass flow rate, differing only in magnitude. The baseline test
had a maximum mass flux of 4950 kg/sec-m^2, and the enhanced method peaked at 4250
kg/sec-m^2.

After peaking, the mass flow rates and pressures declined faster than the baseline.
After the initial depressurization, vapor bubbles were only visibly being formed on the
electric heater with none found on the vessel wall or in the bulk liquid. The increased
vapor generation from the immersion heater raised the pressure within the vessel which
resulted in the flow being choked for the entire 60 seconds as compared to the baseline
case which was choked for only 9.8 seconds. The additional vapor caused a larger total
mass flashed from the vessel. In this case, the enhanced test flashed 0.159 kg as
compared to the baseline experiment which flashed 0.074 kg (shown in Figure 6.31).

The second test used the largest orifice (5.6 mm) and the greatest amount of
initial refrigerant (0.68 kg) at an initial pressure setting of 840 kPa. The 102 mm inside
diameter vessel (Vessel 1) was used. Figure 6.32 shows the mass flow rate for both the
baseline and the active enhanced boiling experiments. Mass flow rates for both cases had
approximately the same value for the first 0.6 seconds until boiling began on the
immersion heater. The immersion heater test case reached a local minimum at 1.0
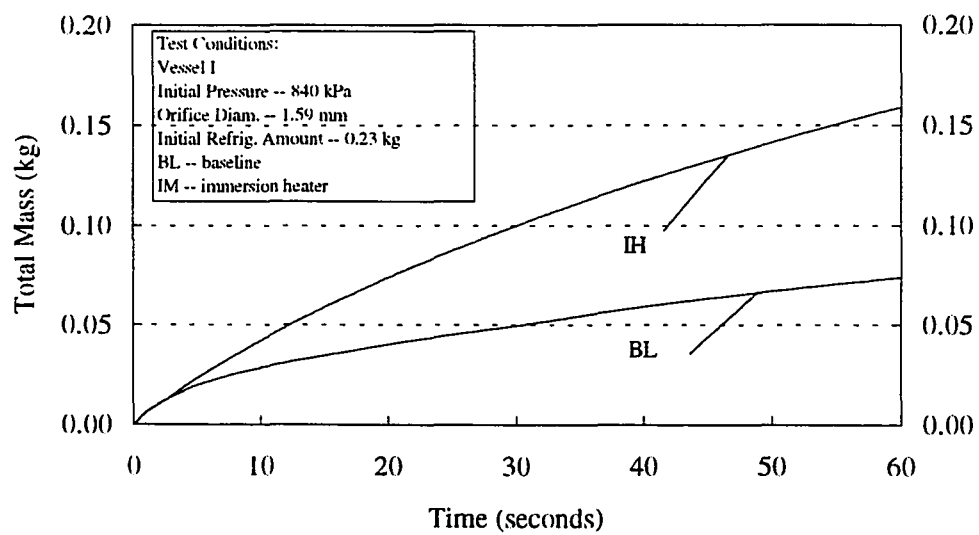
Figure 6.31. Total mass flashed for baseline and immersion heater tests.
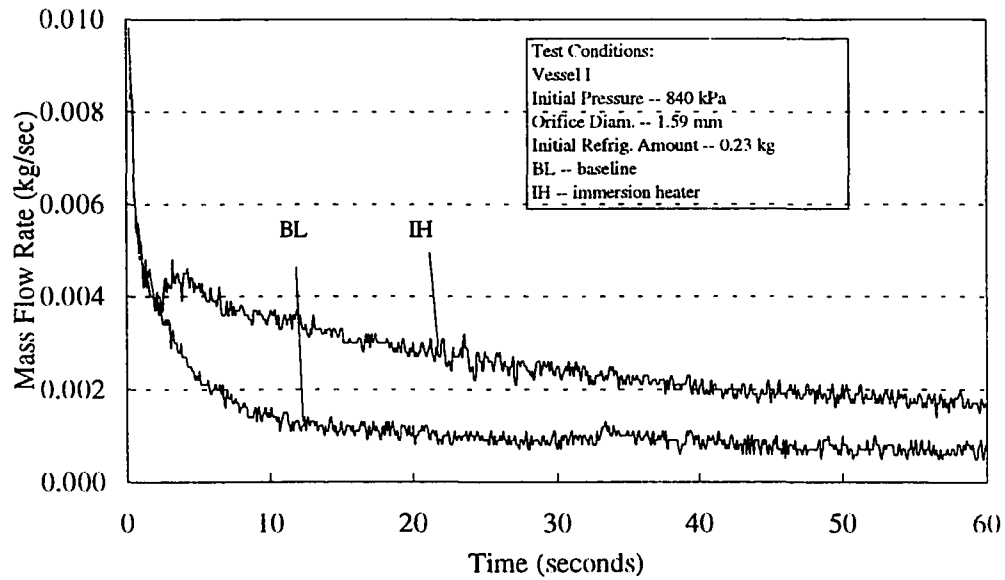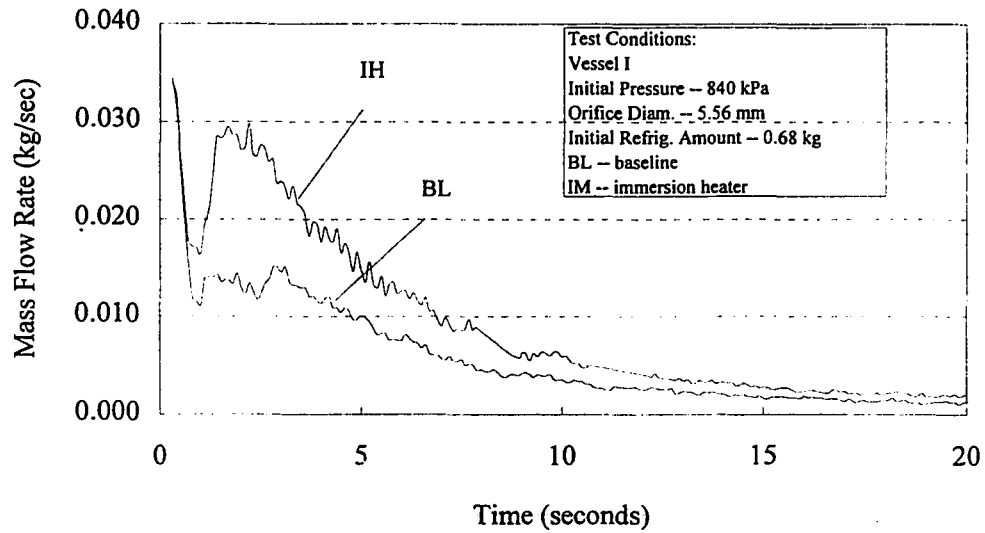
Figure 6.32. Mass flow rate vs. time for baseline and immersion heater tests.
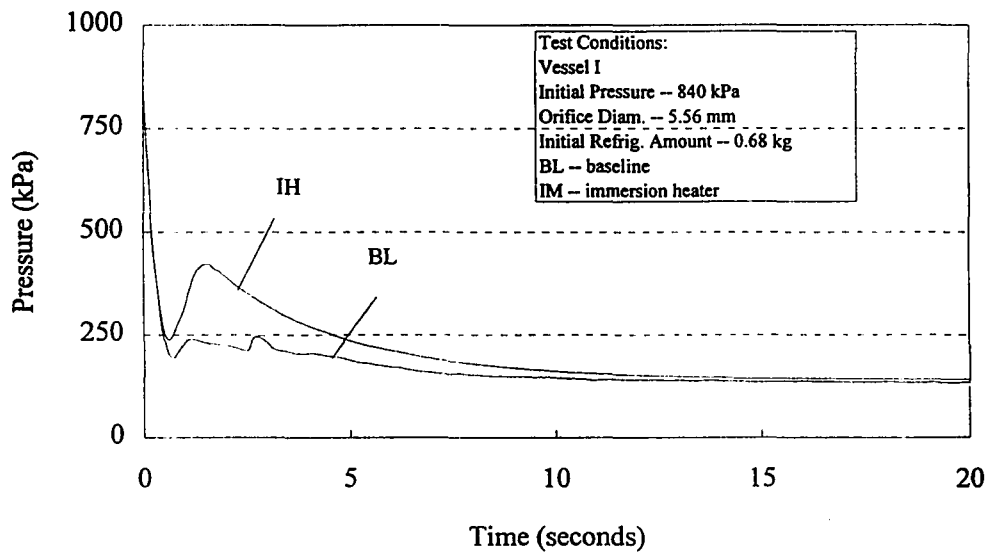
Figure 6.33. Pressure vs. time for baseline and immersion heater tests.

second (0.016 kg/sec) before nearly doubling to 0.030 kg/sec at 2.2 seconds. The baseline case followed the same trends as the enhanced method reaching a minimum mass flow rate of 0.011 kg/sec at 1.0 seconds and rising to 0.015 kg/sec at 2.8 seconds before proceeding downward for the rest of the test.

Both cases had drops in pressure (Figure 6.33) to a local minimum before the superheated liquid began generating vapor within the vessel and increasing the pressure. The enhanced case reached a minimum at 0.6 seconds and a pressure of 238 kPa. This corresponded to 38 °C superheat . The pressure for the baseline case dropped below that of the enhanced method to 194 kPa at 0.7 seconds which corresponded to the liquid being five degrees more superheated, based on the measured vessel pressure. The temperature of the immersion heater was measured during three experiments. The data showed the heater surface to be warmer than the liquid, resulting in a superheated surface with potential for bubble growth. In one experiment, boiling began on the heater surface after about one second. The heater became hotter than the liquid at nine seconds and maintained an average 2.3 °C superheat during the last 50 seconds of the experiment. Calculations showed that the heater was operating with a heat flux of about 40 kW/m². The boiling was found to be nucleate pool boiling, because the heat flux was well below the calculated maximum pool boiling heat flux (360 kW/m²) for a large horizontal cylinder (Lienhard and Khir, 1973). This heater's measured heat flux corresponded to a wall superheat of approximately 7.5 °C based on dimensional analysis and optimal fit correlations by Stephan and Abdelsalam (1980) for nucleate boiling of

refrigerant. It was hypothesized that the difference may have occurred because of two factors, 1) the accuracy of the heat flux correlation and 2) the method of temperature measurement. First, highly accurate models for predicting heat flux are not available. Existing models of nucleate boiling heat transfer are "at best, crude idealizations" (Carey, 1992). Secondly, a 44-gauge thermocouple was placed on the surface of the immersion heater with only the base of the thermocouple bead in contact with the surface. Bubble formation near (or under) the thermocouple junction may have skewed the temperature reading by cooling the portion of the thermocouple bead not in contact with the heater surface.

Pressures increased to local maximums as vapor was released from bursting bubbles. The baseline test increased 45 kPa (or 23%) before receding again, while the enhanced case increased 183 kPa (or 77%) with respect to the minimum pressures.

The mass flux for the baseline case had a maximum value of 1400 kg/sec-m^2, while the enhanced method peaked at 1420 kg/sec-m^2. Figure 6.34 shows the total mass flashed during each 60 second test. The enhanced case diverged from the baseline values throughout the entire test because of the increased vapor production and therefore, increased mass flow. The electric enhanced case released 0.245 kg (or 36% of the initial amount) from the vessel while the baseline test flashed 0.147 kg (or 22% of the initial amount).

The immersion heater used in all of the active enhanced experiments had a rated power of 215-watts. Measurements during actual experiments found that the heater
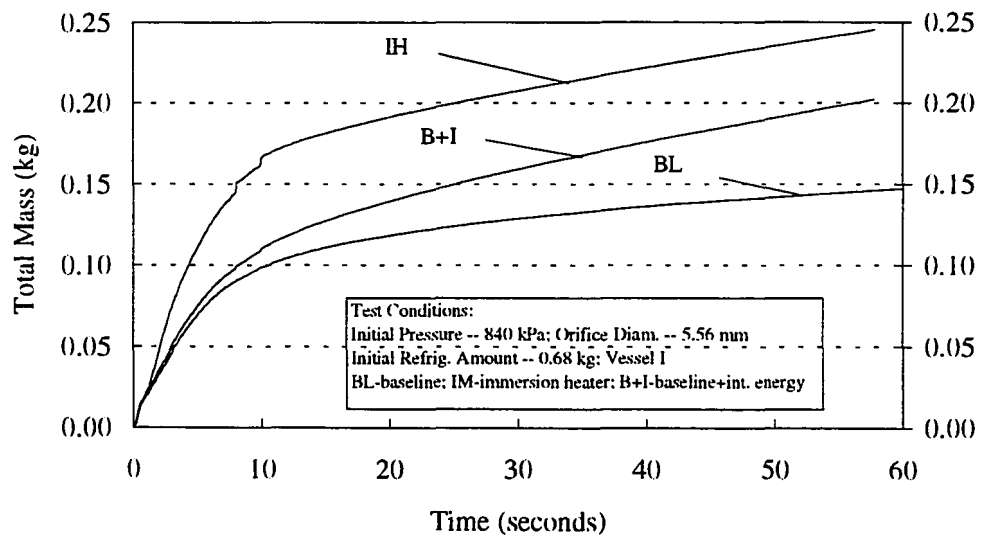
Figure 6.34. Total mass flashed for baseline test, baseline plus steel ball internal energy,
and immersion heater test.

drew 1.75 amps at 122 volts, resulting in a measured power of 214-watts. This heat

energy input into the liquid refrigerant provided additional energy for the heat of

vaporization. This energy was primarily taken from the bulk liquid and glass vessel in

the baseline experiments causing the rapid cooling of the liquid. During each sixty

second test, the heater added approximately 12.8 kJ of energy to the liquid. This

corresponded to 25% of the calculated energy transferred from the liquid refrigerant

during the vaporization process at the lower initial setting discussed above (0.45 kg

initial amount, 840 kPa, 1.59 mm orifice diameter, and 0.159 kg flashed) and 16% of the

energy transferred at the maximum setting presented (0.68 kg initial amount, 840 kPa,

5.56 mm orifice diameter, and 0.245 kg flashed). Furthermore, it was calculated that the

12.8 kJ of energy input had the potential to vaporize about 0.056 ± 0.006 kg of

refrigerant based on the corresponding heat of vaporization for the entire range of

possible pressures. Figure 6.34 also shows this graphically for the given initial test

condition. The added energy (and vaporization) compared closely to the measured

increase of refrigerant released during the electric tests which averaged 0.068 ± 0.02 kg

increase in flashed refrigerant.

The stainless steel surface of the electric heater maintained a temperature higher

than the liquid (which was near the saturation temperature) creating a superheated

surface (2.3 °C) that promoted large and steady quantities of vapor bubbles. These

measurements were confirmed by the semi-theoretical model derived by Hsu (1962).

This model can be arranged to predict the amount of superheat required for active

nucleation sites to exist or it can predict the size of surface cavities that would be active with a given surface superheat. Calculations at conditions seen near the end of an experiment (saturated at 125 kPa) found that small cavities on the heater surface (or any other surface for that matter) would be capable of becoming active bubble nucleation sites with a minimum wall superheat of 1.6 °C.

SUMMARY OF RESULTS FOR ENHANCEMENT EXPERIMENTS

A selection of three enhancement techniques were chosen to determine their influence on the mass flow characteristics during flash boiling from a small vessel. They included two passive techniques: the addition of 3.6 mm diameter steel balls to the base of the vessel and the addition of 4% (by volume) of mineral oil to the refrigerant. The other method tested was an active method: the addition of electric resistance heat by immersing a heater into the liquid. Like the baseline tests, experiments were run for 60 seconds and used varied orifice diameters (1.59 and 5.56 mm), initial refrigerant amounts (0.23, 0.45, and 0.68 kg), initial pressures (575 and 840 kPa), and vessel geometries (I and II). A visualization study along with the analysis and discussion of the measured experimental results from using each potential enhancement method compared with baseline experiments were discussed in this chapter.

A 10 mm layer of 3.6 mm diameter steel balls (or steel shot) was added to the vessel during some of the flashing experiments. A visualization study showed that vapor generation was greater for the tests with steel balls compared to baseline tests at the

same condition. Two-phase liquid-vapor swell of the entire fluid was also more

common. Observations of the experiments showed that most of the bubble formation

within the steel balls occurred at the bottom layer at the intersection of the glass and

each steel ball. Measured results showed an increase in the total mass flashed for the

steel shot tests ranging from an average 21% to 81%. A comparison between two

baseline tests and two steel ball enhancement tests at the same initial conditions revealed

differences in the mass flow rates and pressures once boiling within the layer of steel

balls began. In general, the tests with steel shot had greater increases in mass flow rates

and pressures after boiling began because larger amounts of vapor were produced.

When the smaller orifice (1.59 mm diameter) was used, pressures were substantially

greater during the tests and flow was choked for the entire test. The steel shot added the

equivalent of 3.5 kJ to 4.5 kJ of energy to the vessel during the flashing process.

Calculations showed that the steel balls were superheated, but by less than 1°C.

Measurements of the inner wall found that it was superheated during most of the test and

it was hypothesized that the majority of bubble growth occurred at the intersection of the

steel balls and the superheated glass wall. This supported the findings of Chuah and

Carey (1987) who found that the layer height of small copper and glass beads had very

little influence on the heat flux since the majority of the boiling took place below the

lowest layer of spherical balls.

A series of tests were run with a mixture of refrigerant and mineral oil. A 4%

concentration (by volume) was used and a visualization study showed the boiling to be

similar to baseline experiments except for a layer of foam that developed at the liquid surface. It was hypothesized that the foam inhibited bubble growth and release of vapor. Measured results revealed a general decrease in average mass flashed during each sixty second test. Compared to baseline experiments, two out of eight test conditions averaged an increase in total mass flashed and six averaged a decrease, ranging from a 21% increase to a 27% decrease. Measured results showed the same general mass flow and pressure trends with the oil mixture tests maintaining slightly lower values. It was hypothesized that more energy was required to grow a bubble under the same conditions except the viscosity was higher for the refrigerant-oil mixture.

A nominal 215-watt immersion heater was mounted inside the vessel for some of the flash boiling experiments. Video results revealed that boiling first began on the lead arm of the heater traveling inward to the center. The vessel quickly filled with a two-phase mixture as bubbles continued to form on the heater. Based on observations, the bubbles were spherical and more consistent in size as compared to the baseline tests and the other enhancement tests. Measured results showed that the immersion heater tests increased the total mass flashed ranging between 47% and 111%. As compared to the baseline tests, the tests including the immersion heater had higher mass flow rates and maintained higher pressures within the vessel during flashing. The temperature of the heater was measured and found to be superheated for the last 50 seconds of the test. The amount of superheat averaged 2.3 °C which was 0.7 °C higher than the calculated amount of superheat necessary for a cavity on the heater surface to actively produce

vapor bubbles. Finally, the immersion heater added a measured 12.8 kJ of energy to the liquid during each sixty second test. This corresponded to less than 25% of the calculated energy transferred from the liquid during the vaporization tests.

In conclusion, two of the three enhancement techniques (steel balls and immersion heater) showed consistent increases in the mass flow during flash boiling from a small vessel. The author believes that the passive enhanced boiling technique would be the better method to use for increase mass flow during flashing. The steel balls would have two major advantages over the immersion heater. First, the implementation cost would be much lower. Electric resistance heaters would cost orders of magnitude more than a layer of steel balls ($100 vs. less than $1 for this case) and operation costs would be negligible for the steel balls, while the immersion heater would have a continuous energy charge associated with its operation. However, if these two cost factors were considered unimportant, the immersion heater would provide a more stable increased mass flow.

CHAPTER VII

COMPARISON OF BASELINE TESTS WITH MODEL PREDICTIONS

Experimental data from the baseline experiments were compared with model predictions for each of the varied test parameters (initial pressure, initial refrigerant amount, orifice diameter, and vessel volume). The model was developed to predict the vessel's rate of depressurization (dP/dt) during flash boiling. The one-dimensional lumped model was derived from basic thermodynamic principles (Chapter 3). Mass flux expressions for single-phase choked flow and the homogeneous frozen model were used in the model. A relatively high mixture quality of 0.9 was chosen for use in the HFM because the visualization study of baseline experiments revealed that the flow through the orifice was seldom two-phase. The model predicted the general pressure and mass flux trends that were observed during the experimental study for each changed test parameter. In some cases, the model predictions deviated from the experimental data and some reasons for their differences are discussed below. Opportunities for modifying and improving the model are also discussed.

INFLUENCE OF VARIED TEST PARAMETERS ON PRESSURE PROFILES

Figures 7.1 through 7.4 give the baseline and predicted pressure profiles for each of the varied test parameters (initial pressure, initial refrigerant amount, orifice size, and vessel volume). In each graph either the HFM or the SPM is presented. A mixture

Figure 7.1 Pressure profiles for baseline data and model predictions at varied initial pressures.

Figure 7.2. Pressure profiles for baseline and model predictions at varied initial refrigerant amounts.

Figure 7.3. Pressure profiles for baseline and model predictions at varied orifice diameters.

Figure 7.4. Pressure profiles for baseline data and model predictions with varied vessel volumes.

quality of 0.9 was used for the HFM resulting predictions close to those predicted by the

SPM. Therefore, only one or the other was given to compare with the baseline data.

When both are shown on one graph, the models would overlay one another. Results for

varied initial vessel pressures (575 kPa and 840 kPa) are shown in Figure 7.1. The

HFM was within 4% (575 kPa) and 8% (840 kPa) of the experimental data during the

first 2 seconds as the pressures fell to around 200 kPa. As in the baseline tests,

predicted pressures for tests at both initial pressures, approached the same values by 4

seconds. For times greater than 4 seconds, pressure predictions dropped below

measured values and continued to diverge from measured values. In each simulated test

case, predicted pressures approached the value of zero because the mass flux models

were critical flow models which are independent of the downstream pressure. The actual

depressurization process approached the reservoir pressure (120 kPa) downstream of the

orifice. An improved depressurization model should include a mechanism to constrain

the pressure from dropping below the downstream reservoir pressure.

Figure 7.2 shows the pressure profiles for flashing tests at the same conditions

except for varied initial refrigerant amounts (0.23 kg and 0.68 kg). A pressure rise in

the experimental data was experienced by the test having the higher initial refrigerant

amount. However, model predictions did not reflect the same type of increase as

pressure values gradually declined near zero. The model was also unable to predict the

pressure increases because of the varying vapor production rates within actual R-22

flashing experiments. Future adjustment to the model might include a correlated

parameter attempting to predict the vapor production rates based on the varied initial

parameters. Figures 7.3 shows the pressure profile for the tests with varied orifice

diameters (3.18 mm and 5.56 mm). Model predictions using the larger orifice (5.56

mm) were closer to the experimental measurements. Finally, predicted pressures for the

case of varied vessel volume (Figure 7.4) showed good agreement during the initial

depressurization process. The model also closely predicted two of the trends that were

observable in the baseline tests: 1) the larger vessel (1106 ml) volume had a faster

pressure drop than the smaller vessel (665 ml) and 2) pressures for both vessels

approached the same value after 7 seconds.

INFLUENCE OF VARIED TEST PARAMETERS ON MASS FLUX PROFILES

Figures 7.5 through 7.8 give the baseline and predicted mass flux profiles for

each of the varied test parameters (initial pressure, initial refrigerant amount, orifice

size, and vessel volume). As with the pressure profiles, only one of the model

predictions (either the HFM or the SPM) was used to compare against baseline data for

each graph. In general, the predicted mass flux followed the same trends as measured

values. Predicted values for the mass flux for varied initial pressures (575 kPa and 840

kPa), shown in Figure 7.5, were higher than measured baseline values for the first five

seconds and were in good agreement, thereafter. In each varied test case, mass flux

values were initially overpredicted by both the single-phase model (SPM) and the

homogeneous frozen model (HFM). Lower baseline mass flux values during the initial
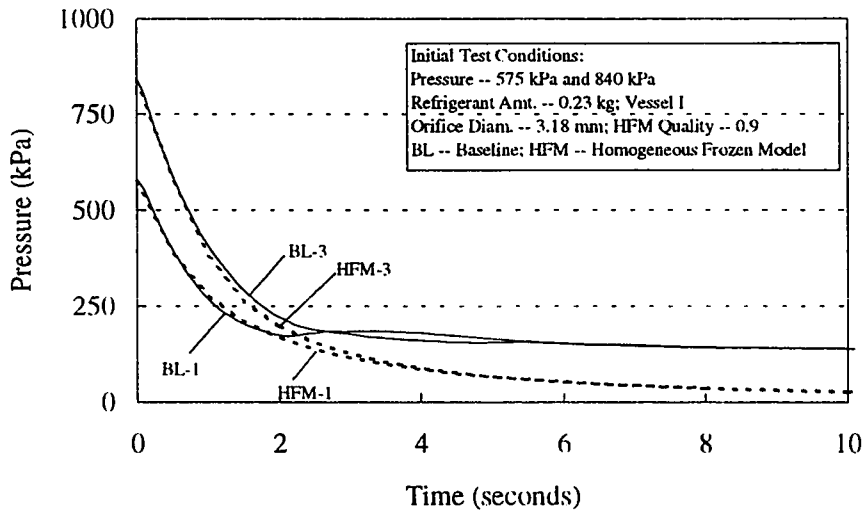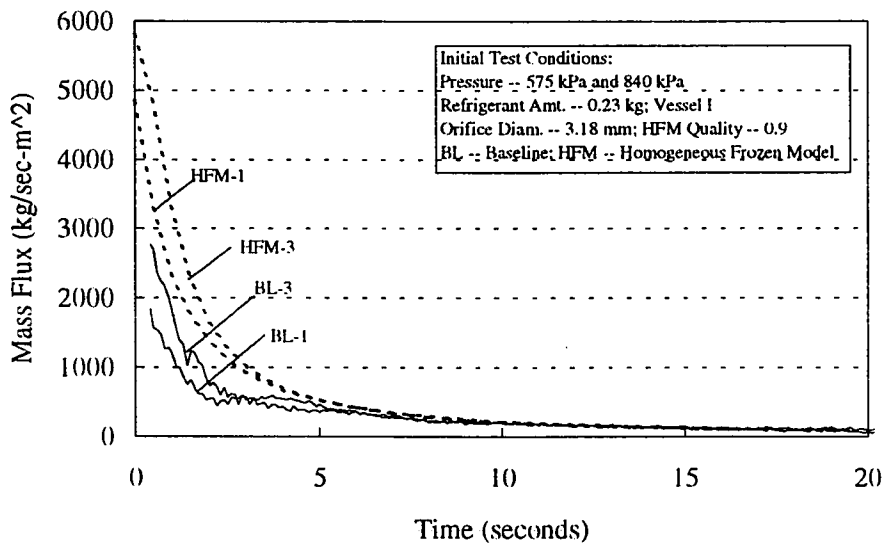
Figure 7.5. Mass flux profiles for baseline data and model predictions at varied initial pressures.
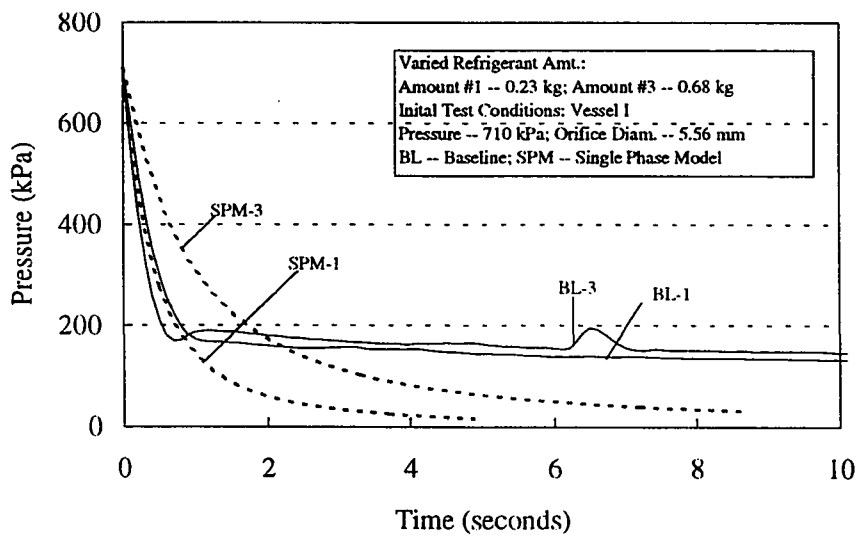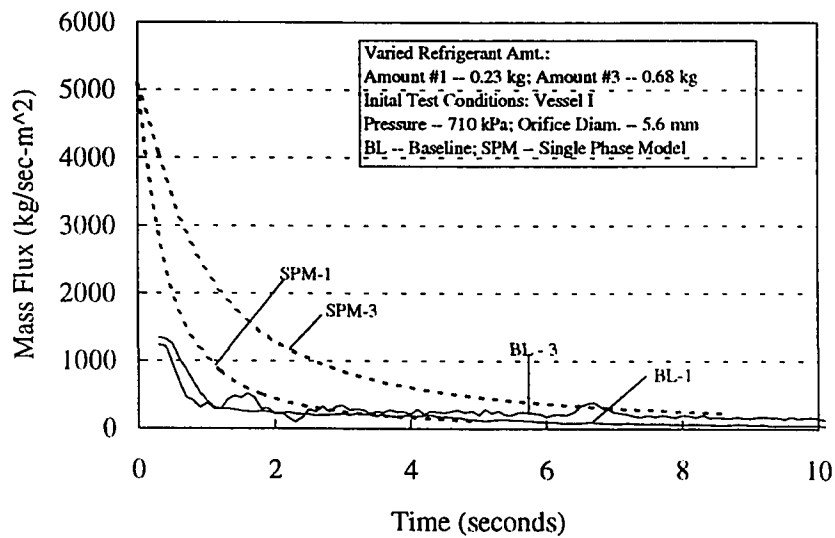

Figure 7.6. Mass flux profiles for baseline and model predictions at varied initial refrigerant amounts.
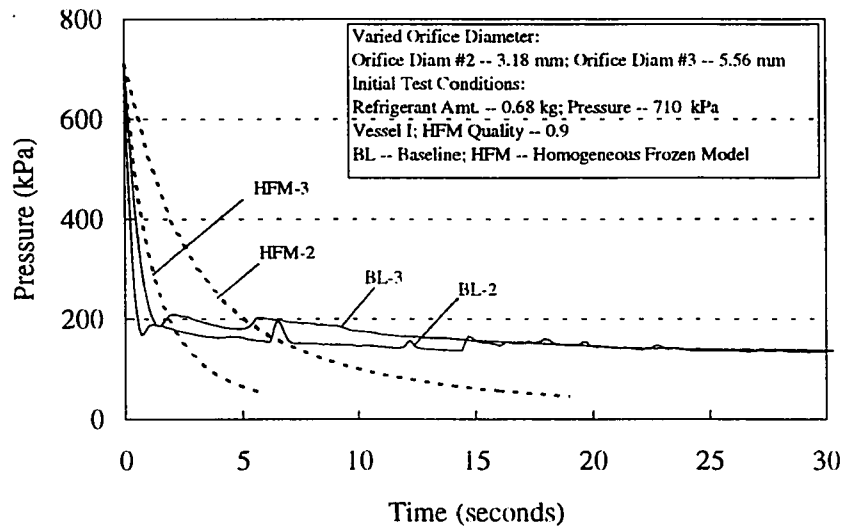
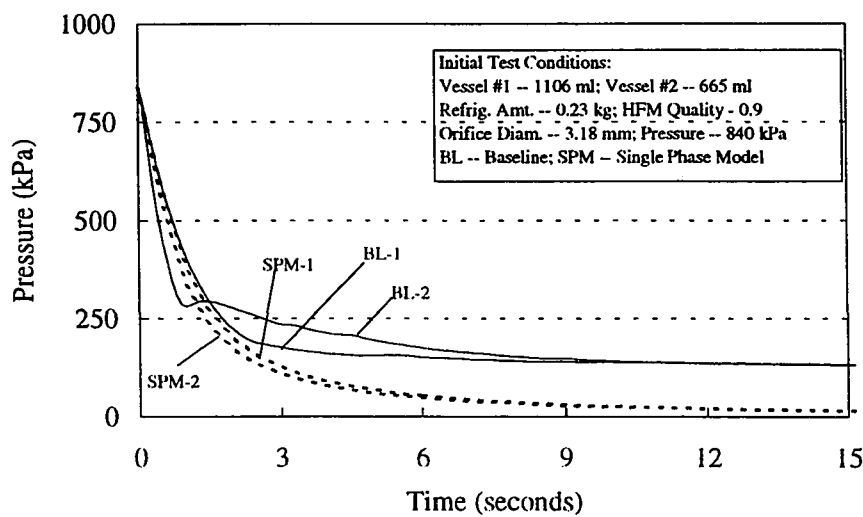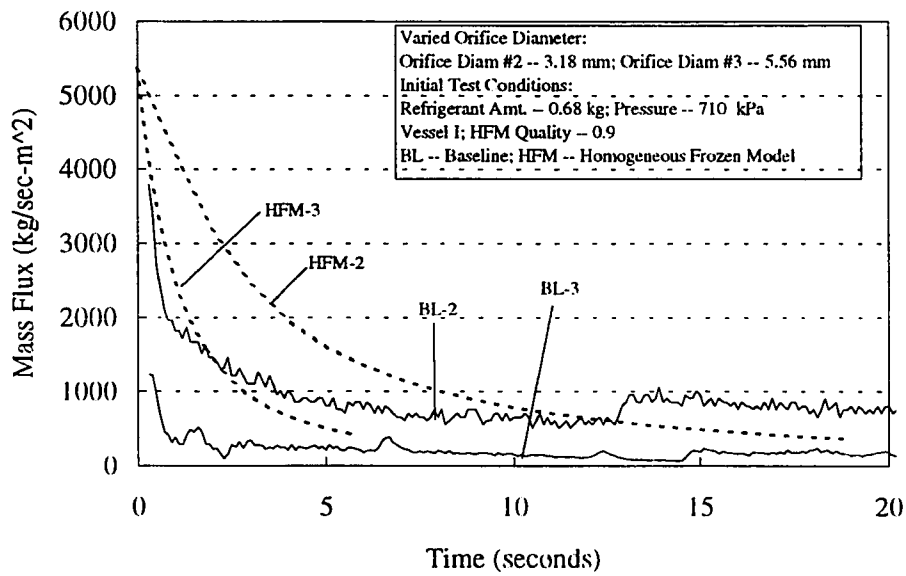Figure 7.7. Mass flux profiles for baseline data and model predictions at varied orifice sizes.
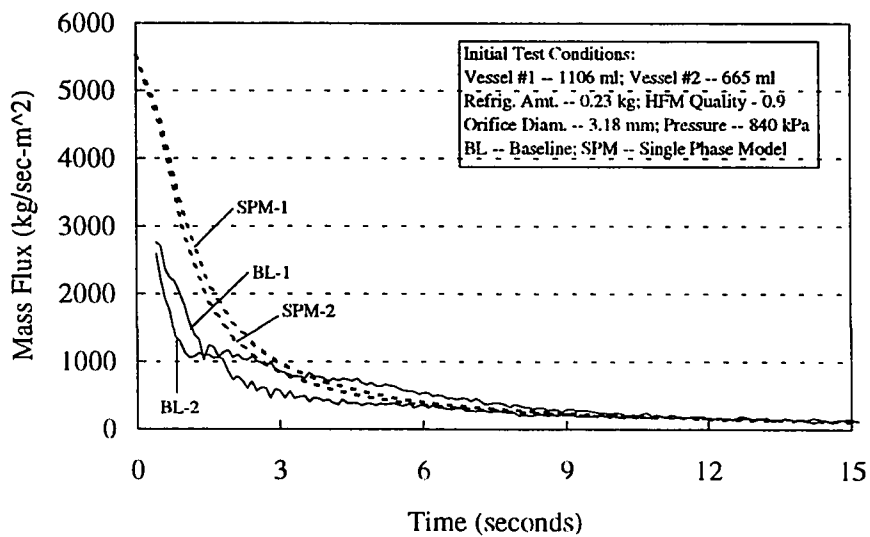
Figure 7.8. Mass flux profiles for baseline data and model predictions at varied vessel volumes.

depressurization would be expected since the flow was choked for a very short period of time (3.18 mm diameter orifice -- 0.7 seconds). Figure 7.6 gives baseline and predicted mass flux profiles for varied initial refrigerant amounts (0.23 kg and 0.68 kg). Initial predictions of the mass flux were high before falling near measured values at 2 seconds (0.23 kg) and 7 seconds (0.68 kg).

Figure 7.7 shows the mass flux for baseline data and model predictions for tests with varied orifice diameters. Mass flux values were overpredicted and the HFM (0.9 mixture quality) had higher values than those predicted using the SPM which assumes a quality of 1.0. At 13 seconds, the increase in the baseline mass flux came as a result of a sudden increase in vapor generation which was not currently predicted by the model. A comparison of the mass flux profiles for varied vessel volumes (Figure 7.8) resulted in overpredicting the values during the initial depressurization process, and closely predicted the measured values after 3 seconds.

REVISIONS TO THE DEPRESSURIZATION MODEL

Opportunities to modify and improve the analytical model exist. Two immediate ways to refine the model are to include effects of stored energy from vessel wall and to include expressions that would better represent the flow through an orifice that is at less than critical flow conditions. The general impact of both model modifications are discussed below.

One of the assumptions used in the derivation of the depressurization model was that the vessel was adiabatic and the stored energy within the vessel walls was negligible (or did not enter the control volume). By relaxing this assumption and including a heat transfer rate term, equation (3.27) changes to (7.1) below. A term estimating the heat transfer rate of energy added to the control volume can be

$$\frac{dP}{dt} = \frac{\dfrac{\dot{Q}}{M} - \dfrac{GA}{M}\left[(u+Pv)_o - u + u_{fg}\dfrac{v}{v_{fg}}\right]}{T\dfrac{v_{fg}}{h_{fg}}\left[C^* - \phi\dfrac{u_{fg}}{v_{fg}}\right]} \tag{7.1}$$

determined. Calculations based on the vessel wall acting as a semi-infinite solid (slab) where the glass is infinitely thick and is subject to an abrupt temperature change at the inner surface (Krieth, 1973). The semi-infinite solid assumption is used since the glass has a low thermal conductivity and the duration of each test is short. The general conduction equation can be reduced to (7.2) for one-dimensional transient heat conduction with constant thermal properties. The solution to (7.2) is given in (7.3) for the case where there is no thermal resistance at the solid's surface which would be the maximum conditions observed during a flashing test. The variables are defined as follows: T -- temperature, t -- time, α -- thermal diffusivity, and x -- distance inward from solid's surface.

$$\frac{\partial T}{\partial t} = \alpha \frac{\partial^2 T}{\partial x} \qquad (7.2)$$

$$\frac{T - T_\infty}{T_i - T_\infty} = erf\left(\frac{x}{2\sqrt{\alpha t}}\right) \qquad (7.3)$$

The instantaneous rate of heat transfer at the glass wall, shown in (7.4), can be found by using Fourier's law and evaluating (7.3) where k_s is the thermal conductivity of the solid.

$$\dot{Q} = k_s A \frac{T_\infty - T_i}{\sqrt{\pi \alpha t}} \qquad (7.4)$$

A temperature difference of 30 °C was used in the calculations. Thermal properties for the glass were assumed to be constant over the small temperature difference. The total energy transferred during a sixty second test (21.5 kJ) was determined by integrating the heat transfer rate equation. The addition of the stored energy term slowed the rate of depressurization, dP/dt, which resulted in higher vessel pressures, as shown in Figure 7.9.

The second adjustment to the model was to modify the model by including an expression for flow through an orifice at conditions that are less than critical flow. Equation (7.5) is the classical equation for flow through an orifice based on horizontal, one-dimensional frictionless flow with a coefficient used to account for viscous and
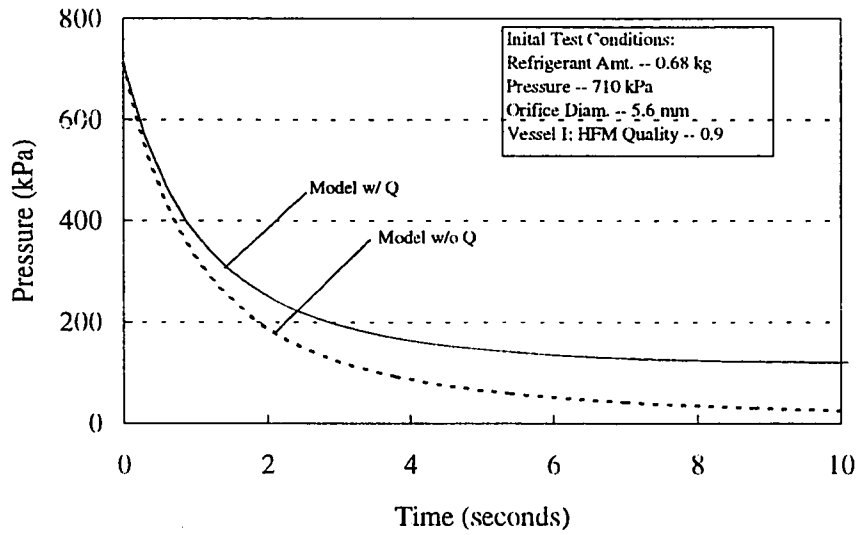
Figure 7.9. Pressure profiles for model predictions with and without added wall energy term.
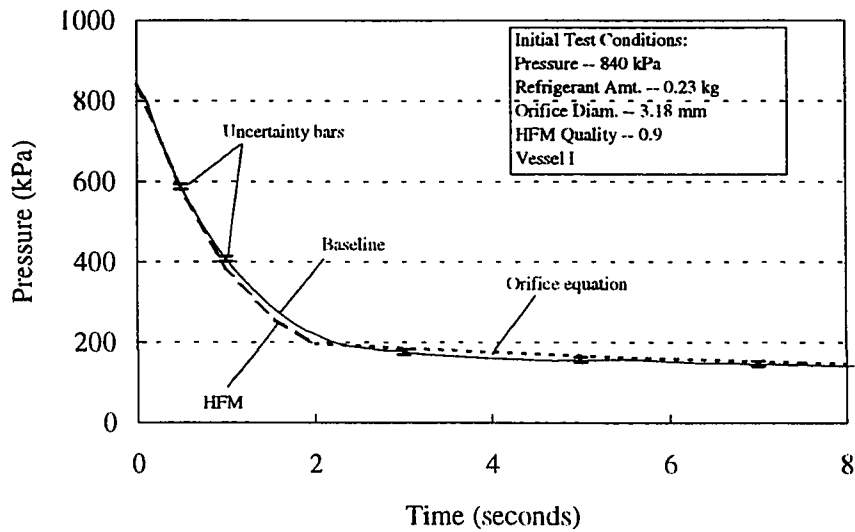
Figure 7.10. Pressure profiles for baseline data and revised model using the HFM and orifice equation.

elastic effects. An averaged flow coefficient (for measured vessel pressures below 250

kPa) of 0.25 was used in the calculations to determine the general impact of such a

revision to the model. The flow coefficient is defined in (7.6) where C_d is the discharge

coefficient. The revised model used the current model to predict the pressure drop

during the initial few seconds and then introduce the orifice equation (Doebelin, 1983)

to properly predict the mass flux as the pressure approaches the reservoir pressure.

Figure 7.10 shows results from the revised model which used the HFM for the first

$$G = C\sqrt{2\rho(P_{in} - P_{out})} \qquad (7.5)$$

$$C = \frac{C_d}{\left[1 - \left(\frac{A_{pipe}}{A_{orifice}}\right)^2\right]^{\frac{1}{2}}} \qquad (7.6)$$

1.5 seconds before changing to a mass flux value described by the orifice equation. For

the case shown in Figure 7.10 (with initial test conditions of 840 kPa, 0.23 kg R-22,

3.18 mm orifice diameter, and Vessel I), results were improved as compared to the

original model. Predicted values were within ±11% of the baseline data for the entire

depressurization process. Other test conditions were not predicted as closely because

the original depressurization process was not predicted as well.

GROLMES AND FAUSKE MODEL

The analytical model used in this chapter and the model developed by Grolmes and Fauske (1984) were developed from the same basic thermodynamic principles. However, the final models differed slightly. Grolmes and Fauske reference at least three critical flow models that could be used in their depressurization model, but the exact one used was not stated. They also developed an expression for a varying mixture quality based on a vapor holdup correlation and the churn turbulent flow regime. A curve-fit discharge coefficient of 0.71 was also found to fit the measured R-12 flashing data. In addition, the R-12 experiment began from an initially full vessel two-phase discharge during the first few seconds. Revisions to the current model (which used a constant quality) added an relation for heat gain to the fluid from the vessel walls as well as developing a different discharge coefficient for better predicting non-critical flow throught the orifice. This model has now been successfully used to predicted the rate of depressurization from a small vessel for two different refrigerants (R-12 and R-22) at different initial conditions. A second validation of this model supports the idea that this model (or some variation of this model) could be used to predict depressurization rates for many other refrigerants and possible other non-refrigerant fluids.

SUMMARY OF MODEL COMPARISON

The experimental results were compared to those predicted by the analytical depressurization model. The one-dimensional lumped parameter model was derived from basic thermodynamic principles. Two critical flow models were used to characterize the mass flux of R-22 leaving the vessel during the depressurization process. The two models were the homogeneous frozen model (HFM) and single-phase choked flow. A two-phase mixture quality of 0.9 was selected for use in the HFM.

A comparison was given for each of the varied test parameters (initial vessel pressure, initial refrigerant amount, orifice diameter, and vessel volume). It was found that the model's pressure estimates were generally in good agreement with baseline experiments during the first few seconds of the flashing process (except for varied orifice diameter tests). The model predictions deviated from the baseline data as the pressure declined toward zero while experimental pressure approached the downstream reservoir pressures. The predicted pressures approached zero because the critical flow models are independent of the downstream pressure. The predicted mass flux profiles generally were overpredicted during the first few seconds of each test, but closely followed the general trend of the baseline data. Predicted mass flux values neared the mass flux of the experimental data during the later stages of the flashing tests.

Opportunities to modify and improve the analytical model exist. The general impact of two refinements to the current model were discussed. The first was to modify the current model by including effects of stored energy from vessel wall. The added

heat transfer term resulted in higher predicted vessel pressures. The second refinement was include an expression for predicting the mass flow during the later stages of the test when critical flow does not exist through the orifice. The revised model showed improved results with pressure predictions within ±11%.

Finally, the model presented begins from the same basic thermodynamic model that was used by Grolmes and Fauske (1984) with different expressions used for predicting mass flux and mixture quality. This research supports the idea that the model (or some variation of this model) could be used to predict depressurization rates for many other refrigerants and possible other non-refrigerant fluids.

CHAPTER VIII

CONCLUSIONS AND RECOMMENDATIONS FOR FUTURE WORK

The mass flow characteristics for flashing Refrigerant-22 from a small vessel was

investigated. Baseline experiments were run to compare with three enhanced boiling

techniques and the derived analytical model. Baseline tests with varied initial settings

were run. The varied parameters were initial vessel pressure, initial refrigerant amount,

orifice diameter, and vessel geometry. Experiments were run using two passive

enhancement methods (additions of a layer of 3.6 mm steel balls and small amounts of

mineral oil) and one active enhancement method (addition of a 215-watt coil immersion

heater). A literature review found that no flash boiling research had been performed

using R-22 as the experimental fluid. The results from the current study could have

immediate applications in the air-conditioning industry. A summary of the study and

overall conclusions and recommendations for further work are discussed in this chapter.

CONCLUSIONS

Mass flow experiments were run establishing a baseline to compare

against the enhanced boiling techniques and model predictions. A literature review led

to the investigation of the effects of four variables on the mass flow during flash boiling.

The four variables were initial orifice diameter, initial refrigerant amount, initial pressure,

and vessel geometry. A visualization study showed that tests run at the lowest initial

conditions (575 kPa, 1.59 mm orifice diameter, and 0.23 kg refrigerant) had a cloud of

vapor and minuscule droplets rise from the liquid surface just after opening the solenoid

valve. Next, larger vapor bubbles appeared at the surface of the liquid primarily around

the perimeter and decreased in number as the test continued.

The orifice size was found to directly impact the mass flow. A smaller orifice

caused a slower depressurization rate within the vessel and reduced mass flow rates.

Tests using a smaller orifice experienced choked flow conditions for a longer duration.

The mass flux was inversely influenced by the orifice size. Higher mass fluxes for test

conditions using a smaller orifice were due to the flow being at, or closer to, critical (or

maximum) conditions for longer periods of time. The initial refrigerant amount was

found to influence the mass flow as well. A higher initial refrigerant amount caused

increased two-phase mixture swelling and increased the overall amount of refrigerant

that was flashed. The initial pressure setting of the refrigerant within the vessel was

changed to determine its impact on the mass flow. The data showed that an increased

initial pressure only changed the mass flow during the initial few seconds of the test, but

did slightly increase the total mass flashed over a 60 second experiment. The fourth and

final variable investigated was the vessel's geometric configuration. Two vessels had

approximately the same volume and two had the same height. A review of the

experiments found varied results with respect to the total mass flashed. Therefore, three

statistical studies of the data were performed to determine the importance of each varied

parameter. Results from the statistical analysis showed that the vessel geometry was not significant when compared against the other parameters.

Refrigerant temperatures were also measured to determine the temperature characteristics within the vessel. A large temperature gradient was found to exist in the vapor region. After the solenoid valve was opened, the pressure quickly dropped below the saturation pressure causing the liquid to be superheated. The liquid was superheated as much as 34°C before vaporization quickly cooled the bulk liquid near the saturation temperature. Between one and seven seconds, the measured corresponded to saturated conditions. Afterwards, a temperature gradient developed in the vapor region with cooler temperatures near the liquid surface and increased temperatures as the vapor approached the orifice. The vapor was superheated as much as 46°C at the top of the vessel near the end of a test. The temperature gradient formed due to the lack of mixing within the vapor region and the poor heat transfer characteristics of the Pyrex glass vessel. Temperature characteristic results agreed quite well with those presented by Guhler, et al. (1979).

The baseline data were used to compare with the enhanced flash boiling test results with primary interest in the mass flow characteristics. A 10 mm layer of 3.6 mm diameter steel balls (or steel shot) was added to the vessel during some of the flashing experiments. A visualization study showed that vapor generation was greater for the tests with steel balls as compared to baseline tests at the same condition. Two-phase liquid-vapor swell of the entire fluid was also more common. Observations of the

experiments showed that most of the bubble formation within the steel balls occurred at the bottom layer at the intersection of the glass and each steel ball. Measured results showed an increase in the total mass flashed for the steel shot tests ranging from an average 21% to 81%. When the smaller orifice (1.59 mm diameter) was used, pressures were substantially greater during the tests and flow was choked for the entire test. Furthermore, measurements of the inner wall found that it was superheated during most of the test and it was hypothesized that the majority of bubble growth occurred at the intersection of the steel balls and the superheated glass wall. Overall, the steel ball passive-type enhanced boiling method was found to consistently increase the mass flow of R-22 while flash boiling. Therefore, the use of small steel shot as a flash boiling enhancement method would be an inexpensive alternative.

A series of tests were run with a mixture of refrigerant and mineral oil. A 4% concentration (by volume) was used and a visualization study showed the boiling to be similar to baseline experiments except for a layer of foam that developed at the liquid surface. It was hypothesized that the foam inhibited bubble growth and release of vapor. Measured results revealed a general decrease in average mass flashed during each sixty second test. Compared to baseline experiments, two out of eight test conditions averaged an increase in total mass flashed and six averaged a decrease, ranging from a 21% increase to a 27% decrease. Measured results showed the same general mass flow and pressure trends with the oil mixture tests maintaining slightly lower values.

A nominal 215-watt coiled immersion heater was mounted inside the vessel for some of the flash boiling experiments. The vessel quickly filled with a two-phase mixture as bubbles continued to form on the heater. Based on observations, the bubbles were spherical and more consistent in size as compared to the baseline tests and the other enhancement tests. Measured results showed that the immersion heater tests increased the total mass flashed ranging between 47% and 111%. Therefore, of the three enhancement methods investigated in this study, the immersion heater would be the most reliable flash boiling enhancement method. The immersion heater would, however, have a higher implementation cost and a continuous operational cost associated with it.

The experimental baseline results were compared to those predicted by the analytical depressurization model. The one-dimensional lumped parameter model was derived from basic thermodynamic principles. Two critical flow models were used to characterize the mass flux of R-22 leaving the vessel during the depressurization process. The two models were the homogeneous frozen model (HFM) and single-phase critical flow model.

A comparison was given for each of the varied test parameters (initial vessel pressure, initial refrigerant amount, orifice diameter, and vessel volume). It was found that the model's pressure estimates were generally in good agreement with baseline experiments during the first few seconds of the flashing process (except for varied orifice diameter tests). The model predictions deviated from the baseline data as the pressures declined toward zero while experimental pressures approached the downstream reservoir

pressure. The predicted pressures approached zero because the critical flow models are independent of the downstream pressure. The predicted mass flux profiles generally were overpredicted during the first few seconds of each test, but closely followed the general trend of the baseline data. Predicted mass flux values neared the mass flux of the experimental data during the later stages of the flashing tests.

Two revisions to the model were made. First, the assumption of an adiabatic vessel was relaxed and the addition of a heat transfer term was added to the model. This was based on experimental measurements of the inner and outer vessel wall temperatures decreasing during flashing tests. The heat transfer rate equation was based on the vessel wall acting as a semi-infinite slab subject to an abrupt temperature change at the surface. The rate of depressurization was decreased resulting in higher predicted internal vessel pressures. The second revision adjusted the model by including an expression for flow through an orifice at conditions less than critical flow. The orifice equation was used to predict the mass flux in the model after the initial depressurization was predicted by the HFM. Modeled pressure values were improved and predicted within ±11% for the test condition shown.

In conclusion, the expected contributions of this investigation include the following: 1) accumulation of experimental data for flash boiling of R-22 from a small vessel, 2) determination and verification of two enhanced flash boiling methods that consistently increase the mass flow during flash boiling of R-22, 3) determination of the influence of orifice diameter, initial vessel pressure, initial refrigerant amount, and vessel

geometry with respect to mass flow during flashing R-22, and 4) development of a model that predicts the general trends of flashing R-22 from a small vessel and may be adaptable for predicting vessel pressure chararistics for other fluids.

RECOMMENDATIONS FOR FUTURE WORK

The present treatment investigated flash boiling of Refrigerant-22 from a small vessel with four varied test conditions -- orifice diameter, initial vessel pressure, initial refrigerant amount, and vessel geometry. Three enhanced flash boiling methods were also investigated. Further work is needed to improve and build on the findings of the present study. The recommendations for future work are listed below.

The present study investigated a range of parameters based on operational conditions for a residential sized heat pump during defrost. The flash boiling process occurs in other stages of heat pump operation like during the transient start-up period. Therefore, a need exists to run flash boiling tests at conditions beyond those investigated in the current study.

To better understand the flash boiling phenomena, further visualization studies are recommend with a greater emphasis on the bubble growth characteristics during flashing.

Many new refrigerants and refrigerant mixtures are being used and developed for use in the future. Experiments using some of the newer alternative refrigerants

(including refrigerant mixtures) would allow for the use of flash boiling data in accumulator (and other) designs and models that use a refrigerant other than R-22.

Experiments with other passive enhancement balls should be run. These experiments could provide data and optimal passive enhancement method. Different size steel balls should be tested as well as balls made of different materials such as glass.

An experimental study of enhanced flash boiling methods for refrigerant-oil mixtures should be performed. The study would be important since refrigeration equipment contains small amounts of oil as a lubricant. Similarly, performance tests on a heat pump system with the addition of an immersion heater and small steel balls placed within the accumulator should be run. This would support the experimental findings and could lead to design changes within manufactured heat pump systems.

Finally, refinement of the depressurization model is needed. Potential improvements to the model would require the addition of an expression for 1) predicting vapor generation for known nucleation sites, 2) heat transfer from vessel walls, and 3) non-choked flow after the initial depressurization.

REFERENCES

Alamgir, Md. and Lienhard, J. H., 1981. Correlation of pressure undershoot during hot-water depressurization. *Transactions, ASME Journal of Heat Transfer*, 103: 52-55.

ANSI/ASME, 1985. Measurement Uncertainty -- Instruments and Apparatus. *ANSI/ASME PTC 19.1-1985*, Part 1.

ASHRAE Handbook of Fundamentals, 1993. Atlanta, Georgia: American Society of Heating, Refrigerating and Air-Conditioning Engineers, Inc., pp. 16.1-16.10.

ASHRAE Handbook of Refrigeration Systems and Applications, 1994. Atlanta, Georgia: American Society of Heating, Refrigerating and Air-Conditioning Engineers, Inc., pp. 8.1-8.21.

Beckwith, T. G., Buck, N. L., and Marangoni, R., D., 1982. *Mechanical Measurements*, 3rd ed., Massachusetts: Addison-Wesley Publishing Co., pp. 261-273.

Bergles, A. E., 1988. Some perspectives on enhanced heat transfer -- second generation heat transfer technology. *Transactions, ASME Journal of Heat Transfer*, 110: 1082-1096.

Blander, M. and Katz, J. L., 1975. Bubble nucleation in liquids. *AIChE*, 21(5): 833-843.

Bolz, R. E. and Tuve, G.L., 1973. *Handbook of Tables for Applied Engineering Science*, Florida: CRC Press, Inc., p. 387.

Bonnet, F. W., 1966. Critical two-phase flow of nitrogen and oxygen through orifices. *Advances in Cryogenic Engineering*, 12: 427-437.

Bosworth, C. M., 1952. Predicting the behavior of oils in refrigeration systems, *Refrigerating Engineering*, June, pp. 617-655.

Carey, V. P., 1992. *Liquid-Vapor Phase-Change Phenomena*. Washington: Hemisphere Publishing Corp., pp. 326-331.

Chuah, Y. K. and Carey, V. P., 1987. Boiling Heat Transfer in a Shallow Fluidized Particulate Bed. *Transactions, ASME Journal of Heat Transfer*, 109: 196-203.

Clegg, G. T. and Papadakis, G., 1986. Rates of evaporation accompanying the depressurization of a pool of saturated Freon-11. *Chemical Engineering*, 41(12): 3037-3043.

Cole, R., 1974. Boiling nucleation. *Advances in Heat Transfer*, 10: 85.

Coleman, H. W., and Steele, W. G., 1989. *Experimentation and Uncertainty Analysis for Engineers*, New York: John Wiley and Sons, pp. 75-118.

Doebelin, E. O., 1983. *Measurement Systems*, 3rd ed., New York: McGraw-Hill Book Co., pp. 528-535.

Edwards, A. R. and O'Brien, T. P., 1970. Studies of phenomena connected with the depressurization of water reactors. *The British Nuclear Energy Society*, 9(2): 125-135.

El-Wakil, M. M., 1984. *Powerplant Technology*. New York: McGraw Hill, Inc., pp. 395-411.

Fauske, H. K., 1985. Flashing flows or: Some practical guidelines for emergency releases. *Plant/Operations Progress*, 4(3): 132-134.

Fauske, H. K., 1988. Emergency relief system design for reactive and non-reactive systems: extension of the DIERS methodology. *Plant Operations Progress*, 7(3): 153-158.

Fauske, H. K., Epstein, M., Grolmes, M. A., and Leung, J. C., 1986. Emergency relief vent sizing for fire emergencies involving liquid-filled atmospheric storage vessels. *Plant Operations Progress*, 5(4): 205-208.

Fauske, H. K., Grolmes, M. A., and Leung, J. C., 1984. Multi-phase flow considerations in sizing emergency relief systems for runaway chemical reactions. *Multi-Phase Flow and Heat Transfer III. Part B: Applications*. pp. 899-907.

Favrat, D. and Denisart, J. P., 1984. Vaporization of superheated water under depressurization. *Multi-Phase Flow and Heat Transfer III. Part A: Fundamentals*. pp. 513-526.

First, K. E. and Huff, J. E., 1989. Design chart for two-phase flashing flow in emergency pressure relief systems. *Plant Operations Progress*, 8(1): 40-54.

Fox, R. W. and McDonald, A. T., 1978. *Introduction to Fluid Mechanics*, 2nd ed., New York: John Wiley and Sons.

Grolmes, M. A. and Fauske, H. K., 1974. Axial propagation of free surface boiling into superheated liquids in vertical tubes. *Proceedings, 5th International Heat Transfer Conference*, Tokyo, pp. 30-34.

Grolmes, M. A. and Fauske, H. K., 1984. An evaluation of incomplete vapor phase separation in freon-12 top vented depressurization experiments. *Multi-phase Flow and Heat Transfer III, Part A: Fundamentals*, pp. 539-548.

Grolmes, M. A. and Leung, J. C., 1984. Scaling considerations for two-phase critical flow. *Multi-phase Flow and Heat Transfer III, Part A: Fundamentals*, pp. 549-565.

Guhler, M., Hannemann, R. J., and Sallet, D. W., 1979. Unsteady two-phase blowdown of a flashing liquid from a finite reservoir. *Two-phase Momentum, Heat and Mass Transfer in Chemical, Process, and Energy Engineering Systems*, pp. 781-795.

Hanaoka, Y., Maeno, K., Zhao, L., and Heymann, G., 1990. A study of liquid flashing phenomenon under rapid depressurization. *JSME International Journal, Series II*, 33(2): 276-282.

Hardy, P. G. and Richter, H. J., 1986. Pressure transient and two-phase swelling due to a small top break. *Nuclear Engineering and Design*, 95: 207-220.

Henry, R. E. and Fauske, H. K., 1971. The two-phase critical flow of one-component mixtures in nozzles, orifices, and short tubes. *ASME*, paper 70-WA/HT-5.

Hooper, F. C. and Abdelmessih, A. H., 1966. The flashing of liquids at higher superheats. *Proceedings, 3rd International Heat Transfer Conference*, Chicago, Illinois, pp. 44-50.

Hooper, F. C. and Kerba, N. A., 1969. A law of flashing. *Proceedings, 2nd Canadian Congress of Applied Mechanics*, Waterloo, Ontario, pp. 259-260.

Hooper, F. C. and Luk, P. S. K., 1974. The mechanisms controlling the static pressure in a flashing liquid. Proceedings, *5th International Heat Transfer Conference*, Tokyo, pp. 70-74.

Hooper, F. C. and Struk, P., 1967. The time delay in flashing of superheated water. Proceedings, *Canadian Congress of Applied Mechanics*, 2: 265-266.

Huff, J. E., 1982. Emergency venting requirements. *Plant Operations Progress*, 1(4): 211-223.

Huff, J. E., 1984. Emergency venting requirements for gassy reactions from closed system tests. *Plant Operations Progress*, 3(1): 50-59.

Huff, J. E., 1985. Multiphase flashing flow in pressure relief systems. *Plant/Operations Progress*, 4(4): 191-199.

Incropera, F. P. and DeWitt, D. P., 1990. *Fundamentals of Heat and Mass Transfer*, 3rd ed., New York: John Wiley and Sons.

Jung, D. S., Venart, J. E. S., and Sousa, A., C., M., 1987. Effects of enhanced surfaces and surface orientation on nucleate and film boiling heat transfer in R-11. *International Journal of Heat and Mass Transfer*, 30(12): 2627-2639.

Kim, Y., 1993. *Two-phase flow of HCFC-22 and HFC-134a through short tube orifices.* Dissertation, Texas A&M University, College Station, Texas.

Klein, S. and Alvarado, F., 1993. *Engineering equation solver.* F-Chart Software, Inc., Middletown, Wisconsin.

Krieth, F., 1973. *Principles of Heat Transfer.* 3rd ed., New York: Harper and Row, Publishing, Inc., pp. 174-178.

Kung, S. P. and Lester, T. W., 1981. Boiling transition during rapid decompression from elevated pressures. *ASME,* paper 81-WA/HT-57.

Leung, J. C. and Fauske, H. K., 1987. Runaway system characterization and vent sizing based on DIERS methodology. *Plant Operations Progress,* 6(2): 77-83.

Levy, S., 1965. Prediction of two-phase critical flow rate. *Transactions, ASME Journal of Heat Transfer,* 86(1): 53-58.

Lienhard, J. H., 1982. Corresponding states correlations of the spinodal and homogeneous nucleation limits. *Transactions, ASME Journal of Heat Transfer,* 104: 379-381.

Lienhard, J. H., Alamgir, Md., and Trela, M., 1978. Early response of hot water to sudden release from high pressure. *Transactions, ASME Journal of Heat Transfer,* 100: 473-479.

Lienhard, J. H. and Karimi, A., 1981. Homogeneous nucleation and the spinodal line. *Transactions, ASME Journal of Heat Transfer,* 103: 61-64.

Little, J. L., 1952. Viscosity of Lubricating Oil-Freon-22 Mixtures. *Refrigerating Engineering,* November, pp. 1191-1195.

Lu, S. M. and Lee, D., J., 1991. The effects of heating methods on pool boiling. *International Journal of Heat and Mass Transfer,* 34(1): 127-134.

Maeno, K., Kosugi, S., and Hanaoka, Y., 1987. A study of R-113 pool flashing under rapid depressurization. *Transactions, JSME*, 53(485B): 193-197.

Mayinger, F., 1982. The state of knowledge of thermohydraulic pressure release phenomena. *German Chemical Engineering*, 5: 297-305.

Mayinger, F., 1988. Two-phase flow phenomena with depressurization -- consequences for the design and layout of safety and pressure relief valves. *Chemical Engineering and Processing*, 23(1): 1-11.

McQuiston, F. C. and Parker, J. D., 1994. *Heating, Ventilating and Air Conditioning Analysis and Design*, 4th ed., New York: John Wiley and Sons, Inc., pp. 384-385

Miller, W. A., 1987. Laboratory examination and seasonal analysis of frosting and defrosting for an air-to-air heat pump. *ASHRAE Transactions*, 93(1): 1009-1025.

Moody, F. J., 1969. Liquid/Vapor action in a vessel during blowdown. *Transactions, ASME Journal of Engineering Power*, 91(1): 53-61.

Moody, F. J., 1965. Maximum flow rate of a single component, two-phase mixture. *Transactions, ASME Journal of Heat Transfer*, 87(1): 134-142.

Moran, M. J. and Shapiro, H. N., 1988. *Fundamentals of Engineering Thermodynamics*, New York: John Wiley and Sons.

Nakamura, S., Matushima, T., and Anzai, S., 1984. Transient characteristics of flashing phenomena of saturated water in vessels and their method of analysis. *Heat Transfer -- Japanese Research*, 13(4): 1-18.

Peterson, R. J., Grewal, S. S., and El-Wakil, M. M., 1984. Investigations of liquid flashing and evaporation due to sudden depressurization. *International Journal of Heat and Mass Transfer*, 27(2): 301-310.

Plesset, M. S. and Zwick, S. A, 1954. The growth of vapor bubbles in superheated liquids. *Journal of Applied Physics*, 25(4): 493-500.

Reay, P. A., 1991. Heat transfer enhancement -- a review of techniques and their possible impact on energy efficiency in the U.K. *Heat Recovery Systems & CHP*, 11(1): 1-40.

Sakurai, A., Shiotsu, M., and Hata, K., 1978. Transient boiling caused by rapid depressurization from initial nonboiling state. *Multiphase Transport: Fundamentals, Reactor Safety, Applications*, 2: 727-747.

Spauschus, H. O. and Speaker, L. M., 1987. A review of viscosity data for oil-refrigerant solutions. *ASHRAE Transactions*, 93(2): 667-680.

Swift, I., et al., 1983. Emergency relief systems for runaway reactions. *Plant Operations Progress*, 2(2): 116-120.

Thome, J. R., 1990. *Enhanced boiling heat transfer*, New York: Hemisphere Publishing Co.

Wallis, G. B., 1969. *One-Dimensional Two-Phase Flow*. New York: McGraw-Hill, Inc., pp. 17-26.

Wallis, G. B., 1980. Critical two-phase flow. *International Journal of Multiphase Flow*, 6: 97-112.

Webb, R. L., 1981. The evolution of enhanced surface geometries for nucleate boiling. *Heat Transfer Engineering*, 2(3-4): 46-69.

Webb, R. L., 1983. Nucleate boiling in porous coated surfaces. *Heat Transfer Engineering*, 4(3-4): 71-82.

APPENDIX A

UNCERTAINTY ANALYSIS

The objective of this analysis was to calculate the systematic uncertainties involved with measuring and predicting the mass flux of the refrigerant leaving the vessel throughout the experiment. Two overall systematic uncertainties were calculated: one for the measured mass flux, G_m; and one for the predicted mass flux, G_p. A diagram of the test apparatus related to the experimental uncertainty is provided below.
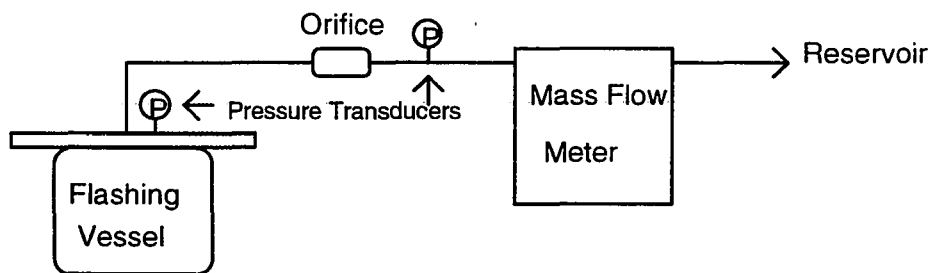

Figure A.1 Mass flux portion of experimental apparatus.

Only the primary independent measurement parameters were included and they are listed in Table A.1 The uncertainty calculation method presented in ANSI/ASME (1985), Coleman and Steele (1989), and Beckwith et al. (1982) was used.

Table A.1 Independent measurement parameters

Independent Measurement Parameter	Rated Bias Limits	Estimated Precision Limits[1]
Mass flow meter	±0.4% of flow or ±0.00016 kg/s (0.02 lb/min) at maximum observed flow of 0.04 kg/s (5.3 lb/min)	±5.5.% of flow or ±0.0022 kg/s (0.29 lb/min) at maximum observed flow of 0.04 kg/s (5.3 lb/min)
Data acquisition system	±0.24%	±0.2% [2]
Pressure transducers	±0.2% full scale or ±3.5 kPa (0.5 psi)	±0.21% full scale or ±3.6 kPa (0.52 psi)
Orifice diameter gauges	±0.8 % or ±0.0127 mm (0.0005 inches) for smallest orifice (1.59 mm or 0.0625 in.)	±0.6 % or ±0.01 mm (0.0004 inches) for smallest orifice (1.59 mm or 0.0625 in.)[3]

Measured Mass Flux

The measured mass flux is determined by dividing the measured mass flow rate (kg/s) by the orifice area. The functional relationship involved is

$$G_m = \frac{\dot{m}}{\pi d^2 / 4}$$ (A.1)

where

G_m = measured mass flux $(kg/s\text{-}m^2)$

$\dot{m}$ = measured mass flow rate (kg/s)

d = measured orifice diameter (m).

---

[1] Precision limits for pressure transducer and mass flow meter were determined by using the standard deviation during first two seconds of depressurization process.

[2] Estimated.

[3] Estimated.

The data reduction bias limits, B_{dr}, can be calculated as

$$B_{dr,G_m} = \left| u_{\dot{m}} \frac{\partial G_m}{\partial \dot{m}} \right| + \left| u_d \frac{\partial G_m}{\partial d} \right| \qquad (A.2)$$

or

$$\frac{B_{dr,G_m}}{G_m} = \sqrt{\left(\frac{u_{\dot{m}}}{\dot{m}} \right)^2 + \left(\frac{2u_d}{d} \right)^2} \qquad (A.3)$$

$$= 1.65\%.$$

Including the bias limit for the data acquisition system, B_{da}, the overall bias limit becomes,

$$B_{G_m} = \sqrt{B_{dr}^2 + B_{da}^2} \qquad (A.4)$$

$$= 1.67\%.$$

Likewise, the data reduction precision limit, P_{dr}, can be calculated as,

$$P_{dr,G_m} = \left| u_{\dot{m}} \frac{\partial G_m}{\partial \dot{m}} \right| + \left| u_d \frac{\partial G_m}{\partial d} \right| \qquad (A.5)$$

or

$$\frac{P_{dr,G_m}}{G_m} = \sqrt{\left(\frac{u_{\dot{m}}}{\dot{m}} \right)^2 + \left(\frac{2u_d}{d} \right)^2} \qquad (A.6)$$

$$= 5.6\%.$$

Include the data acquisition precision limit, P_{da}, of 0.24% and the overall precision limit becomes,

$$P_{G_m} = \sqrt{P_{dr}^2 + P_{da}^2} \qquad (A.7)$$

$$= 5.6\%.$$

Finally, the root-sum squared systematic uncertainty is calculated using eq. A.8 below.

$$U_{RSS,G_m} = \sqrt{B_{G_m}^2 + 2P_{G_m}^2}$$ (A.8)

$$= 8.1\%$$

Predicted mass flux

In the text, several means of predicting the mass flux were presented. Since the predicted models were of similar mathematical form, the uncertainty analysis considered the simplified case of single phase choked flow. The functional relationship involved is

$$G_p = C\sqrt{\frac{h_o - h_1}{v_1}}$$ (A.9)

where

G_p = predicted mass flux $(kg/s\text{-}m^2)$

C = constant (with a negligable influence)

v_1 = specific volume of vapor after orifice (m^3/kg)

h_o = enthalpy of vapor prior to orifice (kJ/kg)

h_1 = enthalpy of vapor after orifice (kJ/kg).

The data reduction bias limits, B_{dr}, can be calculated as

$$B_{dr,G_p} = \left| u_{v_1} \frac{\partial G_p}{\partial v_1} \right| + \left| u_{h_0} \frac{\partial G_p}{\partial h_0} \right| + \left| u_{h_1} \frac{\partial G_p}{\partial h_1} \right| \qquad (A.10)$$

or

$$\frac{B_{dr,G_p}}{G_p} = \sqrt{\left(\frac{u_{v_1}}{v_1} \right)^2 + \left(\frac{1}{2} \frac{u_{h_0}}{h_0} \right)^2 + \left(\frac{1}{2} \frac{u_{h_1}}{h_1} \right)^2} \qquad (A.11)$$

The data reduction precision limits, P_{dr}, can be written as

$$P_{dr,G_p} = \left| u_{v_1} \frac{\partial G_p}{\partial v_1} \right| + \left| u_{h_0} \frac{\partial G_p}{\partial h_0} \right| + \left| u_{h_1} \frac{\partial G_p}{\partial h_1} \right| \qquad (A.10)$$

or

$$\frac{P_{dr,G_p}}{G_p} = \sqrt{\left(\frac{u_{v_1}}{v_1} \right)^2 + \left(\frac{1}{2} \frac{u_{h_0}}{h_0} \right)^2 + \left(\frac{1}{2} \frac{u_{h_1}}{h_1} \right)^2} \qquad (A.11)$$

Both the density and enthalpies were determined using computer program containing curve-fit data of thermodynamic properties for refrigerants. Table A.2, located at the end of the appendix) gives the individual uncertainty for each property measurement. From Eq. A.11, this leads to a data reduction bias limit for the predicted mass flux of

$$\frac{B_{G_p}}{G_p} = 5.5\%.$$

Including in the bias limit of the data acquisition system, the overall precision limit becomes,

Similarly, the precision limit becomes,

$$\frac{P_{G_p}}{G_p} = 5.3\%.$$

Including in the precision limit of the data acquisition system, the overall precision limit becomes.

$$P_{G_p} = \sqrt{P_{dr}^2 + P_{da}^2} \qquad (A.12)$$

$$= 5.3\%.$$

Finally, the root-sum squared systematic uncertainty is calculated below.

$$U_{RSS,G_p} = \sqrt{B_{G_p}^2 + 2P_{G_p}^2} \qquad (A.13)$$

$$= 9.3\%.$$

Table A.2 Individual uncertainty for enthalpies and density.

Property	Upstream pressure kPa	Down-stream pressure kPa	Specific volume m³/kg	Enthalpy kJ/kg	Precision limits %
	840	120			
BIAS LIMITS					
$v_{1,min}$		116.4	0.1868		5.5
$v_{1,max}$		123.6	0.1766		
$h_{0,min}$	836.4			411.07	0.02
$h_{0,max}$	843.6			411.17	
$h_{1,min}$		116.4		389.63	0.16
$h_{1,max}$		123.6		390.24	
PREC. LIMITS					
$v_{1,min}$		116.5	0.1866		5.3
$v_{1,max}$		123.5	0.1767		
$h_{0,min}$	836.5			411.08	0.02
$h_{0,max}$	843.5			411.17	
$h_{1,min}$		116.5		389.64	0.15
$h_{1,max}$		123.5		390.23	

VITA

Darin Wayne Nutter was born on February 4, 1964, in Amarillo, Texas. His parents are Larry Wayne Nutter and Delta Jean Nutter. He graduated from Edmond Memorial High School in 1982. He received a Bachelor and Master of Science in mechanical engineering at Oklahoma State University in the Fall of 1986 and the spring of 1988, respectively. He then accepted a job as a Facilities Engineer with Fleming Companies, Inc. of Oklahoma City, Oklahoma and remained there until November, 1989. He then moved to College Station, Texas where he served as a research associate for the Department of Mechanical Engineering at Texas A&M University and enrolled in the Ph.D. program in mechanical engineering. His area of specialization was thermal science. Darin Wayne Nutter's permanent mailing address is: 3602 W. Backus, Springdale, AR 72762